

AD-A047998

AFAL-TR-77-110



## HOLOGRAPHIC COMBINERS FOR HEAD-UP DISPLAYS

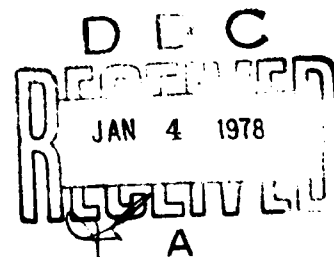
Radar and Optics Division  
Environmental Research Institute of Michigan  
P.O. Box 8618  
Ann Arbor, MI 48107

OCTOBER 1977

Final Technical Report No. AFAL-TR-77-110  
Final Report for Period May 1976 - January 1977

Approved for public release; distribution unlimited.

ORIGINAL CONTAINS COLOR PLATES; ALL DDC  
REPRODUCTIONS WILL BE IN BLACK AND WHITE



AIR FORCE AVIONICS LABORATORY  
AIR FORCE WRIGHT AERONAUTICAL LABORATORIES  
AIR FORCE SYSTEMS COMMAND  
WRIGHT-PATTERSON AIR FORCE BASE, OHIO 45433

CLASSIFICATION


AP front cover


NOTICE

When Government drawings, specifications, or other data are used for any purpose other than in connection with a definitely related Government procurement operation, the United States Government thereby incurs no responsibility nor any obligation whatsoever; and the fact that the government may have formulated, furnished, or in any way supplied the said drawings, specifications, or other data, is not to be regarded by implication or otherwise as in any manner licensing the holder or any other person or corporation, or conveying any rights or permission to manufacture, use, or sell any patented invention that may in any way be related thereto.

This report has been reviewed by the Information Office (OI) and is releasable to the National Technical Information Service (NTIS). At NTIS, it will be available to the general public, including foreign nations.

This technical report has been reviewed and is approved for publication.

  
JOHN O. MYSING  
Project Engineer

  
MAJ. RICHARD L. BUSH  
Acting Chief  
System Technology Branch

FOR THE COMMANDER

  
H. MARK GROVE  
Acting Director  
System Avionics Division

REPORT DOCUMENTATION PAGE		READ INSTRUCTIONS BEFORE COMPLETING FORM
1. REPORT NUMBER AFAL-TR-77-110	2. GOVT ACCESSION NO.	3. RECIPIENT'S CATALOG NUMBER
4. TITLE (and Subtitle) HOLOGRAPHIC COMBINERS FOR HEAD-UP DISPLAYS		5. TYPE OF REPORT & PERIOD COVERED Final Technical Report 1 May 1976-31 January 1977
7. AUTHOR(s) W.S. Colburn B.J. Chang		6. PERFORMING ORG. REPORT NUMBER 122400-9-F
9. PERFORMING ORGANIZATION NAME AND ADDRESS Environmental Research Institute of Michigan P.O. Box 618 Ann Arbor, Michigan 48107		8. CONTRACT OR GRANT NUMBER(s) F33615-76-C-1182
11. CONTROLLING OFFICE NAME AND ADDRESS Air Force Avionics Laboratory (AFAL/AAT) Air Force Wright Aeronautical Laboratories Wright-Patterson AFB, Ohio 45433		10. PROGRAM ELEMENT PROJECT, TASK AREA & WORK UNIT NUMBERS Project 2003 Task 06 Work Unit 31
14. MONITORING AGENCY NAME & ADDRESS (if different from Controlling Office)		12. REPORT DATE October 1977
		13. NUMBER OF PAGES 106
		15. SECURITY CLASS. (of this report) Unclassified
		15a. DECLASSIFICATION/DOWNGRADING SCHEDULE
16. DISTRIBUTION STATEMENT (of this Report) Approval for public release; distribution unlimited.		
17. DISTRIBUTION STATEMENT (of the abstract entered in Block 20, if different from Report)		
18. SUPPLEMENTARY NOTES		
19. KEY WORDS (Continue on reverse side if necessary and identify by block number) Head-up Displays            Hologram Optical Elements Holography                    Hologram Materials Optics                         Dichromated Gelatin Computer Design		
20. ABSTRACT (Continue on reverse side if necessary and identify by block number) The use of holographic optical elements as combiners in Head-Up Displays (HUD) offers performance improvements in two respects; because the holographic combiner has high reflectivity over a narrow spectral region, it can make more efficient use of the light, and by forming the final element of the collimating lens, it can increase the field-of-view. Both improvements were examined separately in an analytical and experimental investigation directed at evaluating holographic combiners in existing HUD systems. To demonstrate the high		

efficiency narrowband property, we designed and fabricated flat holographic combiners that can be substituted on a one-for-one replacement basis for the conventional combiner in an existing HUD. The combiners were fabricated in dichromated gelatin, and were characterized by diffraction efficiencies in excess of 90% and angular bandwidths of 10 to 12°. A computer analysis of curved holographic combiners in the A-10 HUD generated a design that shows promise for increasing the instantaneous field-of-view to 15° and the total field-of-view to 20°.

## FOREWORD

This report was prepared by the Radar and Optics Division of the Environmental Research Institute of Michigan. The work was sponsored by the Air Force Avionics Laboratory under Contract No. F33615-76-C-1182, Project No. 2003.

The report covers work performed between 1 May 1976 and 31 January 1977. The contract monitor is Mr. John Mysing, AFAL/AAT. The principal investigators are B. J. Chang and W. S. Colburn. C. D. Leonard, J. Lewis, and J. A. Losee assisted with the technical effort.

## CONTENTS

I.	INTRODUCTION.....	11
II.	DESIGN OF A FLAT HOLOGRAPHIC COMBINER.....	17
	1. Field-of-View.....	17
	2. Flat Combiner Design.....	25
	3. Curved Combiner.....	35
III.	FABRICATION OF A FLAT HOLOGRAPHIC COMBINER.....	38
	1. Basic Material Investigations.....	38
	a. Dichromated gelatin.....	38
	b. Diffraction efficiency.....	43
	c. Angular bandwidth.....	48
	d. Spectral bandwidth.....	54
	2. Fabrication and Test of Flat Reflection Holographic Combiners.....	60
	a. Fabrication.....	60
	b. Evaluation of the holographic combiners....	65
IV.	COMPUTER ANALYSIS OF A HOLOGRAPHIC COMBINER.....	75
	1. Collimating Combiner.....	76
	2. Relay Lens System.....	94
V.	CONCLUSIONS AND RECOMMENDATIONS.....	100
	REFERENCES.....	103

ACCESSION NO.		
RTS	White Section	<input checked="" type="checkbox"/>
ABC	Buff Section	<input type="checkbox"/>
UNANNOUNCED		<input type="checkbox"/>
JUSTIFICATION		
BY		
DISTRIBUTION/AVAILABILITY CODES		
Dist.	AVAIL. and/or	SPECIAL
A		

## LIST OF ILLUSTRATIONS

Figure 1.	Typical configuration of a conventional HUD.....	12
Figure 2.	Total field-of-view (TFOV) of a HUD optical system.	14
Figure 3.	Instantaneous field-of-view (IFOV) of a HUD optical system. The dashed lines indicate light rays outside the IFOV.....	15
Figure 4.	Head-up display with a holographic combiner.....	18
Figure 5.	Predicted angular bandwidth of a reflection hologram with a thickness of 15 $\mu\text{m}$ and a refractive index modulation of 0.021.....	20
Figure 6.	Predicted angular bandwidth of a reflection hologram with a thickness of 6 $\mu\text{m}$ and a refractive index modulation of 0.0525.....	22
Figure 7.	Predicted angular bandwidth of a reflection hologram with a thickness of 15 $\mu\text{m}$ and a refractive index modulation of 0.0525.....	23
Figure 8.	Predicted spectral bandwidth of a reflection hologram with a thickness of 15 $\mu\text{m}$ and a refractive index modulation of 0.021.....	24
Figure 9.	Predicted spectral bandwidth of a reflection hologram with a thickness of 6 $\mu\text{m}$ and a refractive index modulation of 0.0525.....	26
Figure 10.	Predicted spectral bandwidth of a reflection hologram with a thickness of 15 $\mu\text{m}$ and a refractive index of 0.0525.....	27
Figure 11.	Recording a reflection hologram with fringes parallel to the surface.....	30
Figure 12.	Single-beam recording technique for a reflection hologram with fringes parallel to the surface.....	31
Figure 13.	Raytrace through the F-4 HUD with a holographic combiner.....	34



LIST OF ILLUSTRATIONS (continued)

Figure 14.	Angular bandwidth as a function of refractive index modulation for a volume phase reflection hologram.....	36
Figure 15.	PX58 phosphor characteristic shown with the spectral bandwidth of a hologram with a thickness of 15 $\mu\text{m}$ and a refractive index modulation of 0.0525.....	37
Figure 16.	Absorption of dichromated gelatin as a function of exposure.....	41
Figure 17.	Detail of single-beam recording configuration...	42
Figure 18.	Diffraction efficiency as a function of exposure for reflection holograms recorded in dichromated gelatin.....	47
Figure 19.	Angular bandwidth of single-grating reflection holograms recorded at three exposure levels.....	49
Figure 20.	Angular bandwidth of two-grating reflection holograms recorded at two exposure levels.....	50
Figure 21.	Angular bandwidth of a single-grating reflection hologram in dichromated gelatin sensitized with a 3% sensitizer concentration.....	52
Figure 22.	Angular bandwidth of two-grating reflection holograms in dichromated gelatin sensitized with a 3% sensitizer concentration.....	53
Figure 23.	Spectral bandwidth of a single grating reflection hologram recorded in dichromated gelatin with an exposure of 170 $\text{mJ}/\text{cm}^2$ .....	55
Figure 24.	Spectral bandwidth of a single-grating reflection hologram recorded in dichromated gelatin with an exposure of 320 $\text{mJ}/\text{cm}^2$ .....	56
Figure 25.	Spectral bandwidth of a two-grating reflection hologram recorded in dichromated gelatin.....	57
Figure 26.	Bragg angle deviation as a function of exposure for dichromated gelatin reflection holograms under several drying conditions.....	59

LIST OF ILLUSTRATIONS (continued)

Figure 27. Bragg angle deviation as a function of sensitizer concentration for dichromated gelatin reflection holograms under two drying conditions.. 61

Figure 28. Recording configuration used to fabricate the holographic combiners..... 62

Figure 29. Photograph of the recording system. The parabolic mirror is in the foreground..... 63

Figure 30. Photograph of a complete holographic combiner before cutting to size..... 66

Figure 31. Measurement of angular bandwidth of the holographic combiner..... 67

Figure 32. Angular bandwidth of holographic combiner HUD-76-1. 68

Figure 33. Angular bandwidth of holographic combiner HUD-76-2.69

Figure 34. Angular bandwidth of holographic combiner HUD-76-3.70

Figure 35. Spectral bandwidth (shown in transmission) of holographic combiner HUD-76-1.....72

Figure 36. Spectral bandwidth (shown in transmission) of holographic combiner HUD-76-2.....73

Figure 37. Spectral bandwidth (shown in transmission) of holographic combiner HUD-76-3.....74

Figure 38. Configuration of the A-10 HUD with a holographic combiner/collimator.....78

Figure 39. Two recording configurations for the holographic combiner..... 82

Figure 40. Diffraction efficiency as a function of field angle for the two hologram designs..... 83

Figure 41. Effect of hologram curvature on image tilt for several hologram designs..... 85

Figure 42. Image surfaces formed by varying the vertical field angle for several hologram curvatures..... 86

Figure 43. Effect of hologram curvature on wavefront deviations for two hologram designs..... 87

LIST OF ILLUSTRATIONS (continued)

Figure 44.	Collimation error as a function of field angles for a hologram made with a plane reference beam.....	89
Figure 45.	Collimation error as a function of field angle for a hologram made with a spherical reference beam.....	90
Figure 46.	Raytrace from exit pupil through the holographic combiner at field angles of $0^\circ$ , $\pm 7.5^\circ$ .....	92
Figure 47.	Unfolded optical system with a relay lens.....	95
Figure 48.	Effect of hologram curvature on wavefront deviations.....	98
Figure 49.	Image surfaces formed by varying the vertical field angle.....	99

LIST OF TABLES

Table

1. Construction Parameters of the Flat Holographic Combiner.....	33
2. Preparation of Dichromated Gelatin Plates.....	44
3. Standard Development of Dichromated Gelatin Plates..	45
4. Examples of Chemical Mixing Formulas.....	46
5. Design Parameters of Relay Lens Configurations.....	97

## HOLOGRAPHIC COMBINERS FOR HEAD-UP DISPLAYS

SECTION I  
INTRODUCTION

Current head-up display (HUD) systems tend to be limited in two respects: their field-of-view is often less than desired, and excessive CRT power levels are often necessary to achieve adequate image intensity. The introduction of holographic optics offers potential relief to both limitations. This report describes the results of an investigation into the addition of holographic optics to existing HUD systems; the investigation included both analytical and practical considerations, as well as fabrication of several holographic combiners.

A typical HUD optical system includes a CRT, collimating optics, and a combiner. The CRT is the source of the display information, and is located at the focal plane of the collimating optics. The information displayed on the CRT will therefore be imaged at infinity with a field-of-view determined by the properties of the collimating optics and the distance between the collimator and the pilot's eye. The combiner is a beam-splitter, usually flat, that folds the optical path of the display information so that it is superimposed on the forward view of the pilot. Figure 1 shows a typical configuration for a conventional HUD system.

Let us now examine how, in the context of this typical configuration, the problems of limited field-of-view and excessive CRT power arise. The latter problem is simply a matter of optical efficiency considerations. The HUD combiner must not severely attenuate the light passing through it from the windscreen. Therefore, the reflectivity of the

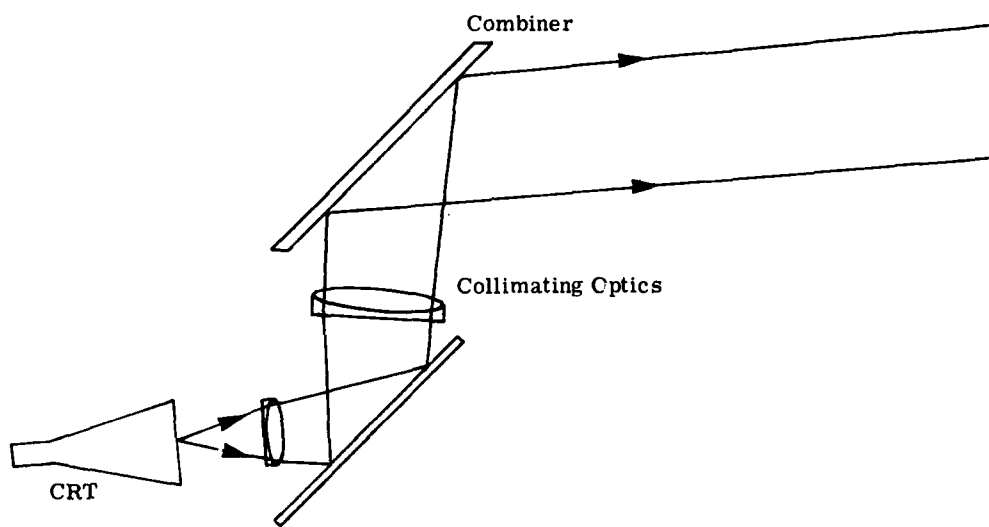
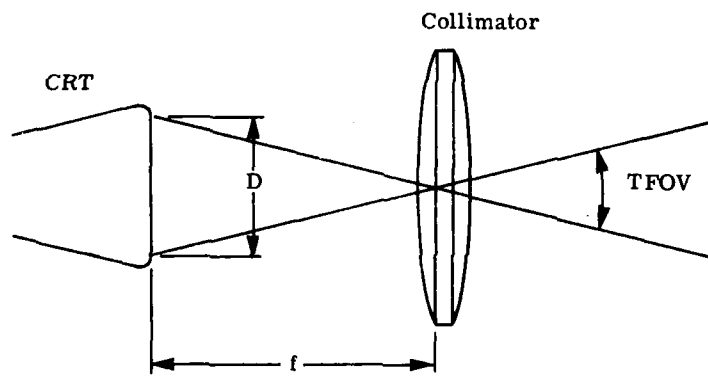


Figure 1. Typical configuration of a conventional HUD.

combiner must be low if it has broad spectral characteristics, or conversely, if the reflectivity is high, it must be high over a very limited spectral range. Since fabrication of a narrow-band combiner is difficult because of the large field-of-view that must be accommodated, typical HUD combiners have broadband reflective coatings with a reflectivity of 20 to 30% in order to transmit 70 to 80% of the light that passes through the windscreen. The combiner is very lossy with respect to the display information, therefore, and the losses are compensated by driving the CRT at high power levels that shorten its lifetime. A holographic combiner can make more efficient use of the display light by having a high reflectivity over a narrow spectral range that corresponds to the CRT peak spectral output. The reflectivity of the holographic combiner must, of course, be high over a relatively large range of angles of incidence.

The total field-of-view (TFOV) of the HUD system is determined by the focal length of the collimator and the diameter of the CRT, as shown in Figure 2. The field-of-view seen by the pilot from a given head position is generally less than the TFOV, and will be referred to as the instantaneous field-of-view (IFOV). Figure 3 shows the geometry that determines the IFOV; note that the system is unfolded and that the combiner is not shown. In a conventional system, the combiner has no optical power and does not affect the field-of-view (unless in a restrictive sense as a limiting aperture). Cockpit design considerations dictate a large eye relief  $R$  (here the distance from the collimator to the pilot's eye) while weight and space considerations dictate a small collimator size. In a typical conventional HUD optical system, the difference between the IFOV and TFOV may be as large as a factor of two; to



$$\text{TFOV} = 2 \tan^{-1} \left( \frac{0.5D}{f} \right)$$

Figure 2. Total field-of-view (TFOV) of a HUD optical system.



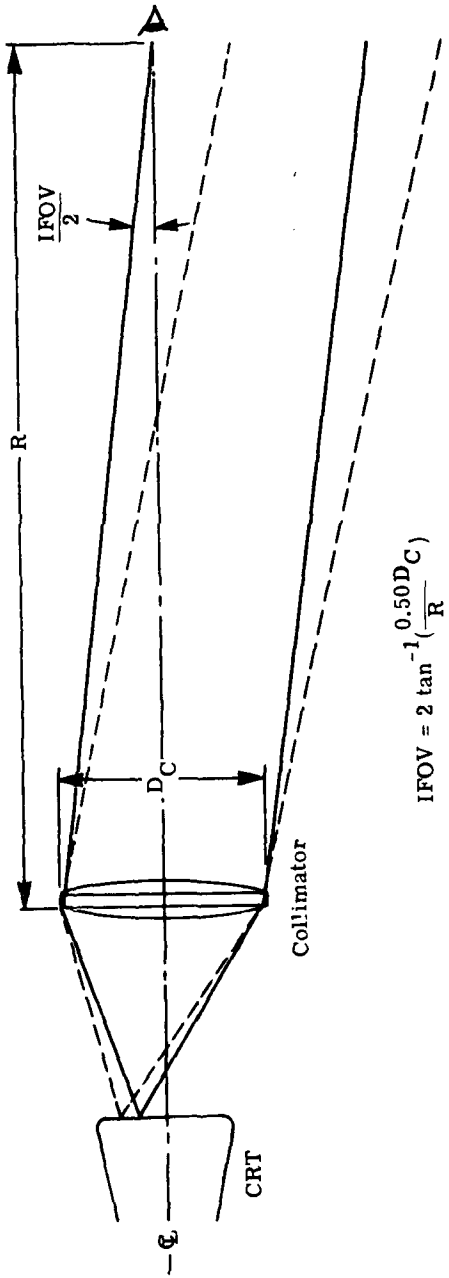


Figure 3. Instantaneous field-of-view (IFOV) of a HUD optical system. The dashed lines indicate light rays outside the IFOV.

see the entire field-of-view, the pilot must move his head. (For a more complete discussion of the field-of-view of HUD optical systems, see Ref. 1). If a holographic lens is substituted for the combiner, the eye relief is reduced by the previous collimator-combiner separation, and with the holographic lens forming the collimator as well as the combiner, the collimator diameter can be increased. Thus a holographic combiner/collimator will increase the IFOV, possibly making it equal to the TFOV.

The investigation of the holographic combiner divided into two major phases that concentrated separately on the efficiency and field-of-view considerations. Under the first phase we designed and fabricated a holographic combiner to fit, as a one-for-one replacement, into the optical system of the F-4 HUD. Because the holographic combiner was to fit into an existing optical system without otherwise modifying the optics, it did not have optical power. It nevertheless demonstrates the feasibility of fabricating high quality holographic optics and is useful in evaluating the performance of a holographic combiner in terms of efficiency. The second phase of the investigation was an analytical effort to determine the performance improvements that could be realized by replacing the combiner in an A-10 HUD with a holographic combiner that has optical power and a curved substrate, with the optical system constrained only to fit within its space in the existing system. The focus of the second phase was on field-of-view improvement, although some discussion is given to certain practical considerations.

## SECTION II DESIGN OF A FLAT HOLOGRAPHIC COMBINER

The objective of this phase of the investigation was to design a flat holographic combiner that could be substituted on a one-for-one replacement basis into an existing HUD optical system as shown in Figure 4. The system chosen was the F-4 HUD, which has a TFOV of approximately  $14^\circ$  and an IFOV (at the design eye) of approximately  $8^\circ$ . The major task here was the development of techniques to form a volume phase reflection hologram having high diffraction efficiency over the  $14^\circ$  TFOV. This effort is discussed in two sections that separately describe the design analyses and the laboratory investigations. In the design analysis we investigated the field-of-view requirements of the holographic combiner and generated the design parameters for fabrication of the element.

### 1. FIELD-OF-VIEW

By field-of-view of the holographic combiner, we are actually referring to the angular bandwidth over which rays are diffracted (or reflected) with high efficiency. This is an important consideration because the requirement for high reflectivity over a narrow spectral band calls for a volume phase type of hologram (see Reference [2] for a discussion of holographic optics and materials). The Bragg effects that are responsible for the high efficiency also limit the angular bandwidth of a volume phase hologram. A typical reflection hologram in a material such as dichromated gelatin might be  $15 \mu\text{m}$  thick and 95% efficient at the Bragg angle. The angular bandwidth of this hologram at the half

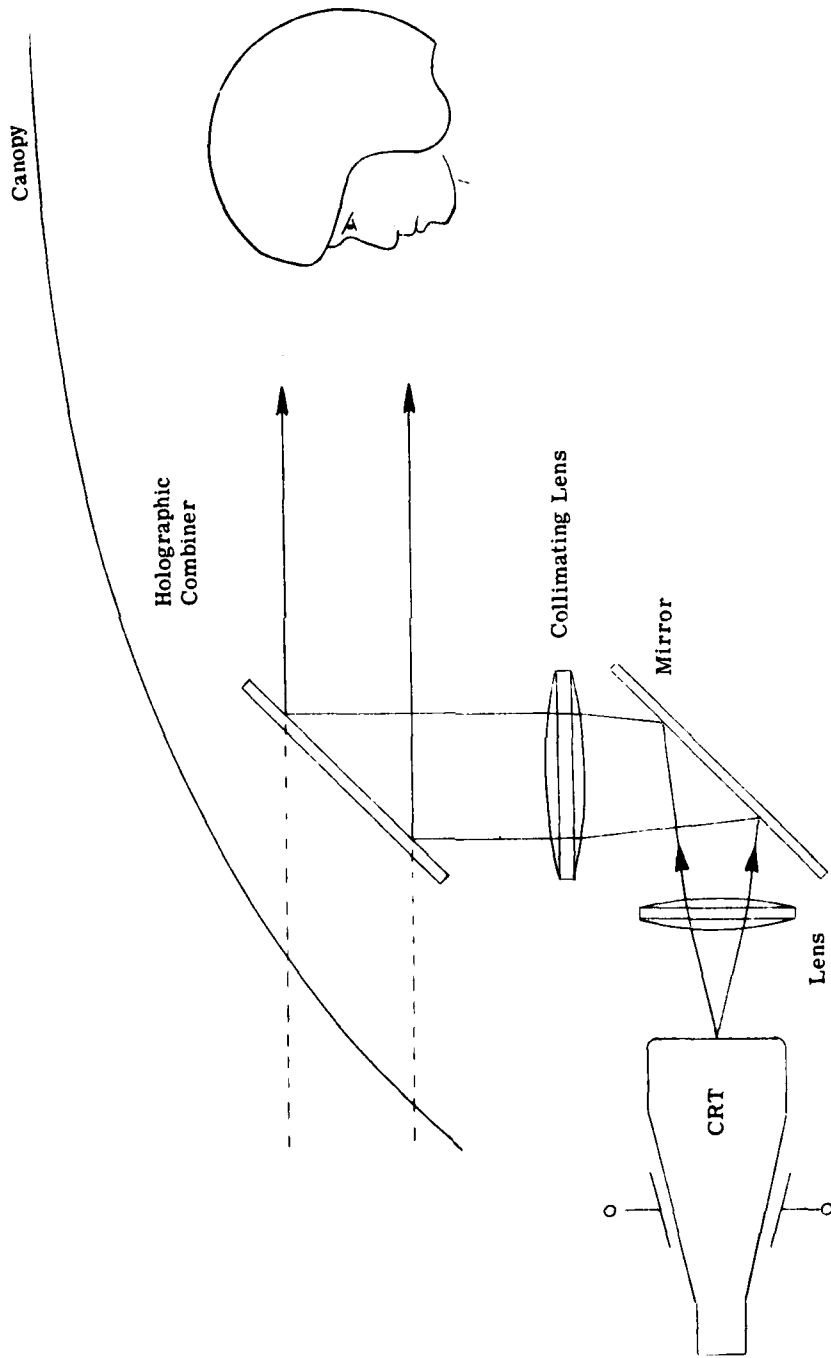


Figure 4. Head-up display with a holographic combiner.

power points would be  $5^\circ$ ; far below our goal of  $14^\circ$ . A curve of diffracted intensity as a function of angle is shown in Figure 5. We generated this curve by simulating a volume phase reflection hologram with our ray tracing programs; the hologram was assumed to be constructed with two plane waves incident from opposite sides of the hologram plate, with the plate bisecting the angle between the beams. With this configuration, the fringe planes are parallel to the hologram surface. The efficiency of a volume phase hologram is strongly dependent on the hologram thickness and on the amount by which the refractive index is modulated. For a  $15 \mu\text{m}$  hologram thickness, the index modulation necessary for a peak diffraction efficiency of 95% is 0.021.

It is well known in holographic research that the angular bandwidth of a volume phase hologram varies inversely with its thickness [2,3]. We can increase the angular bandwidth of our reflection hologram, therefore, by reducing its thickness from  $15 \mu\text{m}$  to  $6 \mu\text{m}$ , but unless we compensate for the reduced hologram thickness by increasing the index modulation, the diffraction efficiency will decrease. At the Bragg angle, the diffraction efficiency of a volume phase reflection hologram is given by [3]

$$\eta = \tanh^2 \left( \frac{\pi n_1 T}{\lambda \cos \theta} \right) \quad (1)$$

where

- $\eta$  = diffraction efficiency
- $n_1$  = refractive index modulation
- $T$  = hologram thickness
- $\lambda$  = reconstruction wavelength
- $\theta$  = angle between reconstruction ray and the normal to the hologram fringes

# EFFICIENCY VS. BRAGG DEVIATION

$T = 15, N1 = 0.021$

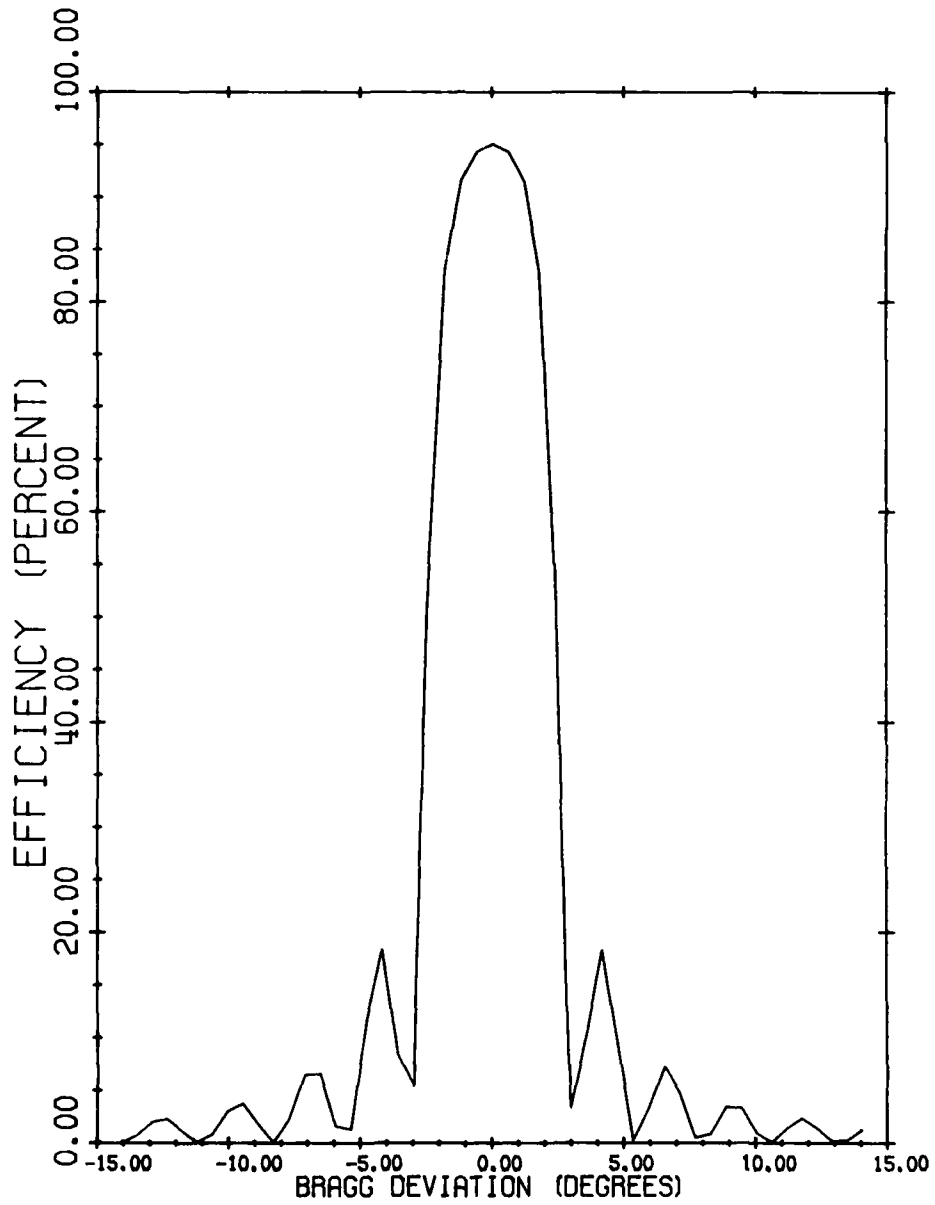


Figure 5. Predicted angular bandwidth of a reflection hologram with a thickness of  $15\mu\text{m}$  and a refractive index modulation of 0.021.

If we keep the product of  $n_1$  and  $T$  constant, reducing the thickness to  $6 \mu\text{m}$  requires an increase in the index modulation from 0.021 to 0.0525 to keep the peak diffraction efficiency at 95%. In this case, the angular bandwidth increases from  $5^\circ$  to  $12^\circ$ , as can be seen in the curve shown in Figure 6.

Finally let us consider increasing the refractive index modulation to 0.525 without decreasing the hologram thickness. Reflection holograms have the interesting property that once all of the light has been diffracted into the signal beam, the light emerges from the hologram and is not further affected, whereas in a transmission hologram, the light can couple back and forth between the reconstruction and signal beams as it passes through the hologram. Increasing the index modulation of a volume phase reflection hologram reduces the effective hologram thickness, in that most of the light only travels a short distance into the hologram before it is reflected back out. Furthermore, the rays near the Bragg angle are diffracted with very high efficiency, with predicted ray efficiencies as high as 99.994%. The overall effect is for the angular bandwidth curve to take on a hard clipped appearance, with greater sidelobe structure, as shown in Figure 7. The bandwidth of the central peak here is  $10^\circ$ , but if the sidelobe structure is smoothed, the bandwidth is approximately  $12^\circ$ , as it was with the  $6 \mu\text{m}$  hologram thickness.

It is interesting to observe the expected spectral bandwidth corresponding to the three holograms we have just discussed. For the first, the index modulation is 0.021 and the thickness  $15 \mu\text{m}$ , a rather typical volume phase reflection hologram. Figure 8 shows the predicted spectral bandwidth of this hologram; in this case the hologram is

# EFFICIENCY VS. BRAGG DEVIATION

$T = 6, N1 = 0.0525$

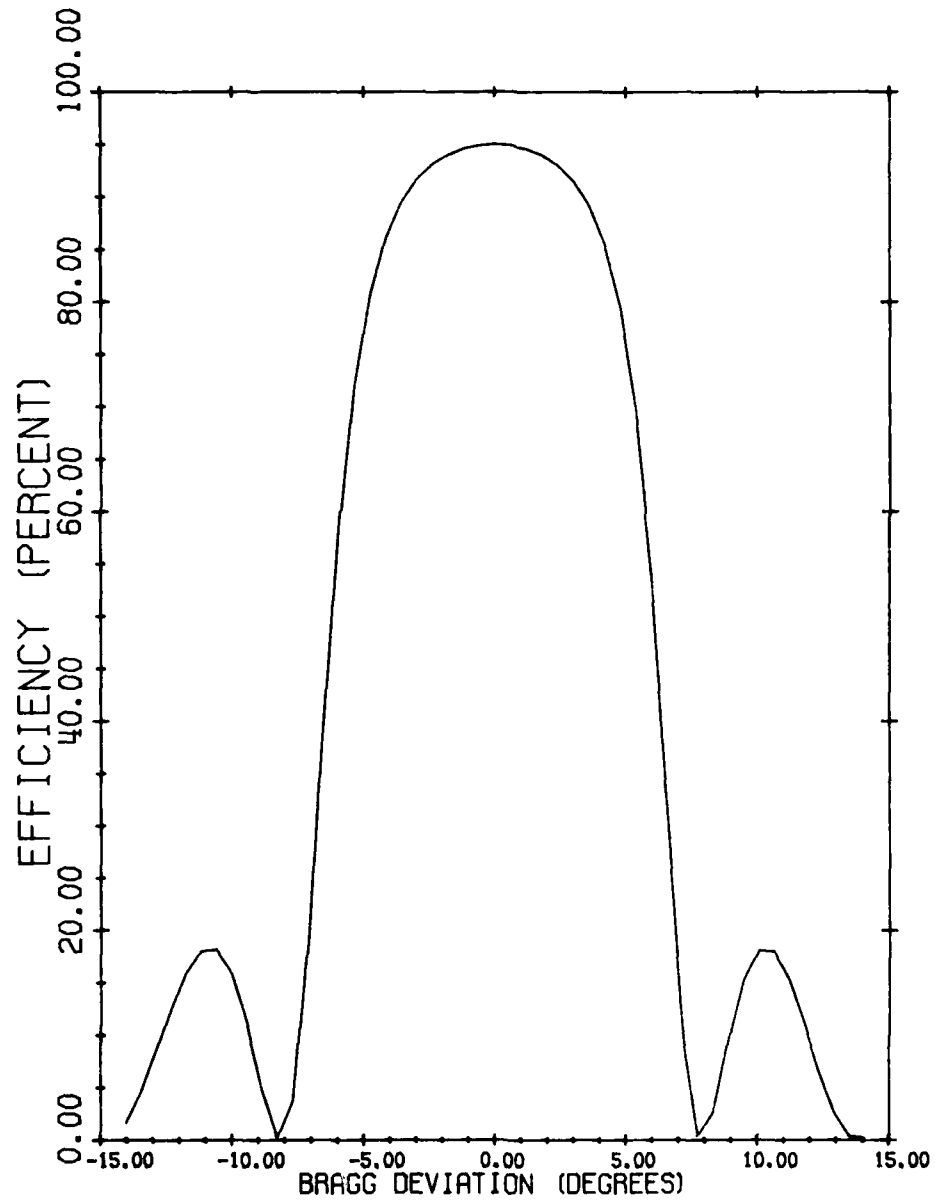


Figure 6. Predicted angular bandwidth of a reflection hologram with a thickness of  $6 \mu\text{m}$  and a refractive index modulation of 0.0525.



# EFFICIENCY VS. BRAGG DEVIATION

$T = 15, N1 = .0525$

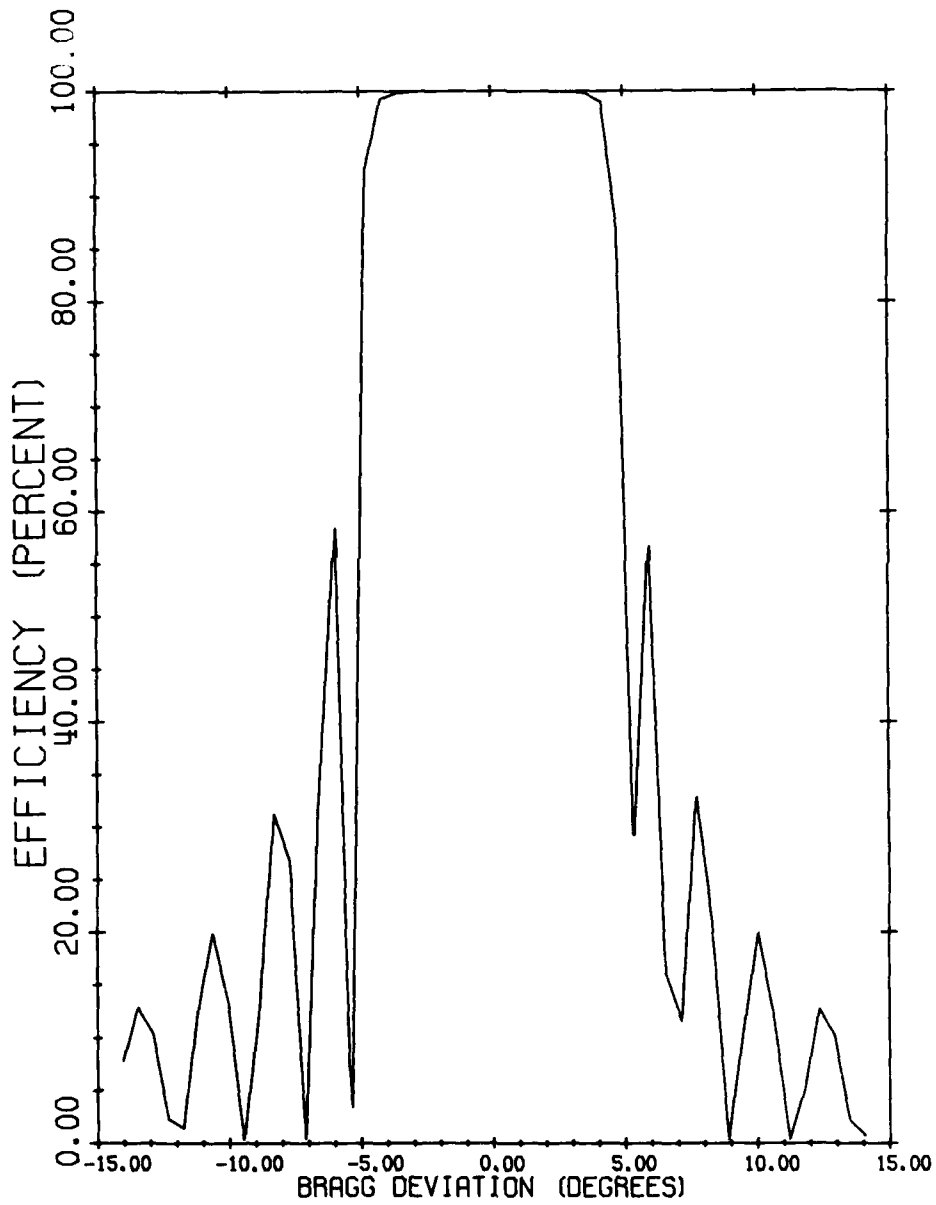


Figure 7. Predicted angular bandwidth of a reflection hologram with a thickness of 15  $\mu$ m and a refractive index modulation of 0.0525.

# EFFICIENCY VS. WAVELENGTH

$T = 15, N1 = 0.021$

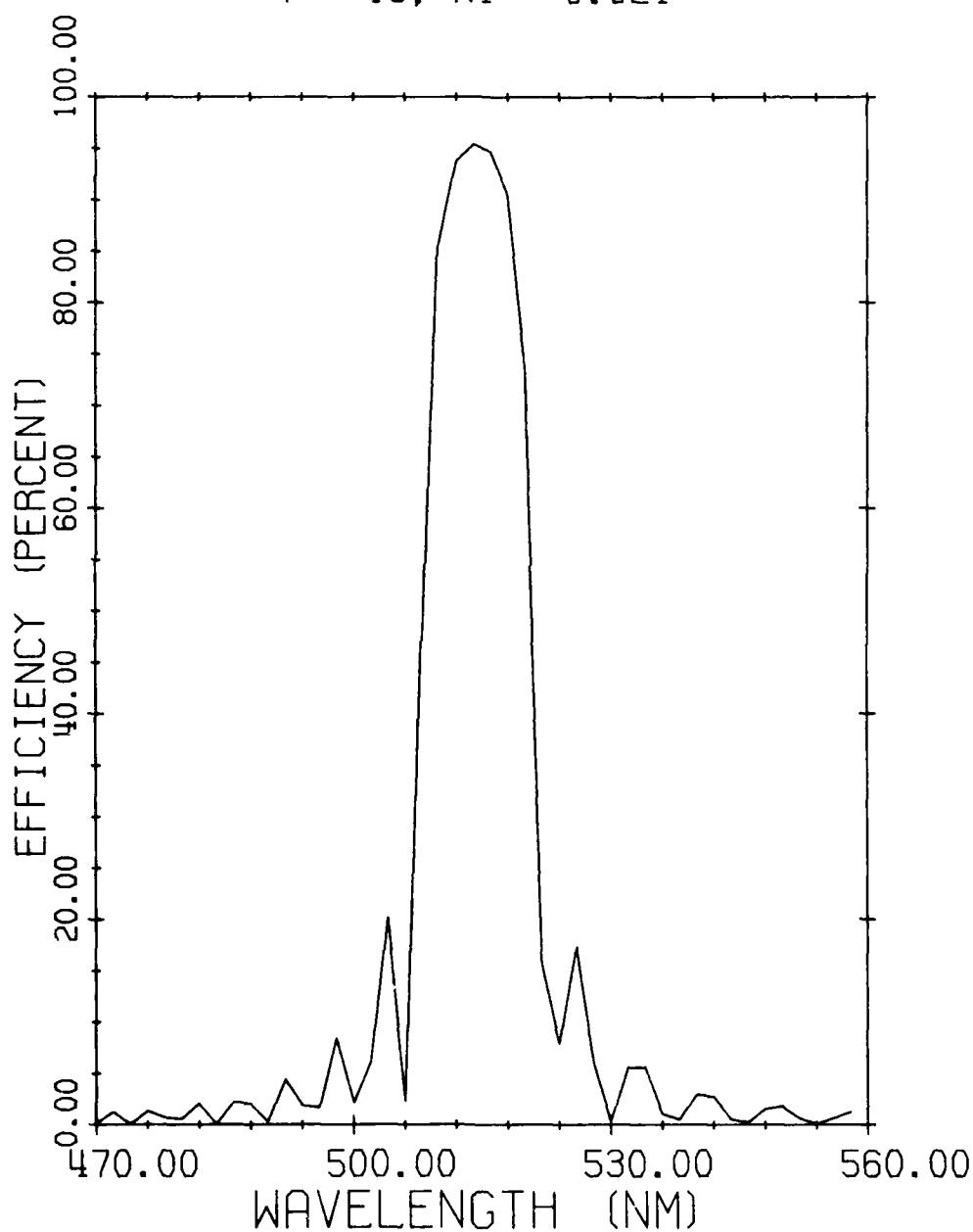


Figure 8. Predicted spectral bandwidth of a reflection hologram with a thickness of  $15 \mu\text{m}$  and a refractive modulation index of 0.021.

reconstructed at the angle corresponding to the central angle in Figures 5-7, and the reconstruction wavelength varied. The bandwidth is 13 nm at the half power points (50% diffraction efficiency). Figure 9 shows the spectral bandwidth of a hologram 6  $\mu\text{m}$  thick with an index modulation of 0.0525; the bandwidth here is slightly over 17 nm. Assuming a hologram thickness of 15  $\mu\text{m}$  and index modulation of 0.0525 produces a spectral bandwidth curve that appears similar to the angular bandwidth curve. Figure 10 shows the spectral bandwidth for this case; at the half power points, the central peak has a width of 27 nm, with the sidelobe structure tending to increase the bandwidth somewhat further.

An alternate method of increasing the angular bandwidth of the hologram is to record two hologram gratings in the gelatin layer, with the angle between the recording beams shifted slightly between exposures. This technique records two holograms, each of which has its own angular bandwidth but with an offset between them to give a broader composite bandwidth. The approach is especially well suited to the special case where each hologram comprises a set of fringes parallel to the hologram surface; because such holograms behave as plane mirrors, there will be no likelihood of a double image forming where the bandwidth curves of the individual gratings overlap. Unfortunately, we are unable to simulate a multiple-grating reflection hologram, and therefore cannot show predicted angular bandwidth curves. Nevertheless, we demonstrated the technique experimentally as is discussed in Section III.

## 2. FLAT COMBINER DESIGN

In this section we discuss the design considerations for the flat holographic combiner that we ultimately fabri-

# EFFICIENCY VS. WAVELENGTH

$T = 6, N1 = 0.0525$

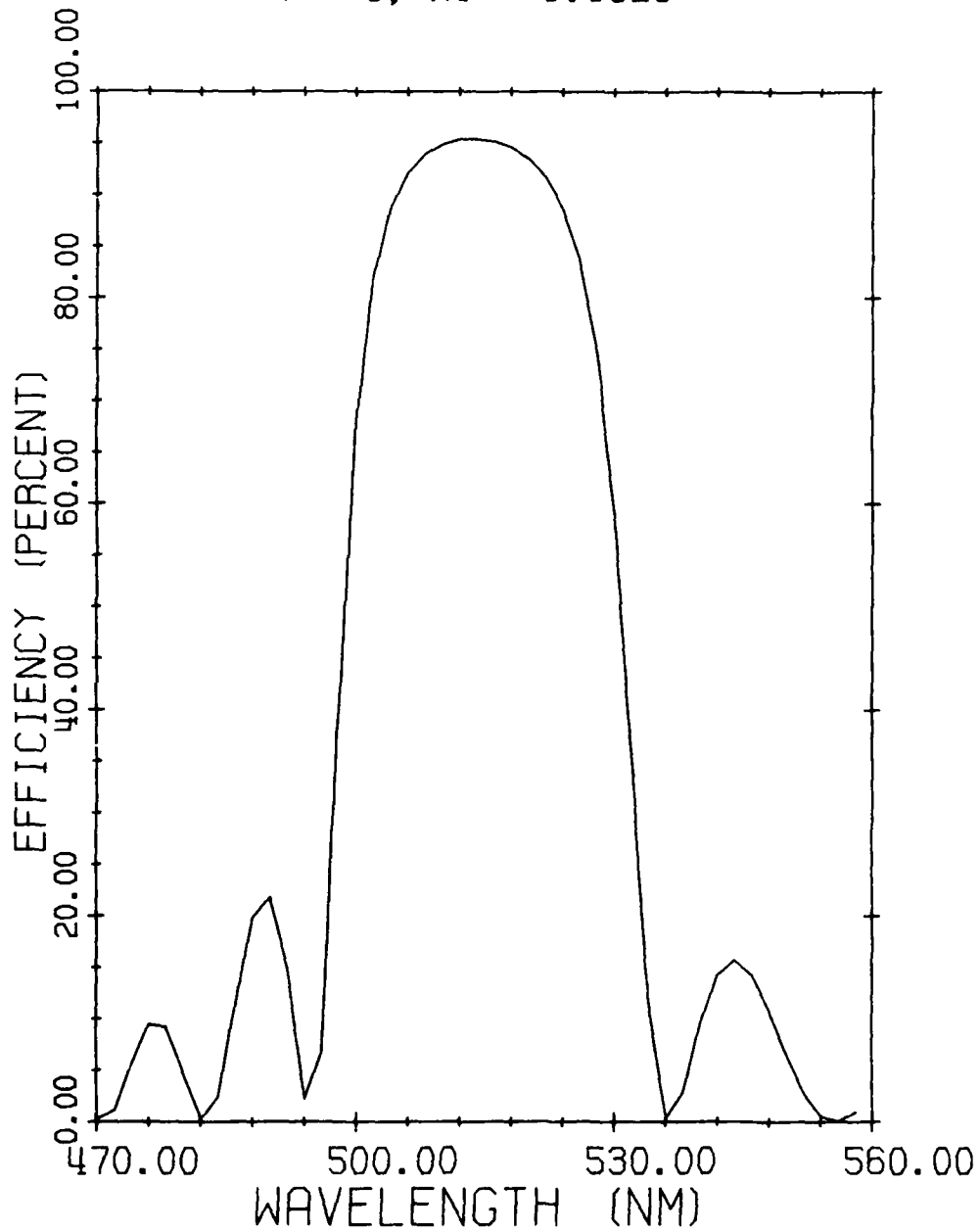


Figure 9. Predicted spectral bandwidth of a reflection hologram with a thickness of  $6 \mu\text{m}$  and a refractive index modulation of 0.0525.

# EFFICIENCY VS. WAVELENGTH

$T = 15, N1 = .0525$

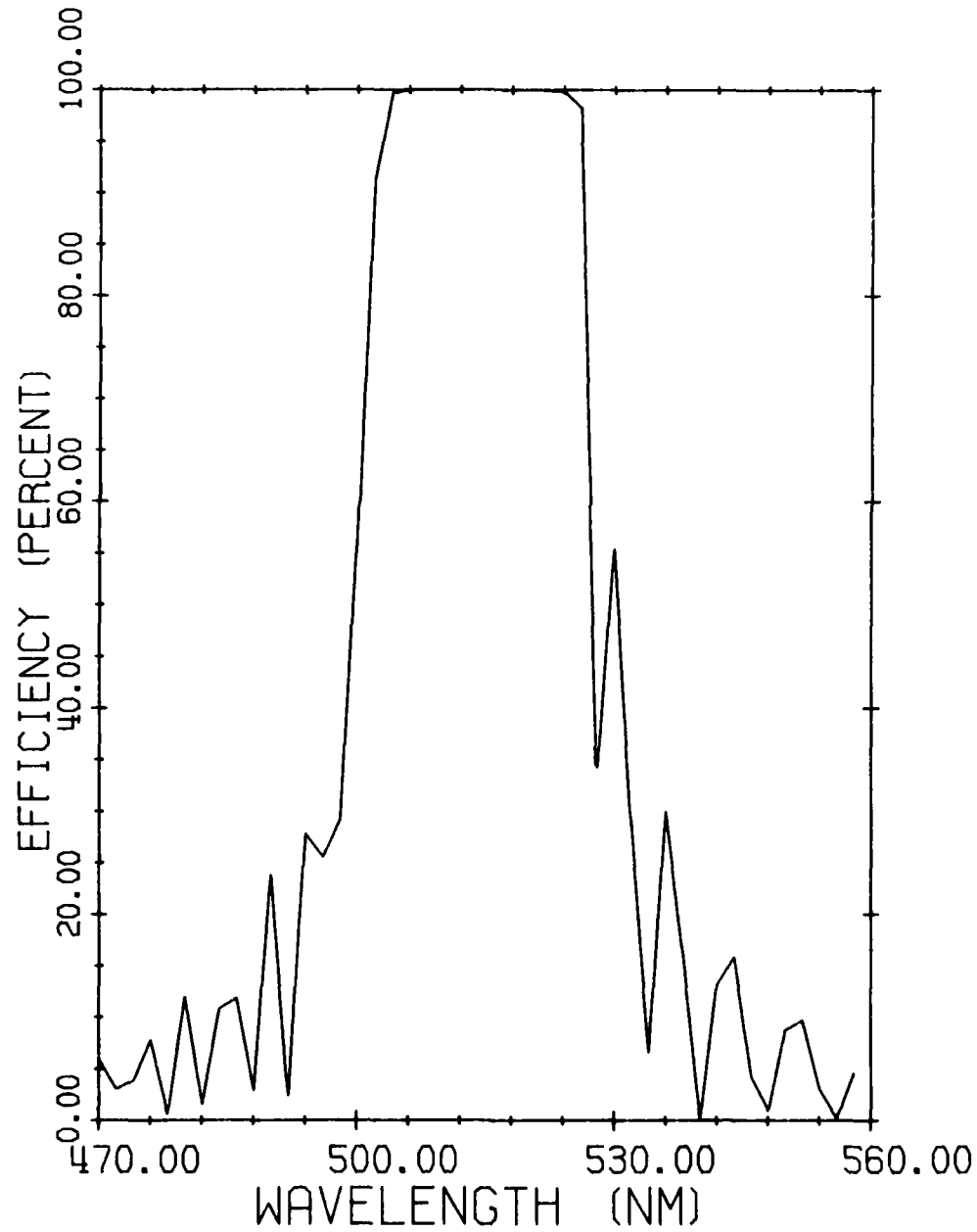


Figure 10. Predicted spectral bandwidth of a reflection hologram with a thickness of  $15 \mu\text{m}$  and a refractive index of 0.0525.

cated and tested. The parameters of major importance are the TFOV of the system and the spectral characteristics of the CRT input. For the F-4, the TFOV is  $14^{\circ}$ , and the CRT phosphor is Type PX58 with a peak at approximately 515 nm and a bandwidth of nearly 100 nm. The primary design constraint is that the holographic combiner replace the conventional combiner of the F-4 HUD on a one-for-one basis, without further changes to the optical train. This constraint implies that the holographic combiner must have no optical power since the conventional combiner is a flat mirror. Furthermore, if the combiner angle is to be unchanged, then the holographic combiner must appear very similar to a flat conventional mirror. The requirement that the holographic combiner replace an existing combiner thus dictates that the holographic combiner must have no optical power, and for high efficiency along the optic axis, that the fringe planes must be parallel to the hologram surface. Although the combiner does not take advantage of all the capabilities of a holographic optical element, it does offer certain other advantages for an optical system with broadband illumination and it simplifies the fabrication process.

A holographic element with fringes parallel to the hologram surface has no optical power and behaves simply as a plane mirror, with all ray directions determined by classical laws of reflection. Thus, (assuming reasonable flatness), no dispersion or aberration is introduced by the holographic combiner, regardless of the bandwidth of the illumination source. The holographic nature of the element will be evident in consideration of the efficiency with which rays are reflected, as the efficiency is a function of the wavelength, incident angle, fringe spacing, and refractive index modulation.

Not only does this method minimize aberrations and eliminate dispersion, but it provides a simple method of fabricating the hologram. To form fringes that are parallel to the hologram surface, we illuminate the hologram with plane waves from either side, making equal but opposite angles with the surface normal as shown in Figure 11a. An optical configuration capable of forming such a hologram is shown in Figure 11b; because of the interferometric nature of the optical system, a high degree of physical stability is required of all elements from the beamsplitter to the hologram plate during the course of the hologram exposure (usually several seconds to several minutes). Although the required stability can be achieved reliably, it requires careful work and high quality optical components. A simpler method of forming fringes parallel to the hologram surface is shown in Figure 12. A single plane wave illuminates the hologram; a portion of the illumination is transmitted through the recording medium, and reflected by a mirror clamped to the back side of the hologram substrate. Not only is the optical system greatly simplified, but since the entire interferometer is formed by the hologram-mirror combination, the only stability requirements are on that combination.

Let us consider briefly how such a hologram is designed to achieve efficient reconstruction at a given wavelength and angle. Efficient reconstruction will occur at or near the Bragg angle, which is given by the Bragg relation.

$$2d \sin \theta = \lambda \quad (2)$$

where  $d$  is the fringe spacing,  $\theta$  is the angle between the reconstruction ray and the fringe plane, and  $\lambda$  is the re-

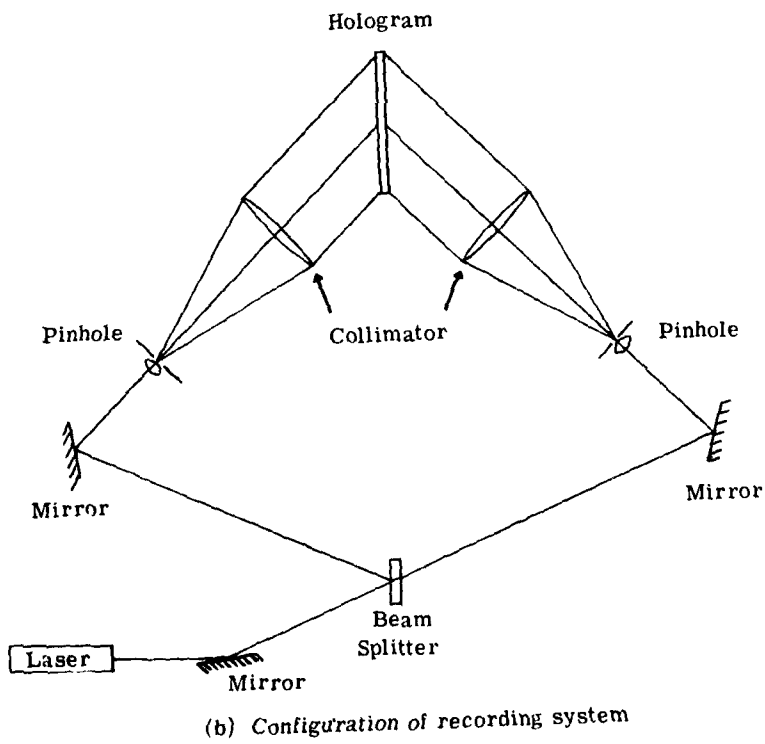
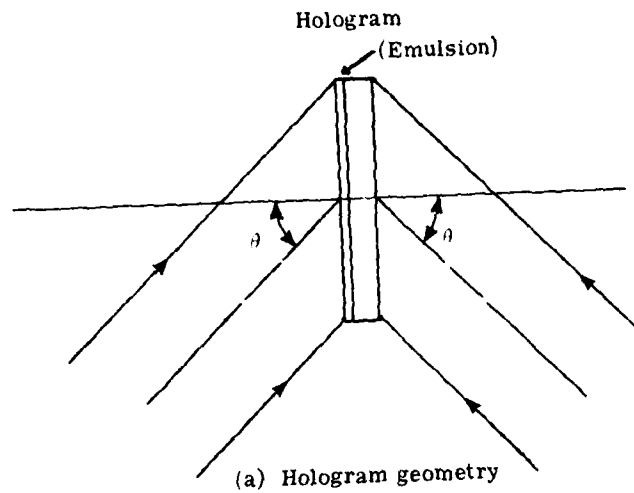


Figure 11. Recording a reflection hologram with fringes parallel to the surface.



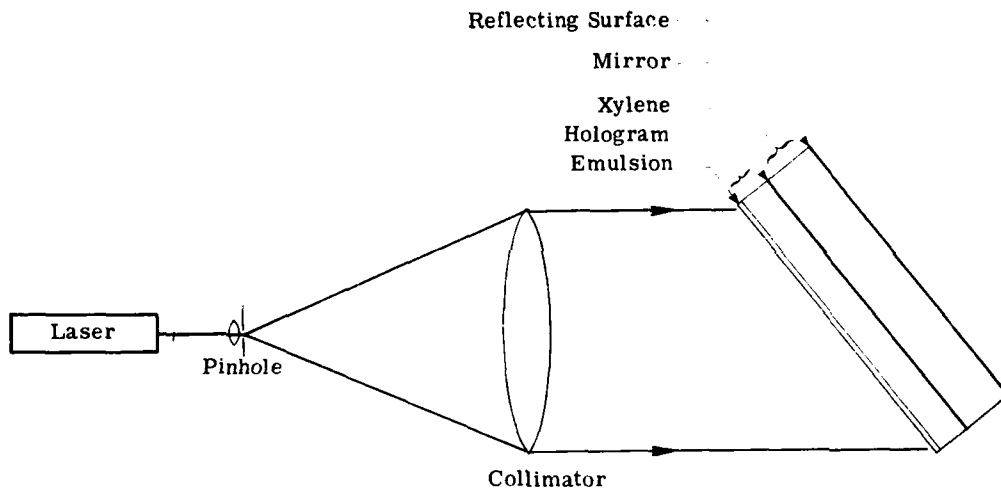


Figure 12. Single-beam recording technique for a reflection hologram with fringes parallel to the surface.

construction wavelength. Choosing the reconstruction wavelength and angle will determine the required fringe spacing. For construction of the hologram, we must choose an appropriate laser wavelength  $\lambda_0$  (we generally use 514 nm for dichromated gelatin). Given  $d$  and  $\lambda_0$ , we can find  $\theta$ ; this, and the constraint that the fringes must be parallel to the hologram surface determine the angles that the recording beams must make with the hologram.

A final point that must be considered in determining the design parameters of a volume reflection hologram is the possibility of a net thickness change of the hologram caused by processing. The effect of a thickness change is to cause  $d$  to be different in construction and reconstruction. In the case of a hologram with fringes parallel to the surface,  $d$  changes by the same ratio as the net thickness change of the gelatin layer.

For the F-4 HUD combiner, the construction wavelength, 514 nm, corresponds to the peak wavelength of the PX58 phosphor, so we assume no wavelength change. Although dichromated gelatin holograms often undergo a net thickness change, we were able to adjust our processing technique to minimize thickness changes (see Section III.1.e). In this case, therefore, it was unnecessary to use Eq. (2), and the design reduced to choosing the construction beam angles to correspond to the angles between the conventional combiner in the F-4 HUD and the folded optic axes,  $48.3^\circ$ . The construction parameters of the holographic combiner are given in Table 1. Figure 13 shows a sketch of the optical system with a set of rays traced through it.

Finally, let us consider once more the expected angular and spectral characteristics of the combiner. For a single grating hologram with a given thickness, the angular bandwidth is a function of the refractive index modulation. If

TABLE 1  
CONSTRUCTION PARAMETERS OF THE FLAT HOLOGRAPHIC COMBINER

Reference Beam:	Plane Wave, $\theta = 48.3^\circ$
Object Beam:	Plane wave, $\theta = -48.3^\circ$
Recording Wavelength:	514.5 nm
Size:	160 x 195 mm
Recording Material:	Dichromated Gelatin
Hologram Thickness:	15 $\mu\text{m}$ (nominal)
Substrate Thickness:	63 mm

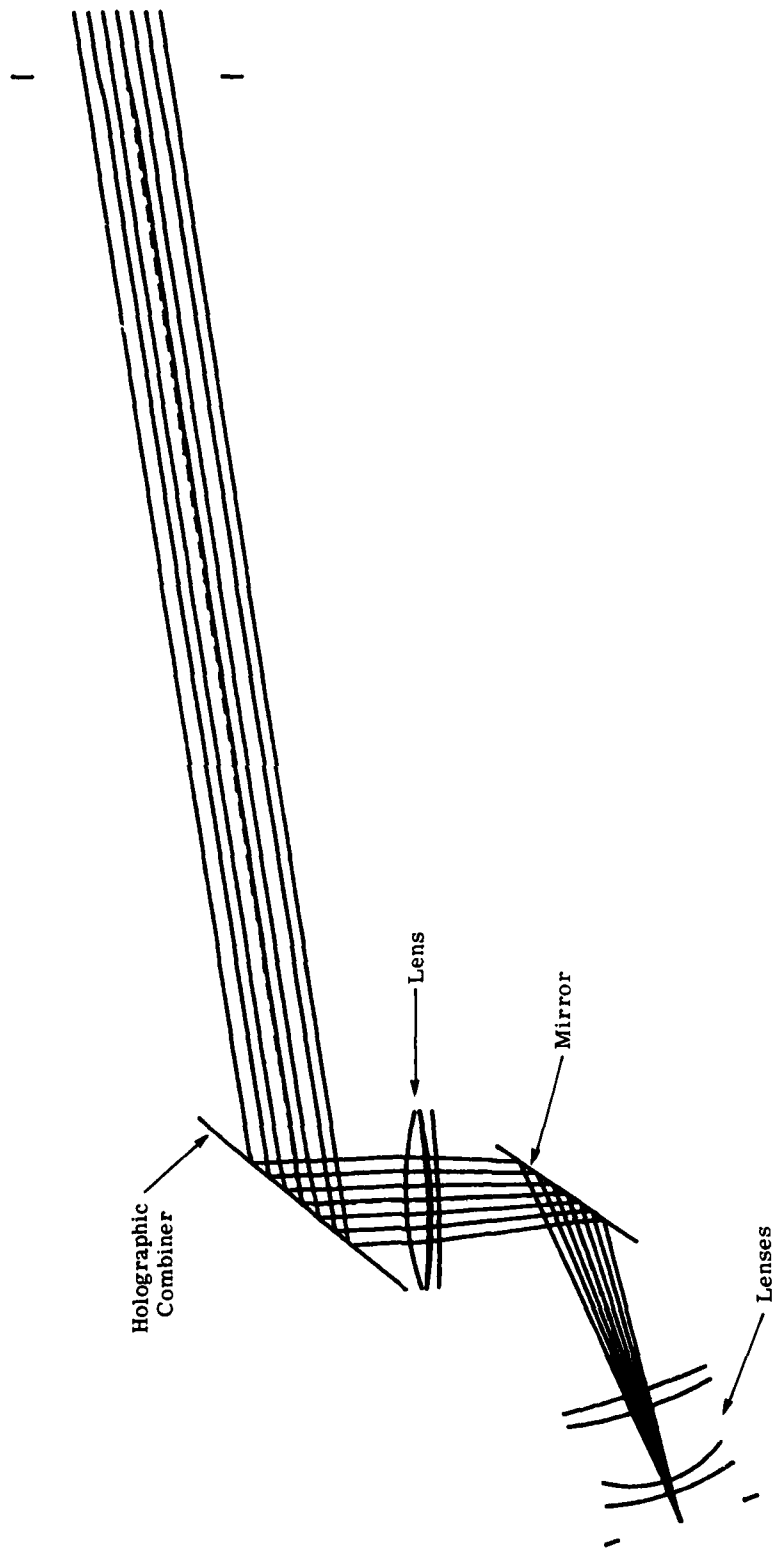


Figure 13. Raytrace through the F-4 HUD with a holographic combiner.

we examine a curve of angular bandwidth as a function of index modulation (see Figure 14), we see that for a 15  $\mu\text{m}$  thick hologram, an index modulation of 0.078 will produce an angular bandwidth of  $14^\circ$ . Although 0.078 is a large index modulation, it is not unreasonable. Alternatively, if we examine the angular bandwidth curves obtained at a lower index modulation, say 0.0525, but at the two different wavelengths corresponding to the 70% points of the phosphor output, then the bandwidth is increased from  $10^\circ$  at a single wavelength of 514 nm to  $25^\circ$  width of the overlapping bandwidths at two wavelengths, 500 nm and 540 nm.

Figure 15 shows a curve of predicted spectral bandwidth superimposed with the phosphor output characteristic. The hologram is assumed to be 15  $\mu\text{m}$  thick and have an index modulation of 0.0525.

### 3. CURVED COMBINER

We briefly investigated the use of a curved combiner in the F-4 HUD system. Because of the constraints that the combiner not add optical power to the system, the flat combiner performance is excellent, leaving little room for improvement. In fact, in our investigations, the curved combiner tended to reduce the angular bandwidth slightly, and more importantly, to introduce aberrations and dispersion that were not present with the flat combiner. Consequently, we did not pursue this approach further, and would not recommend the curved combiner without making other changes to the optical train.

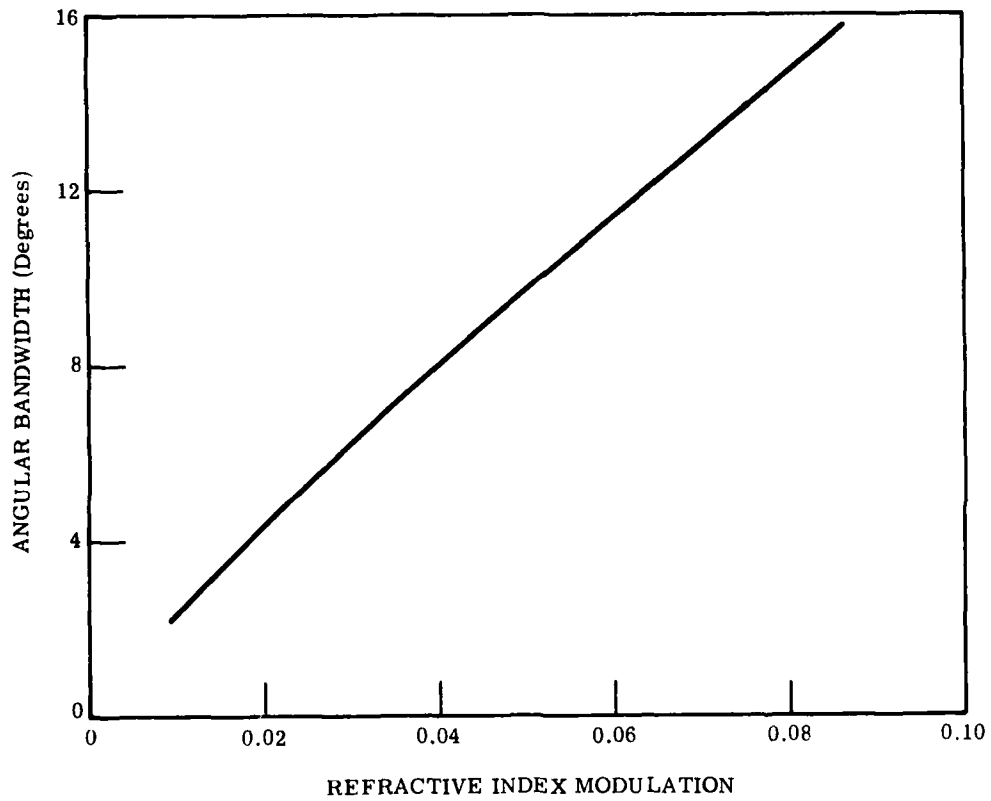


Figure 14. Angular bandwidth as a function of refractive index modulation for a volume phase reflection hologram.

# EFFICIENCY VS. WAVELENGTH

$T = 15, N1 = .0525$

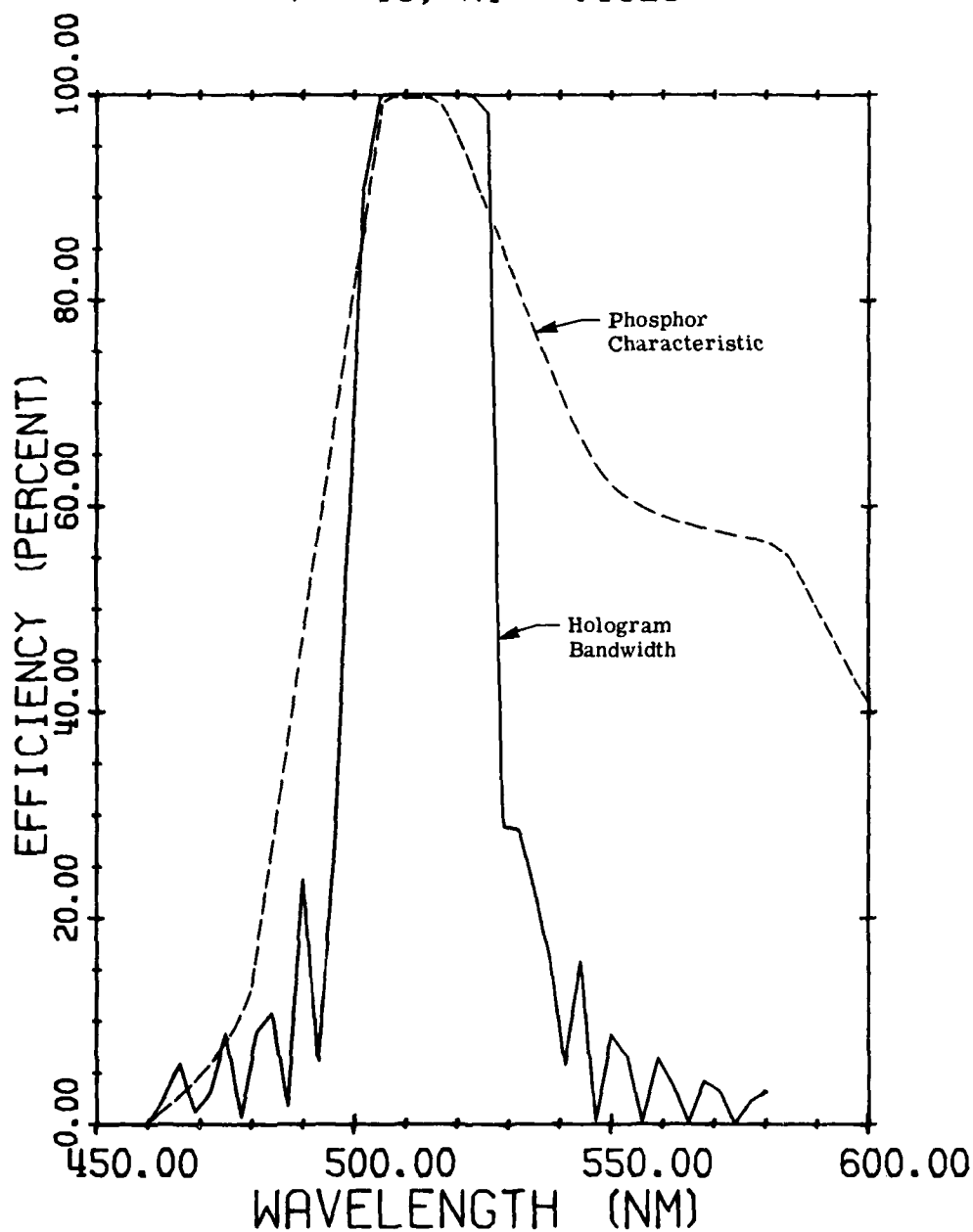


Figure 15. PX58 phosphor characteristic shown with the spectral bandwidth of a hologram with a thickness of  $15 \mu\text{m}$  and a refractive index modulation of 0.0525.

### SECTION III FABRICATION OF A FLAT HOLOGRAPHIC COMBINER

Successful fabrication of high quality holographic combiners required a thorough understanding of the properties of the recording material. Furthermore, the goal of a large angular bandwidth required a certain amount of technique development. The experimental effort therefore divided into two parts: a basic materials investigation concentrating on diffraction efficiency, angular and spectral bandwidth, and hologram thickness changes; and the fabrication of the actual combiners.

#### 1. BASIC MATERIAL INVESTIGATIONS

Since we had determined that the optimum recording configuration for the combiner fabrication was the single beam system shown in Figure 12, all of our materials investigations were carried out with holograms that were recorded in this manner. We used dichromated gelatin exclusively as the recording material, as it is unsurpassed in forming high quality reflection holograms. In this section, we describe this unique material, and the properties of reflection holograms recorded in it.

##### a. DICHROMATED GELATIN

Dichromated gelatin is attractive because it has a large modulation capacity, high S/N ratio, moderate exposure sensitivity, and excellent response to high spatial frequencies [4-9]. With a cover plate or in a dry atmosphere, dichromated gelatin holograms exhibit good environmental stability [5, 7]. In addition, dichromated gelatin holograms can be reprocessed as many times as necessary to produce a desired refractive index modulation [10,11]. Furthermore, unlike many recording materials, the component that absorbs light



during the exposure of dichromated gelatin is removed during subsequent processing, leaving a colorless gelatin material. The absorption on readout is therefore negligible.

The mechanism of hologram formation in dichromated gelatin, hypothesized by Curran and Shankoff [ 8 ], appears to be layering of gelatin by the formation of cracks along fringe planes. Although not entirely satisfying to all, this hypothesis does account for the large refractive index modulation. Briefly, the mechanism is as follows. The gelatin is sensitized with ammonium dichromate prior to exposure; exposure to light in the UV or blue-green region of the spectrum causes the gelatin to harden. The gelatin layer is subsequently washed, removing the sensitizer chemicals, and causing the gelatin to swell with the absorption of water. Rapid dehydration follows by immersing the gelatin in isopropyl alcohol, and the emulsion shrinks back to approximately its original thickness. The sudden shrinkage creates between the exposed (or hardened) regions and the unexposed (or unhardened) regions stresses that crack the gelatin along the fringe planes.

The method of processing dichromated gelatin as described above is simple and straightforward, but it does not always produce high quality results. Certain precautions must be observed to prevent the formation of a certain amount of opacity on the gelatin surface. Our previous experimental investigations of dichromated gelatin holograms revealed that the saturation refractive index modulation, as well as the thickness of the processed hologram, is greatly affected by the processing environment, especially the relative humidity and temperature in the processing room [7, 11 - 13]. Carefully controlling the processing environment in those investigations, we examined the exposure characteristics of dichromated

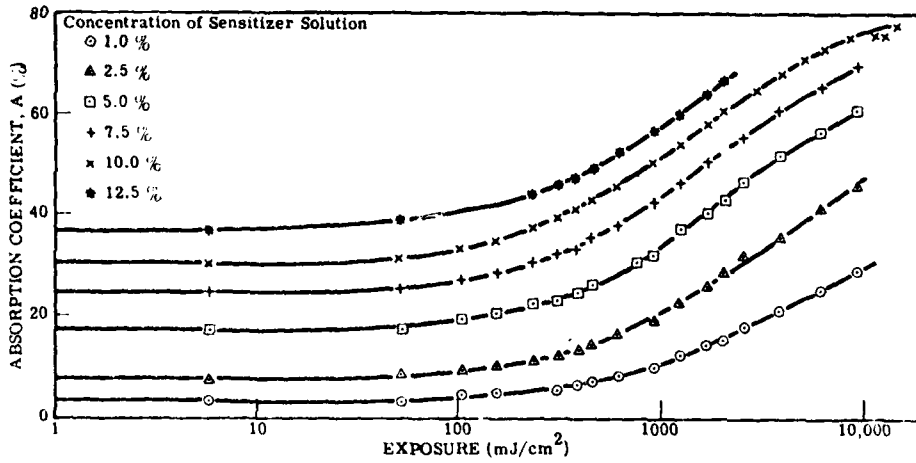
gelatin holograms as a function of various parameters, including sensitizer concentration, prehardening before sensitization, recording beam intensity, lag-time between sensitization and development, spatial frequency and recording beam ratio [11,12]. To analyze the data, we developed a model that expresses refractive index modulation as a function of exposure. This model incorporates the measured absorption coefficients of dichromated gelatin, which we found to increase with exposure, as shown by the curves in Figure 16.

Although those investigations were restricted to transmission holograms, we expect that most of the exposure characteristics can also be applied to reflection holograms. Our current materials research, therefore, concentrated on improving the angular bandwidth of reflection holograms recorded in dichromated gelatin films by varying the sensitizer concentration. We also investigated the diffraction efficiency, spectral bandwidth, and thickness change of dichromated gelatin reflection holograms.

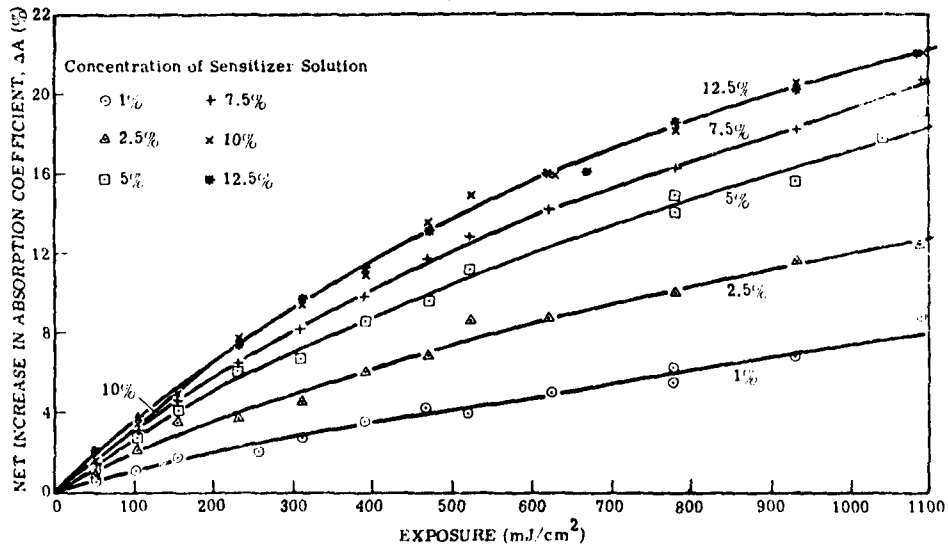
In Figure 17, we show in detail the single-beam recording geometry of reflection holograms. Because of this unique recording method and the dynamic absorption characteristic of dichromated gelatin (Figure 16), we refer to the incident exposure  $E_i$  defined as

$$E_i = (I_{it} \cos \theta_i) t \text{ mJ/cm}^2, \quad (3)$$

where  $I_{it}$  is the intensity of the recording beam transmitted to the dichromated gelatin film,  $\theta_i$  is the angle of incidence, and  $t$  is the exposure time. The actual exposure of the recording material is then approximately equal to  $2E_i$ .



(a) Absorption at several sensitizer concentrations



(b) Change in absorption coefficient with exposure

Figure 16. Absorption of dichromated gelatin as a function of exposure.

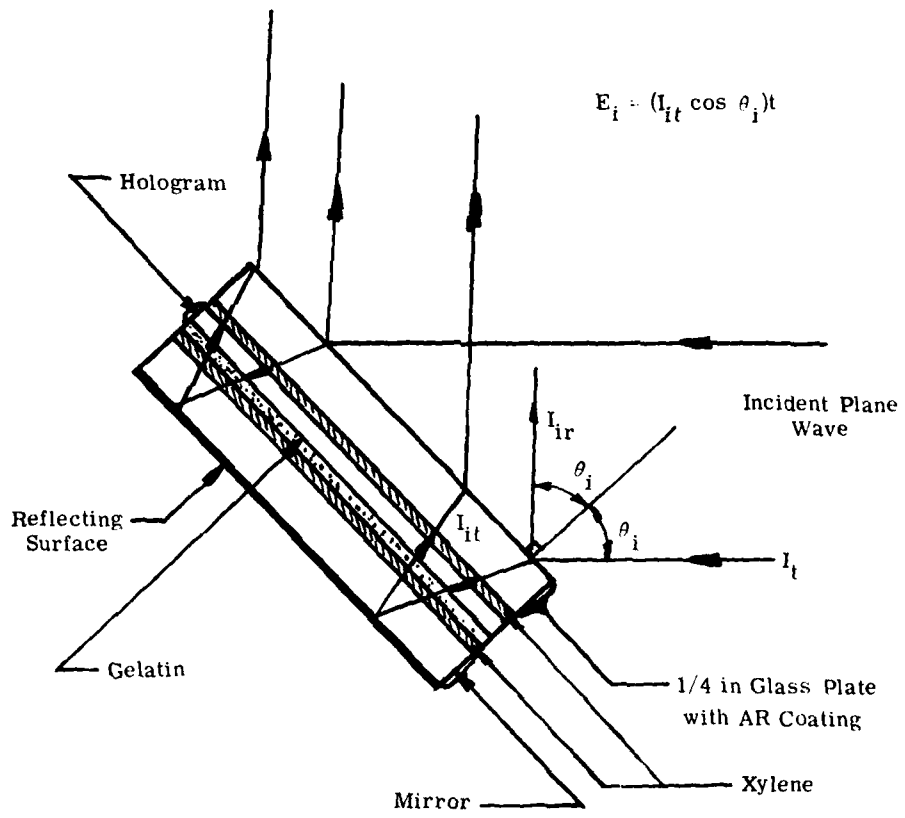


Figure 17. Detail of single-beam recording configuration.

Diffraction efficiency throughout this report is defined as the ratio of the diffracted intensity to the intensity of the incident readout beam, and the Bragg-angle deviation is the angle measured with respect to the original position of the recording beam.

In all of our investigations as well as the combiner fabrication, we used dichromated gelatin plates that were derived from Kodak 649F spectrographic plates. Our standard technique for the preparation of dichromated gelatin plates from Kodak 649F plates is outlined in Table 2, and our standard development procedure of exposed plates is outlined in Table 3. These processing techniques are similar to those of Chang [ 9 ]. Examples of chemical mixing formulas are shown in Table 4. The processing environment for the current work was under constant control; the relative humidity and temperature were 29 to 35% and 75 to 85°F, respectively. Finally we note that except for spectral bandwidth measurements, all holograms were recorded and measured at a wavelength of 514 nm.

#### b. DIFFRACTION EFFICIENCY

We determined the diffraction efficiency of single-grating holograms as a function of exposure at several sensitizer concentrations. The angle of incidence,  $\theta_i$  was 48° (see Figure 17). As shown in Figure 18, the diffraction efficiency curve obtained with a 3% sensitizer is similar to that of a 5% sensitizer. These results show that lowering the sensitizer concentration from 5% to 3% does not reduce the exposure sensitivity of dichromated gelatin; this is due to our unique recording system employing one beam and a mirror, and to the absorption characteristics of dichromated gelatin (Figure 16).

TABLE 2  
PREPARATION OF DICHROMATED GELATIN PLATES

All chemicals are dissolved in distilled water and, except where noted, all steps are at a temperature of 68°F.

Lighting: Room Light

<u>STEP</u>	<u>DIRECTION</u>
P-1*	Soak in fixer without hardener for 10 minutes.
P-2	Wash in running water at 90°F for 5 minutes; start at 68°F and raise temperature 2.5°F/min to 90°F; following wash, lower temperature at same rate to 68°F.
P-3	Soak in fixer with x% hardener (Kodak standard 3.125%) for 10 minutes.
P-4	Wash in running water for 10 minutes.
P-5	Rinse in distilled water for 5 minutes with agitation.
P-6	Dip into a Photo-Flo 200 solution (1 drop/500 ml) for 30 seconds and remove the excess with either a photographic sponge or clean wiper blade.
P-7	With plate in horizontal position, dry overnight at room temperature.

Lighting: Red (dim)

P-8	Soak in x% ammonium-dichromate solution (with 0.x% Photo-Flo 200) for 5 minutes.
P-9	Wipe ammonium dichromate from glass side of plates.
P-10	With plate in horizontal position, dry overnight at room temperature.

\*For mixing formulas, see Table 4.

For our standard processing, we use 3.125% hardener concentration for step P-3 and 5% for Step P-8.

TABLE 3  
STANDARD DEVELOPMENT OF DICHROMATED GELATIN PLATES

All chemicals are dissolved in distilled water, and, except where noted, all steps are at a temperature of 68°F

<u>STEP</u>	<u>DIRECTION</u>	<u>LIGHTING</u>
SD-1*	Soak in 0.5% solution of ammonium dichromate for 5 minutes.	Red (dim)
SD-2*	Soak in fixer with x% hardener for 5 minutes.	Red (dim)
SD-3	Wash in running water for 10 minutes.	Room light
SD-4	Dip into a Photo-Flo 200 solution (1 drop/500 ml) 30 seconds and remove the excess water with photographic sponge.	Room light
SD-5	Soak in distilled water for 2 minutes with agitation.	Room light
SD-6	Dehydrate in a 50/50 solution of distilled water and isopropanol for 3 minutes.	Room light
SD-7	Dehydrate in 100% isopropanol for 3 minutes.	Room light
SD-8	Free-air dry for at least 1 hour.	Room light
SD-9	Either bake for 2 hours over a hot plate at an elevated temperature, or evaporate residual water in a vacuum chamber.	Room light

\* For mixing formulas, see Table 4.

For our standard processing, we use a 3.125% hardener concentration for Step SD-2.

TABLE 4  
EXAMPLES OF CHEMICAL MIXING FORMULAS

1. Fixer without hardener

Water: 60 ml; Fix concentrate: 20 ml

2. Fixer with x% hardener

$$x\% = \frac{\text{hardener volume}}{\text{water} + \text{concentrate volume}} \times 100\%$$

a) Kodak fixer with standard hardener (3.125%)

Water: 60 ml; Fix concentrate: 20 ml;  
Hardener: 2.5 ml.

b) Fixer with 2x hardener (6.25%)

Water: 60 ml; Fix concentrate: 20 ml;  
Hardener: 5 ml.

3. 0.5% ammonium dichromate for development

Water: 800 ml; ammonium dichromate: 4 g

4. x% ammonium dichromate with 0.x% Photo-Flo

$$x\% = \frac{\text{ammonium-dichromate (g)}}{\text{water (ml)}} \times 100\%$$

a) 5% ammonium dichromate

Water: 800 ml; ammonium dichromate: 40 g;  
Photo-Flo: 4 ml.

b) 3% ammonium Dichromate

Water: 800 ml; Ammonium Dichromate: 24 g;  
Photo-Flo: 2.4 ml.



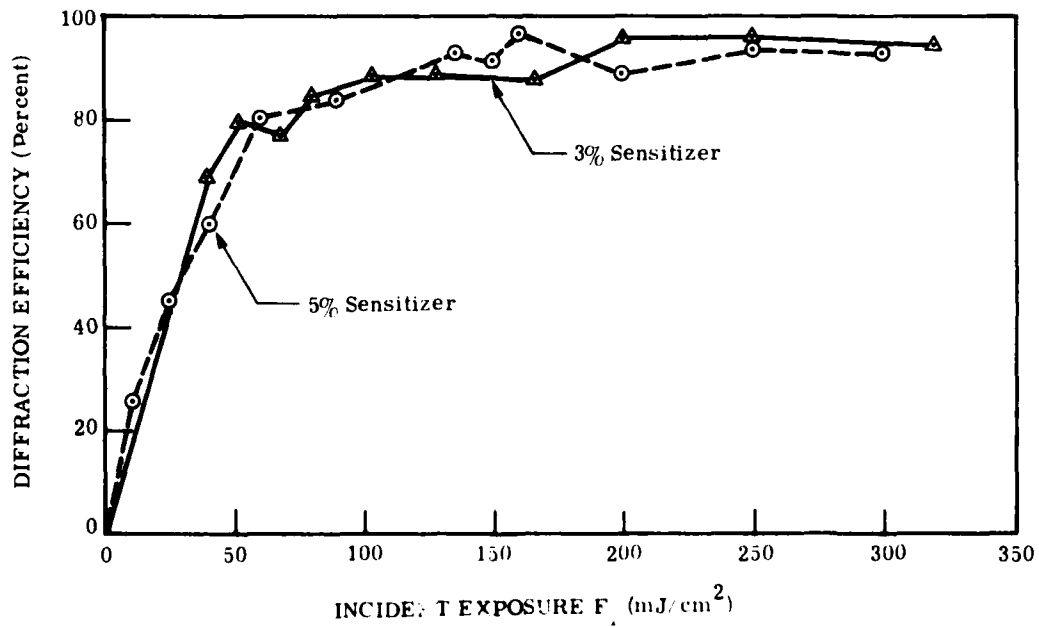


Figure 18. Diffraction efficiency as a function of exposure for reflection holograms recorded in dichromated gelatin.

The diffraction efficiency of reflection holograms as a function of refractive index modulation saturates [3]. Unlike the case of transmission holograms, it is difficult to estimate the refractive index modulation from the curve of diffraction efficiency as a function of exposure. However, the refractive index modulation of saturated reflection holograms can be determined by measuring the angular bandwidth of the holograms, because the angular bandwidth is also a function of the refractive index modulation.

### c. ANGULAR BANDWIDTH

The current conventional lenses in the F-4 HUD system provide a field-of-view of  $14^\circ$ . The flat holographic combiner should provide the equivalent field-of-view, requiring the hologram to have an angular bandwidth of  $14^\circ$ . From our previous experience we expected the task of achieving such a large angular bandwidth to be difficult, and therefore, concentrated much of our effort on increasing the angular bandwidth of reflection holograms. To increase the angular bandwidth, we used two approaches. The first was to maximize the refractive index modulation by optimizing the sensitizer concentration and processing technique. The second was to record two gratings incoherently with slightly different fringe spacings.

First, using a 5% sensitizer, we examined the angular bandwidth of single-grating and two-grating reflection holograms. As shown in Figure 19, the angular bandwidth increases as the exposure (or refractive index modulation) increases. At an incident exposure  $E_i$  of  $300 \text{ mJ/cm}^2$ , the angular bandwidth reaches  $8^\circ$ . The angular bandwidth of two-grating reflection holograms is plotted in Figure 20, where the offset between the recording angles of the two gratings was  $4^\circ$ . As

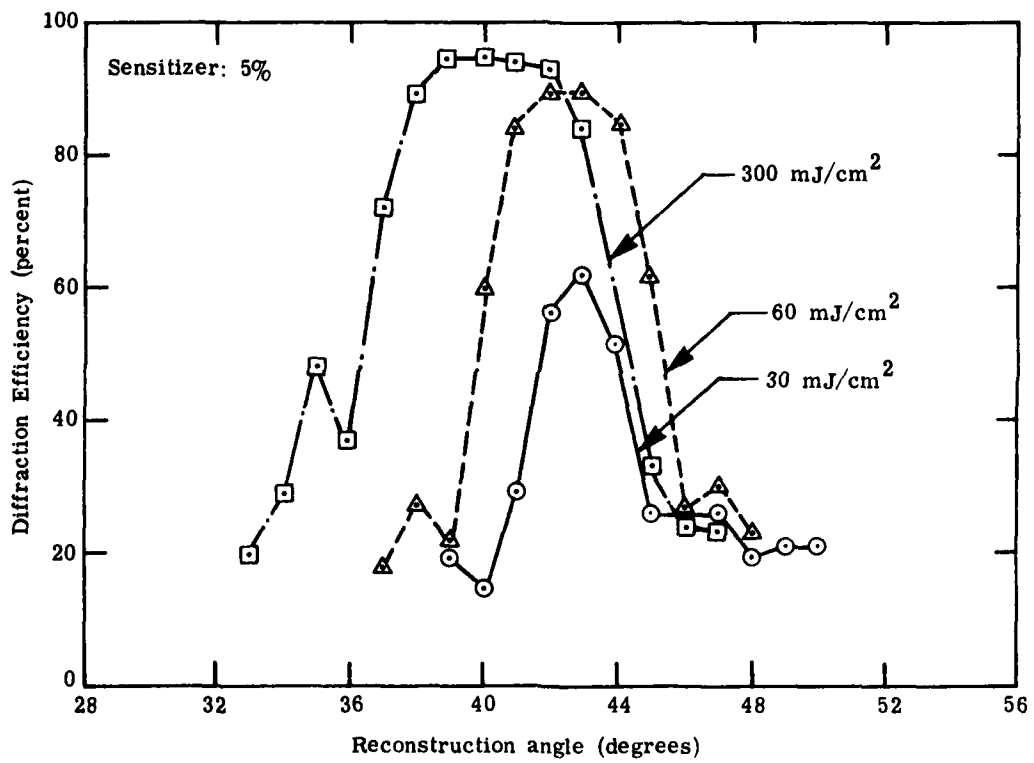


Figure 19. Angular bandwidth of single-grating reflection holograms recorded at three exposure levels.

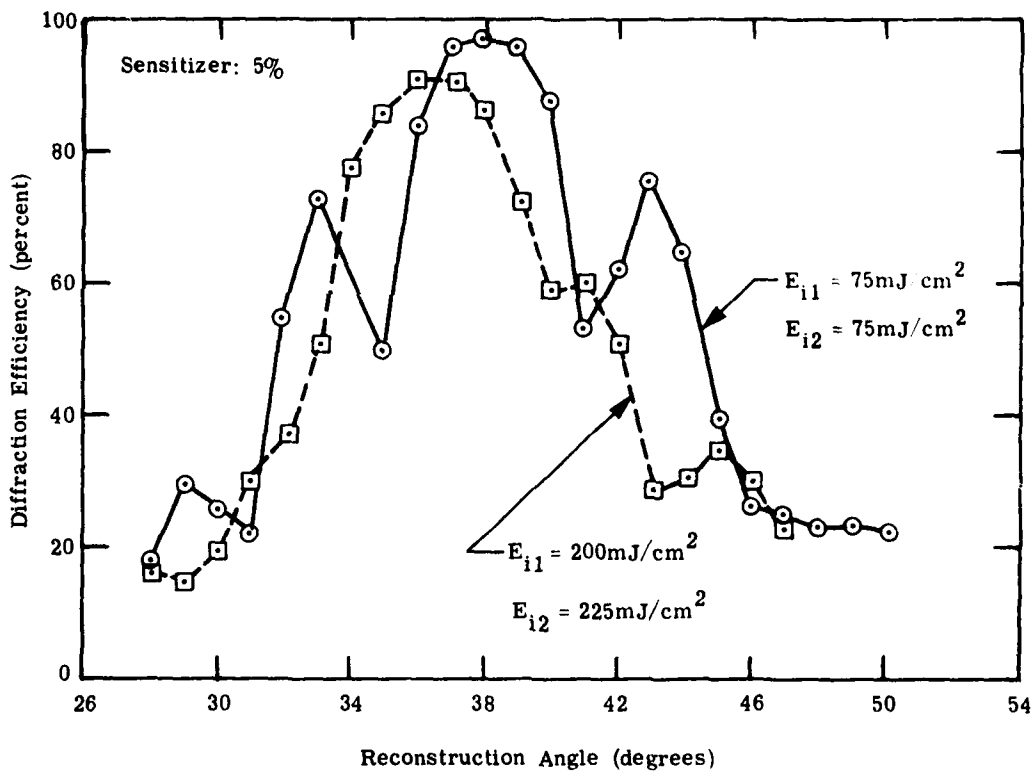


Figure 20. Angular bandwidth of two-grating reflection holograms recorded at two exposure levels.

expected, the angular bandwidth of two-grating holograms is greater than that of single-grating holograms. The deviation of the Bragg-angle from the original recording angle indicates that the hologram thickness undergoes a net shrinkage and increasingly so at heavy exposures (see Figures 19 and 20). The net thickness change after processing will be discussed below in Section III.1.e.

Angular bandwidths obtained with a 3% sensitizer concentration were generally considerably wider than those obtained with the 5% sensitizer. At an incident exposure of  $200 \text{ mJ/cm}^2$ , the angular bandwidth of a single-grating reflection hologram exceeded  $14^\circ$  (Figure 21); we estimate the refractive index modulation of this hologram to be 0.08. In Figure 22, we show the angular bandwidth of two-grating reflection holograms, where, again, the offset between the recording angles of the two gratings was  $4^\circ$ . Unlike the case with a 5% sensitizer, the holograms made with a 3% sensitizer solution appeared to swell, although the relative thickness still decreased with exposure.

We also recorded single-grating and two-grating holograms in a dichromated gelatin plate sensitized with a 1% sensitizer solution. While the exposure sensitivity and angular bandwidths of these holograms were comparable to those obtained with a 3% sensitizer, we observed that the Bragg-angle shift was considerably larger. After drying in vacuum at  $90^\circ\text{C}$  for two hours, these holograms still showed an average Bragg-angle deviation of over  $12^\circ$ . Although the swelling can be compensated by altering the incident angle of the recording beam, it was undesirable to alter the angle by a large amount because the anti-reflection coating of our optical window was optimized for an incident angle of  $45$  to  $48^\circ$ .

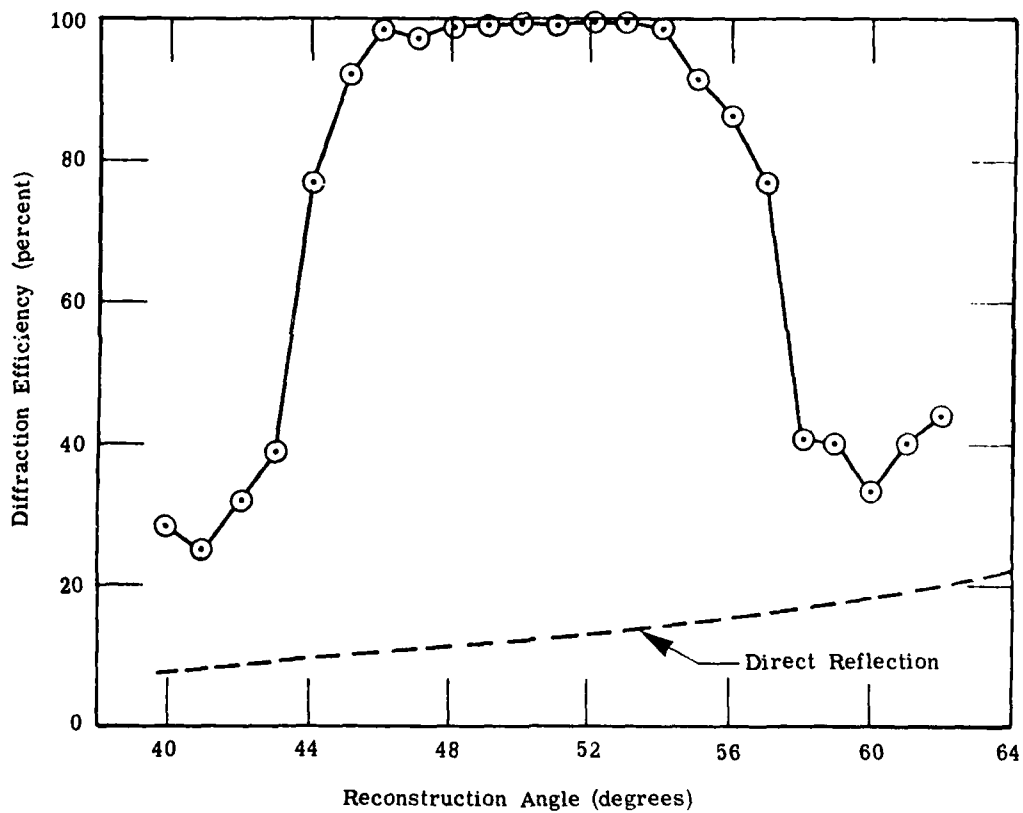


Figure 21. Angular bandwidth of a single-grating reflection hologram in dichromated gelatin sensitized with a 3% sensitizer concentration.

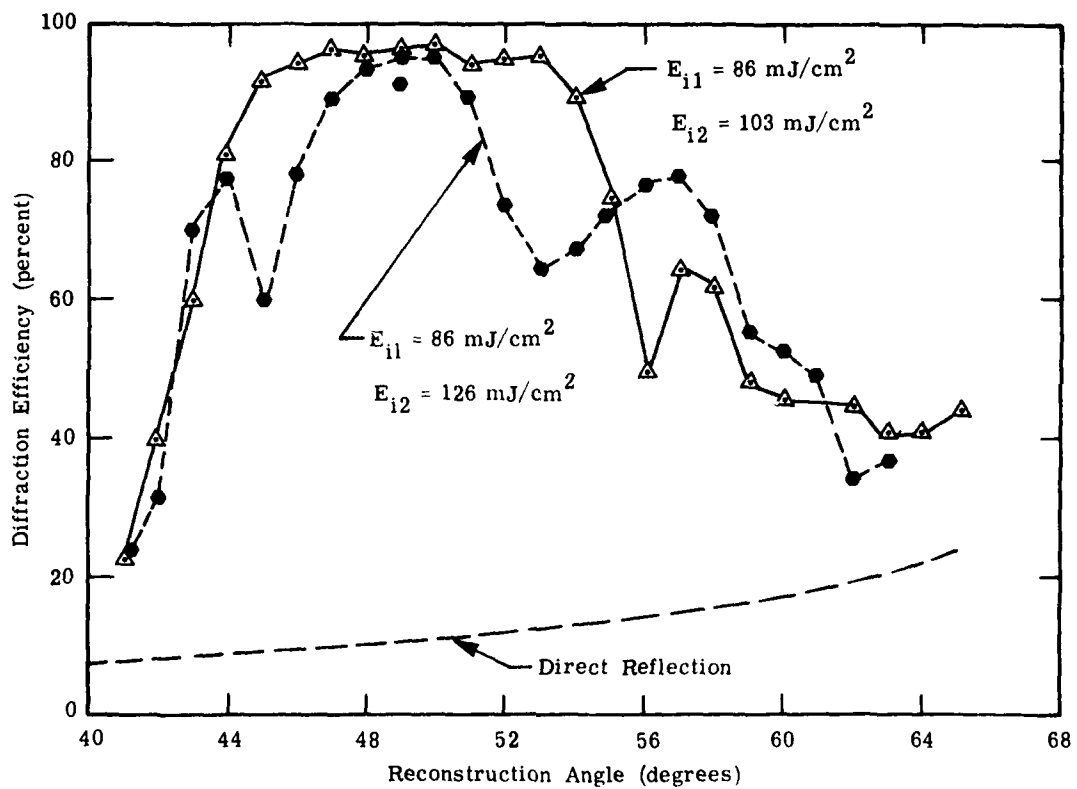


Figure 22. Angular bandwidth of two-grating reflection holograms in dichromated gelatin sensitized with a 3% sensitizer concentration.

From this series of measurements of the angular bandwidth of dichromated gelatin reflection holograms, we concluded that a sensitizer solution of 3 to 5% is optimum for the fabrication of the HUD combiner.

#### d. SPECTRAL BANDWIDTH

The spectral selectivity of reflection holograms was measured in a spectrometer as follows. With the spectrometer set to a wavelength of 512 nm, the peak wavelength of the PX58 phosphor emission of the CRT, we placed a hologram in one of the two spectrometer arms and oriented it to the Bragg-angle. We then measured the transmission of the hologram as a function of wavelength. Assuming no absorption, we transformed the transmission spectrum to a reflection spectrum.

As shown in Figures 23 and 24, the spectral bandwidth of reflection holograms increases with exposure (or refractive index modulation). At an incident exposure of  $320 \text{ mJ/cm}^2$ , the spectral bandwidth is about 15 nm. As shown in Figure 25, the spectral bandwidth of the two-grating reflection holograms is greater than that of the single-grating holograms. In general, a hologram having a wider angular bandwidth also has a wider spectral bandwidth, since both bandwidths are determined by the refractive index modulation, and the grating structure [3].

There appears to be some discrepancy between the predicted and measured spectral bandwidths. In particular, the measured spectral bandwidth was narrower than anticipated for a hologram that has a large angular bandwidth. The trend of the bandwidth to increase with increasing index modulation was observed both experimentally and analytically, however. The theoretical prediction of the spectral bandwidth was made by assuming a refractive index modulation



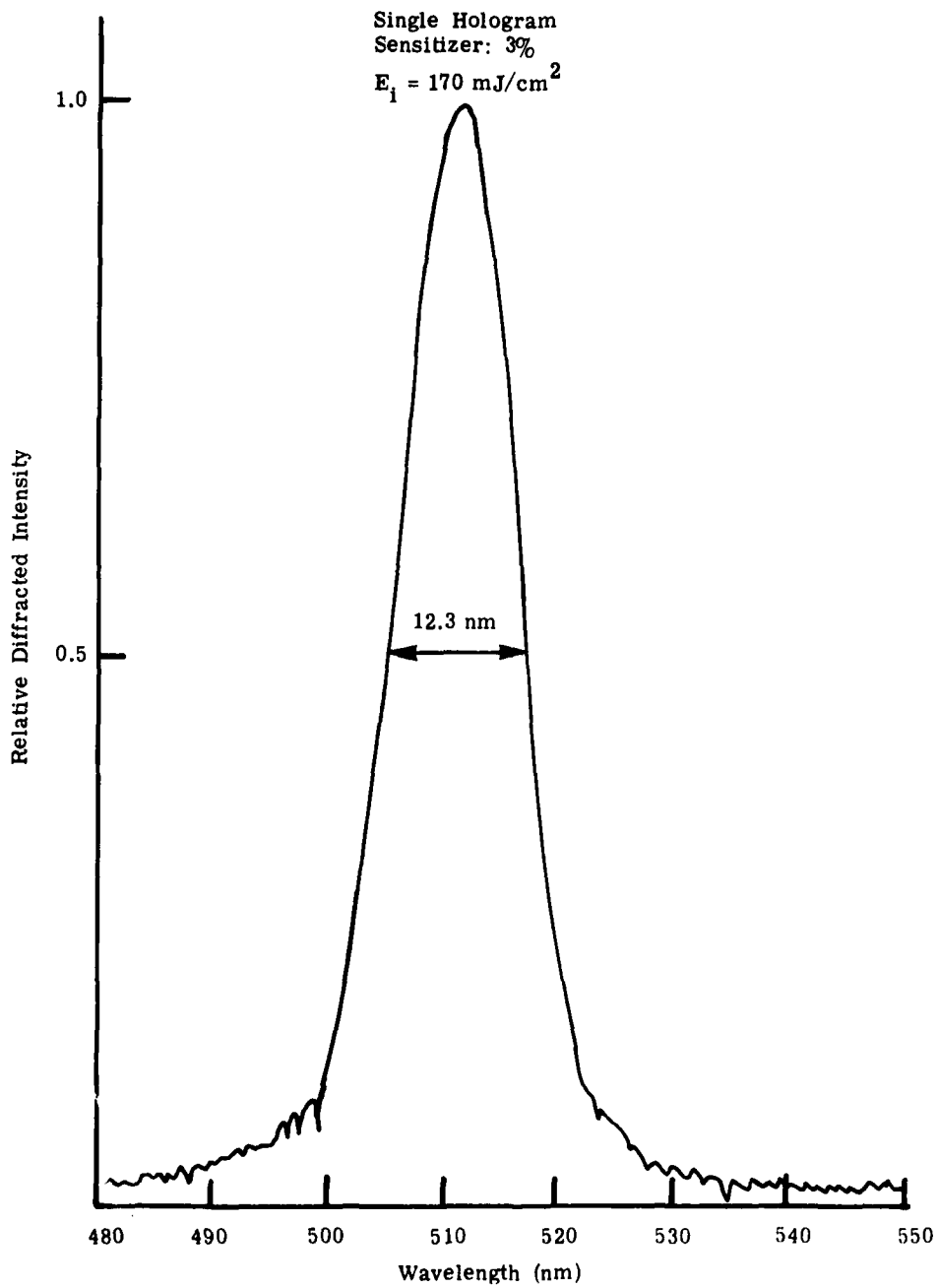


Figure 23. Spectral bandwidth of a single-grating reflection hologram recorded in dichromated gelatin with an exposure of  $170 \text{ mJ/cm}^2$

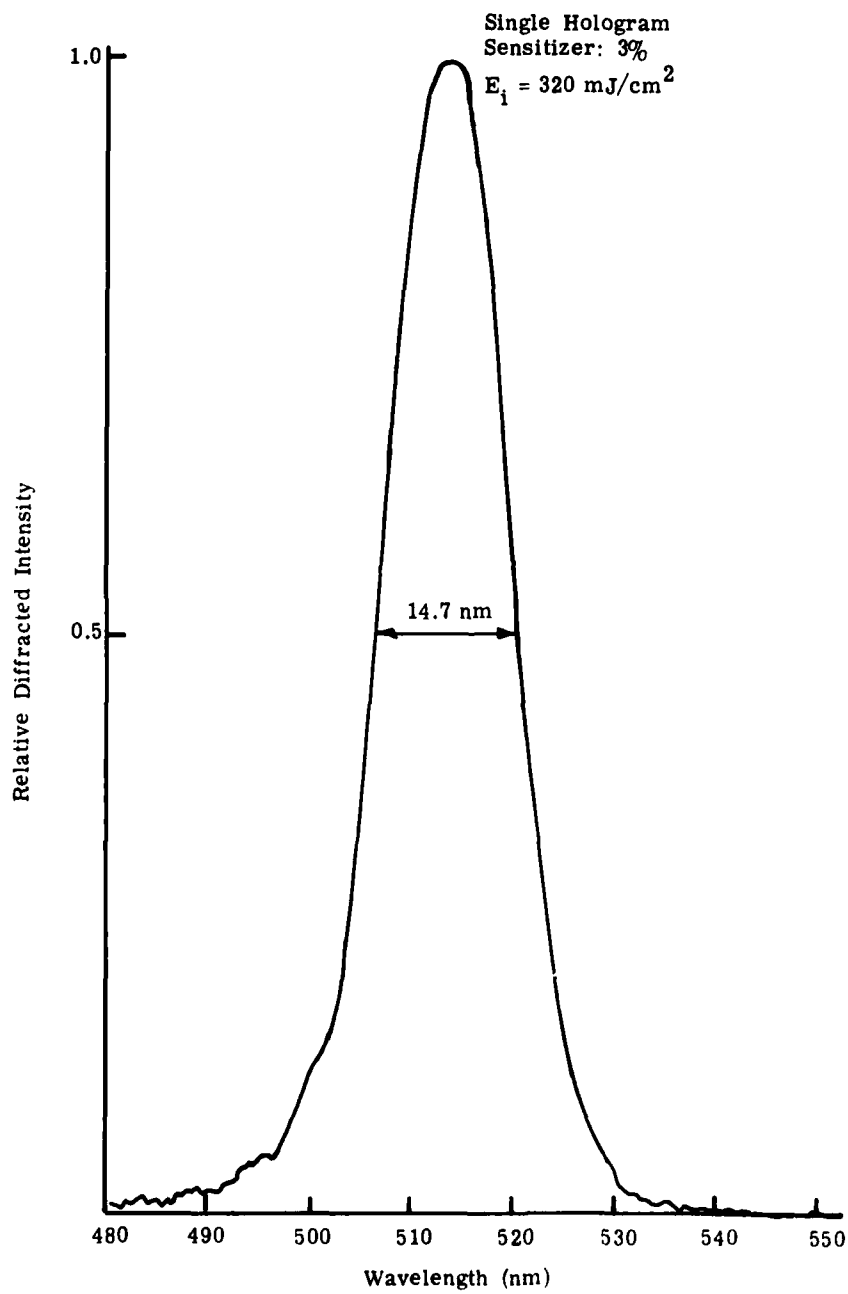


Figure 24. Spectral bandwidth of a single-grating reflection hologram recorded in dichromated gelatin with an exposure of  $320 \text{ mJ/cm}^2$ .

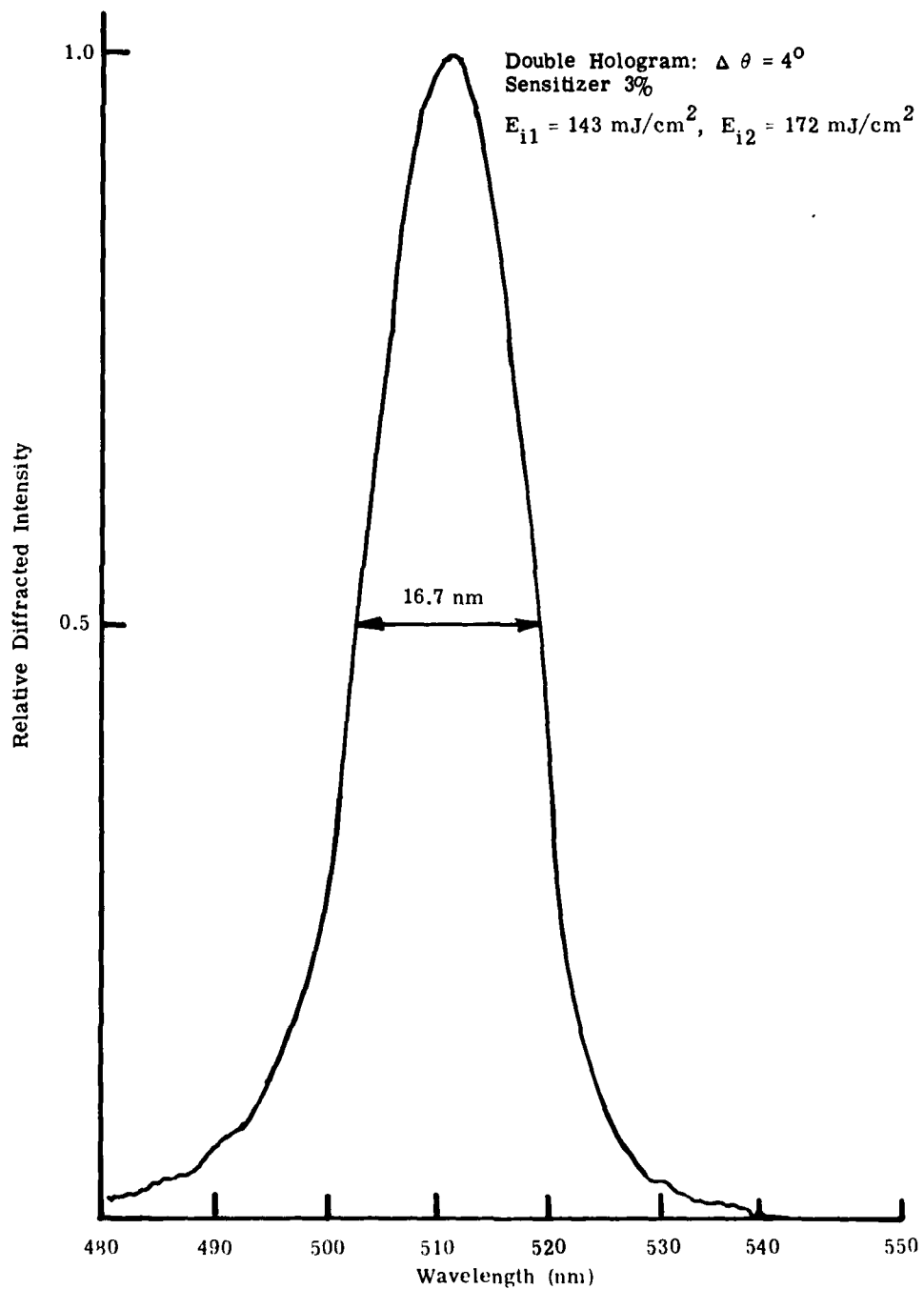


Figure 25. Spectral bandwidth of a two-grating reflection hologram recorded in dichromated gelatin.

that was constant throughout the hologram depth. The index modulation of actual holograms varies with depth, however, and may account for the discrepancy we observed.

A wide spectral bandwidth is desirable in that a greater fraction of the CRT illumination will reach the pilot's eye; the HUD system will be more efficient. At the same time, however, more light passing through the window-screen will be diffracted away from the pilot. If the spectral bandwidth is too large, most of the incident light will be diffracted over a significantly wide band, and the transmitted light will have a tint associated with it.

#### e. HOLOGRAM THICKNESS

The thickness of dichromated gelatin holograms usually changes due to the development processing. The thickness change is rather complicated because it is a function of the exposure level, sensitizer concentration, and processing environment as well as the processing technique [7,12,13]. The primary effect of the thickness change in volume holograms is to cause a shift of the Bragg angle.

Controlling our processing environment and using our standard processing technique (Tables 2 and 3), we studied the thickness change of reflection holograms as a function of exposure and sensitizer concentration. First, we measured the Bragg-angle shift as a function of exposure, under various drying conditions.

The results are shown in Figure 26, in which a positive angle corresponds to a net swelling of the hologram. The Bragg-angle shift is readily converted to the hologram thickness change by applying Eq. (2); a shift of  $+5^\circ$ , for example, corresponds to a thickness increase of 7.5%. Although the drying method affected the hologram thickness, we observed little effect on the hologram efficiency. We also investigated

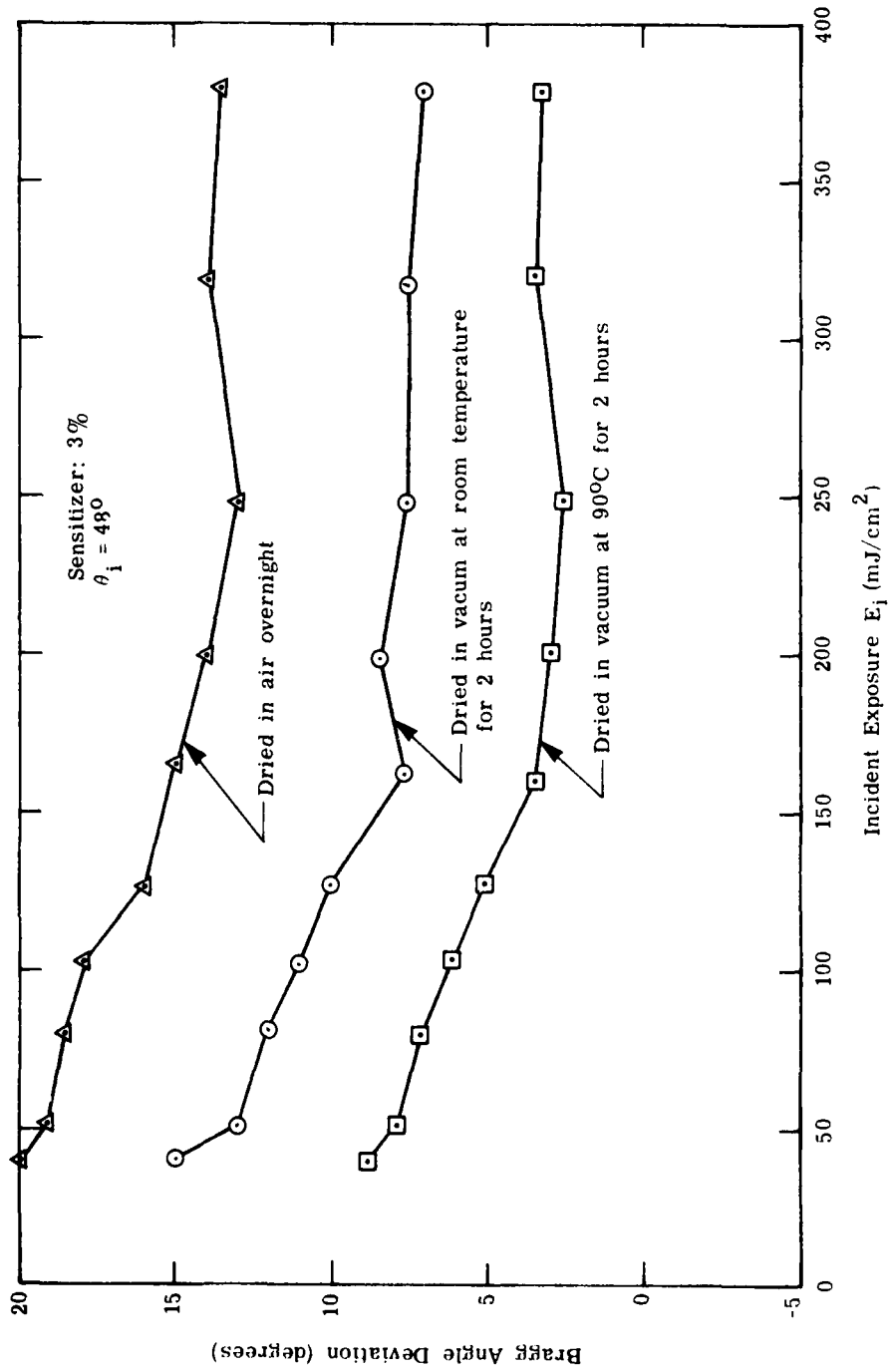


Figure 26. Bragg angle deviation as a function of exposure for dichromated gelatin reflection holograms under several drying conditions.

the hologram thickness as a function of sensitizer concentration. As shown in Figure 27, the hologram thickness decreases linearly as the sensitizer concentration increases. The hologram thickness can thus be controlled either by employing the optimum drying method or by varying the sensitizer concentration.

## 2. FABRICATION AND TEST OF FLAT REFLECTION HOLOGRAPHIC COMBINERS

### a. FABRICATION

To fabricate the holographic combiner, we used a single-beam recording system employing an off-axis parabolic mirror of 28 cm diameter as a collimator, as shown in Figure 28; the focal length of the parabolic mirror is about 2 m (80 inches). Figure 29 shows the major optical components assembled into the recording system. A plate glass window having an anti-reflection coating was used to minimize multiple-reflections between the front surface of the hologram plate and the second surface mirror. This optical window yields less than 0.5% reflection for 514 nm s-polarized light at an incident angle of  $45^\circ$ . For optimum holograms, the optical window and second surface mirror should be extremely flat. The thickness of the optics we used varies by about one wavelength over any 5 cm aperture, however, since the glass is commercial plate glass. Because the present effort aims at demonstrating the feasibility of the holographic combiner, commercial quality materials were used for the optical window and second surface mirror to minimize costs.

To expand the beam of an argon ion laser, we used a microscope objective with a focal length of either 22.7 mm

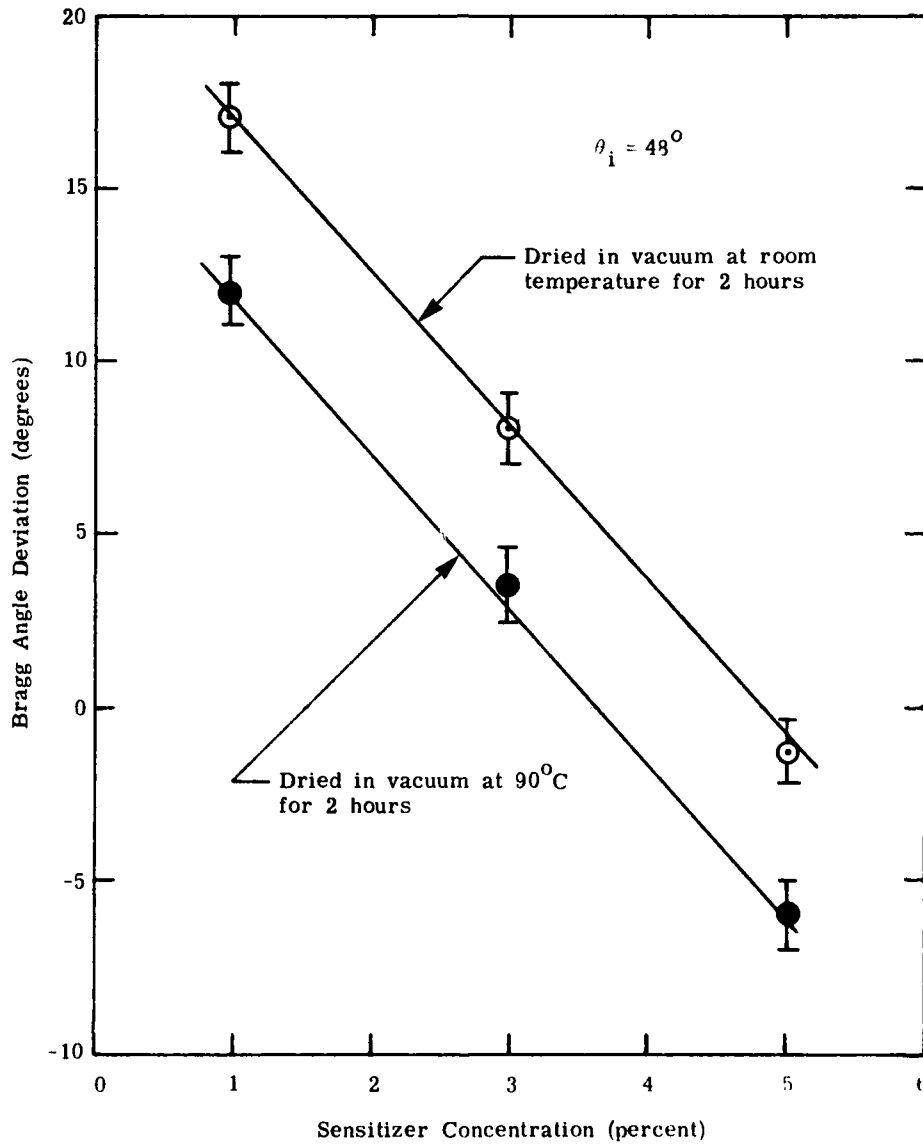


Figure 27. Bragg angle deviation as a function of sensitizer concentration for dichromated gelatin reflection holograms under two drying conditions.

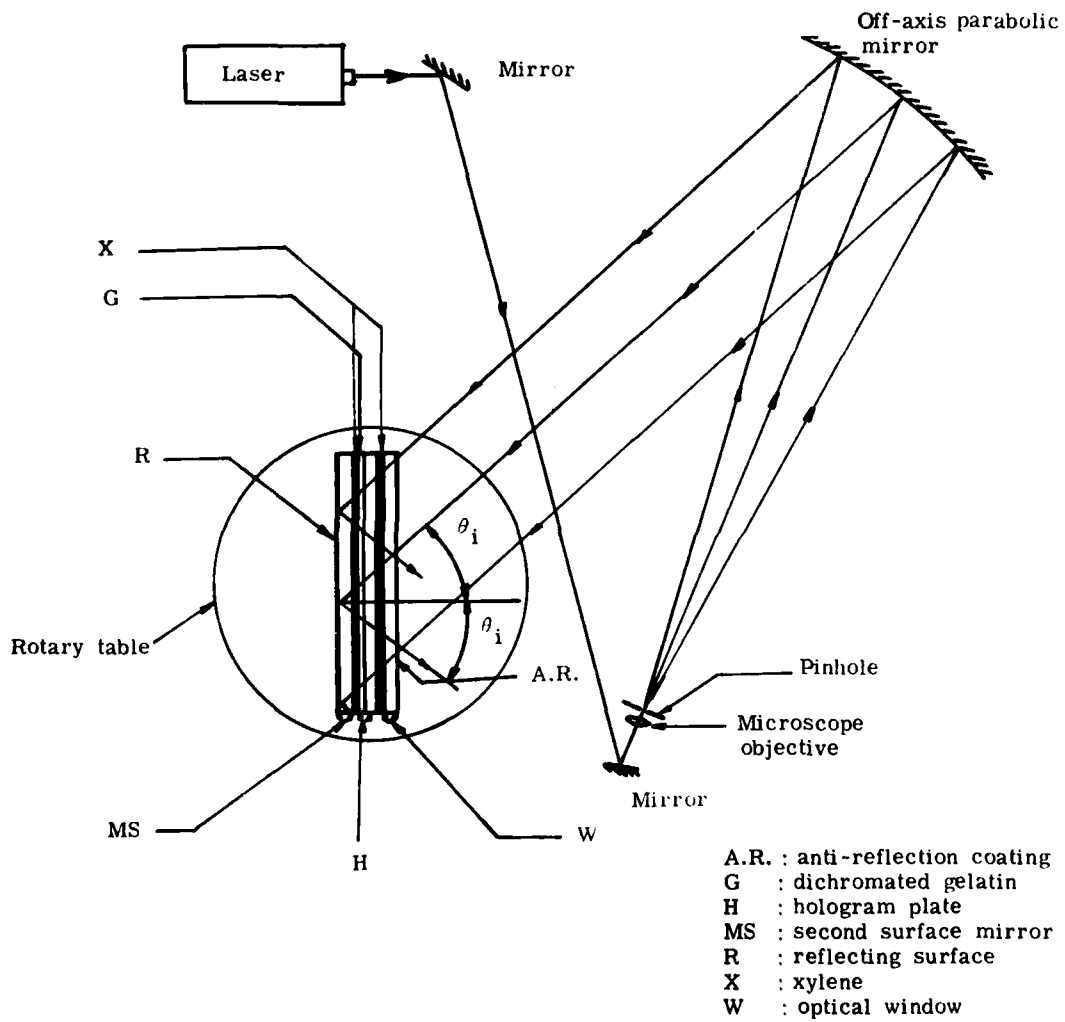


Figure 28. Recording configuration used to fabricate the holographic combiners.



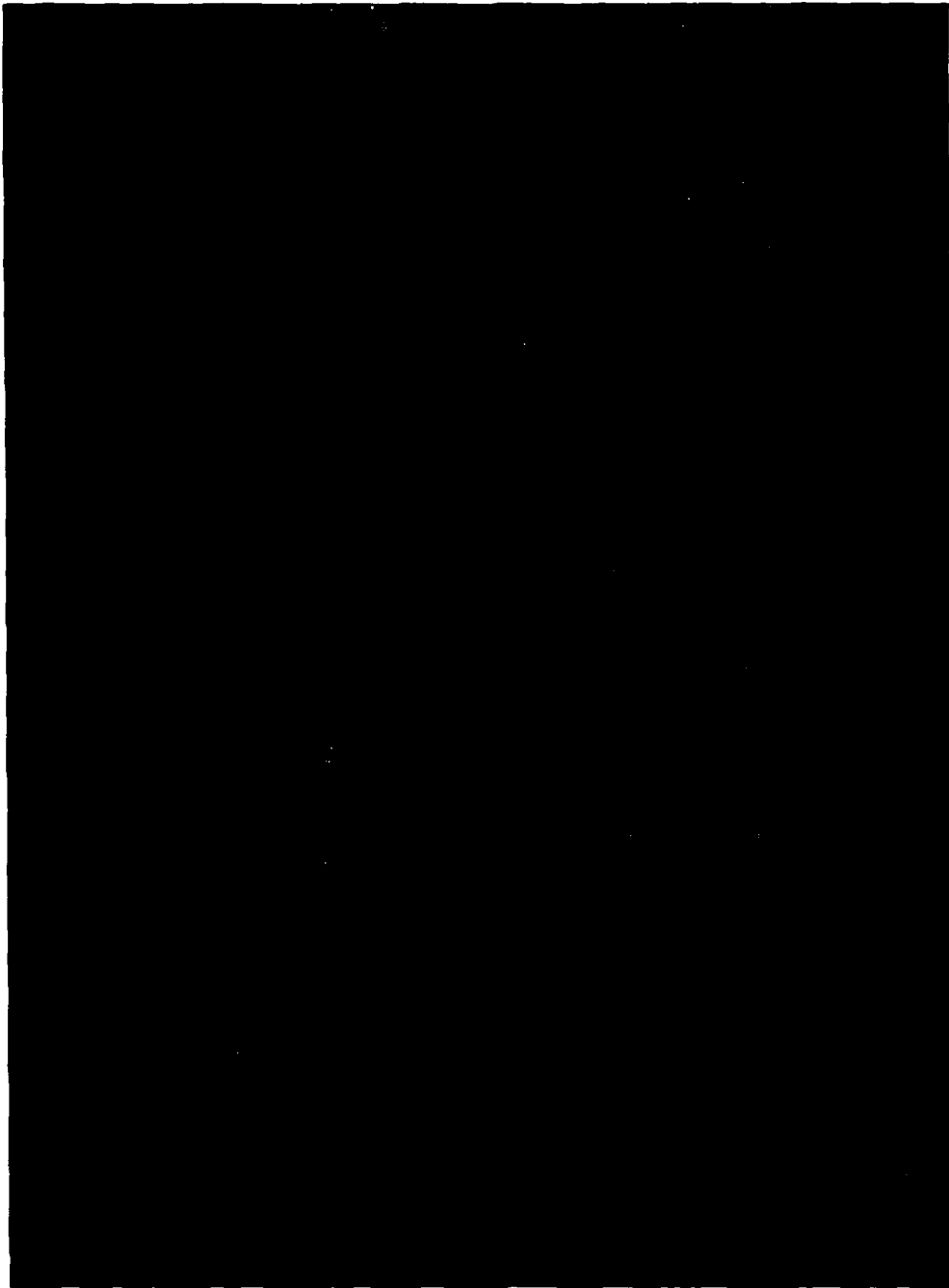
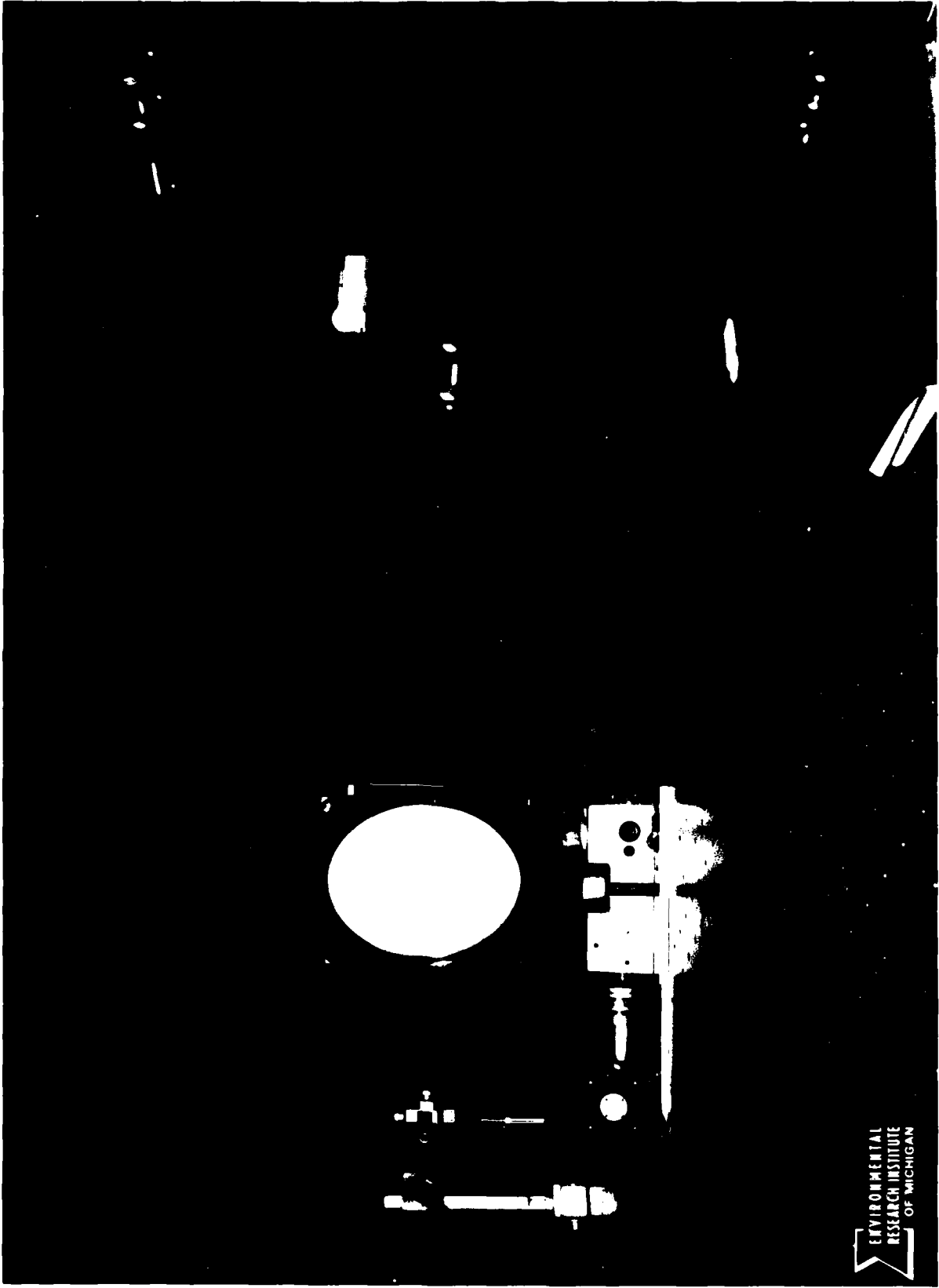


Figure 29. Photograph of the recording system. The parabolic mirror is in the foreground.



ENVIRONMENTAL  
RESEARCH INSTITUTE  
OF MICHIGAN

REDUCE  $9\frac{5}{16}$ " TO  $7\frac{3}{4}$ "

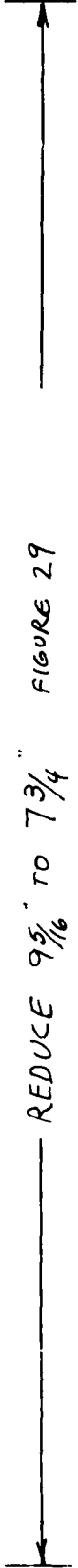


FIGURE 29

or 16 mm. With a microscope objective having a 22.7 mm focal length, the exposure time was about 5 minutes to achieve  $200 \text{ mJ/cm}^2$  exposure at the edge of a circular hologram 25 cm in diameter. In this case, the ratio of the intensity at the center of the hologram to that at the edge was 3.3. With a microscope objective having a 16 mm focal length, this ratio reduces to 1.5, but requires increased exposure time.

The incident angle  $\theta_i$  of the recording beam was adjusted according to the sensitizer concentration to compensate for the expected thickness change of the hologram (see Figure 27). With a 3% sensitizer solution, we set  $\theta_i$  at  $45^\circ$ , and with a 4% solution, we set  $\theta_i$  at  $48^\circ$ , the center angle of the combiner's field-of-view. After processing, and before cementing a cover plate to the hologram, we reduced the gelatin thickness by careful baking, while monitoring the hologram thickness by measuring the Bragg-angle.

The baking process has another important function in that it eliminates residual water in the gelatin layer [7]. Our previous environmental testing indicated that if a dichromated gelatin hologram was not dried completely before cementing the cover plate to the gelatin surface, it was still affected by high temperatures. It is important to dry the gelatin layer completely because the combination of residual water and high temperature apparently soften the gelatin sufficiently to cause degradation of the hologram. Residual water can also be eliminated in a vacuum chamber. Our investigations showed that the diffraction efficiency of a hologram was not affected by one hour in boiling water if the hologram was either baked at a temperature higher than  $85^\circ\text{C}$  for 1 to 2 hours or placed in a vacuum chamber for 1 to 2 hours before cementing.

Using the methods outlined above, we fabricated several flat holographic combiners in dichromated gelatin layers

derived from 11 x 11 inch Kodak 649F Microflat Plates. Figure 30 shows one of the combiners with a cover plate before it was cut to F-4 combiner size, 160 x 195 mm.

#### b. EVALUATION OF THE HOLOGRAPHIC COMBINERS

We evaluated the holographic combiners by measuring the diffraction efficiency and the angular and spectral bandwidths of each of three combiners. The peak diffraction efficiency exceeded 95% in each case, the angular bandwidths were between 11 and 13<sup>o</sup>, and the spectral bandwidths were between 21 and 25 nm. In addition the combiners were of high optical quality, with very low or negligible scattering.

For the measurement of diffraction efficiency as a function of reconstruction angle (angular bandwidth), a dichromated gelatin hologram was placed on a rotary table and illuminated with a plane wave of 514 nm wavelength. As shown in Figure 31, a fiber optics probe was placed as close to the hologram plate as its housing allowed, and the hologram plate and probe were rotated together to make the measurement. To reduce spurious reflections, the hologram was gated with an anti-reflective optical window in front and an absorbing plate behind. Two angular selectivity curves were generated for each hologram; one for illumination from the cover plate side (front side), and another for illumination from the substrate side (rear side). The angular selectivity curves for the three combiners (HUD-76-1, HUD-76-2, and HUD-76-3) are shown in Figures 32, 33, and 34. The third combiner (HUD-76-3) has the widest bandwidth, 13<sup>o</sup>, and is closest to having a Bragg-angle of 48<sup>o</sup>.

The two angular selectivity curves obtained from the same combiner are different. The curve obtained with illumination from the front side has more fluctuations than

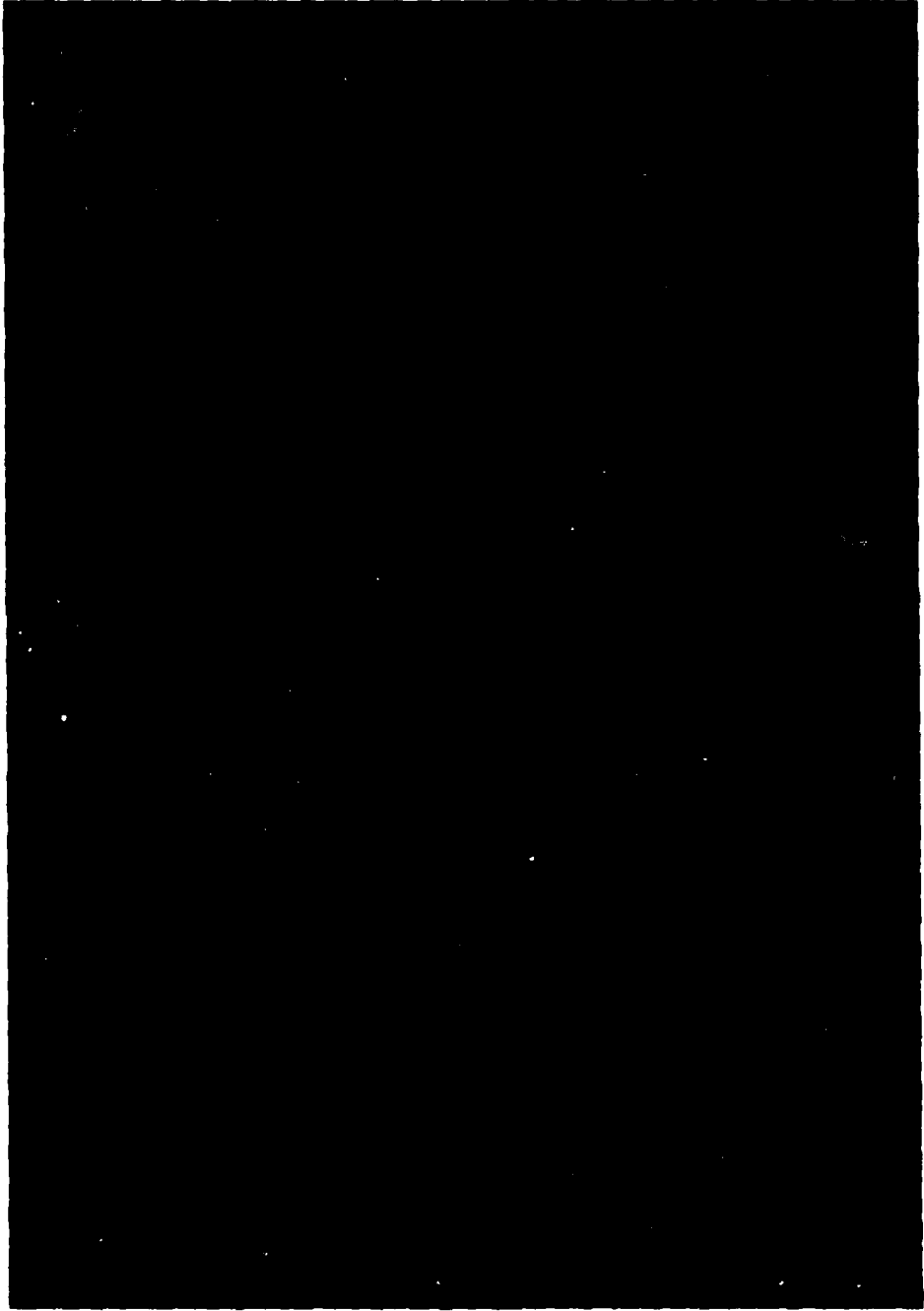
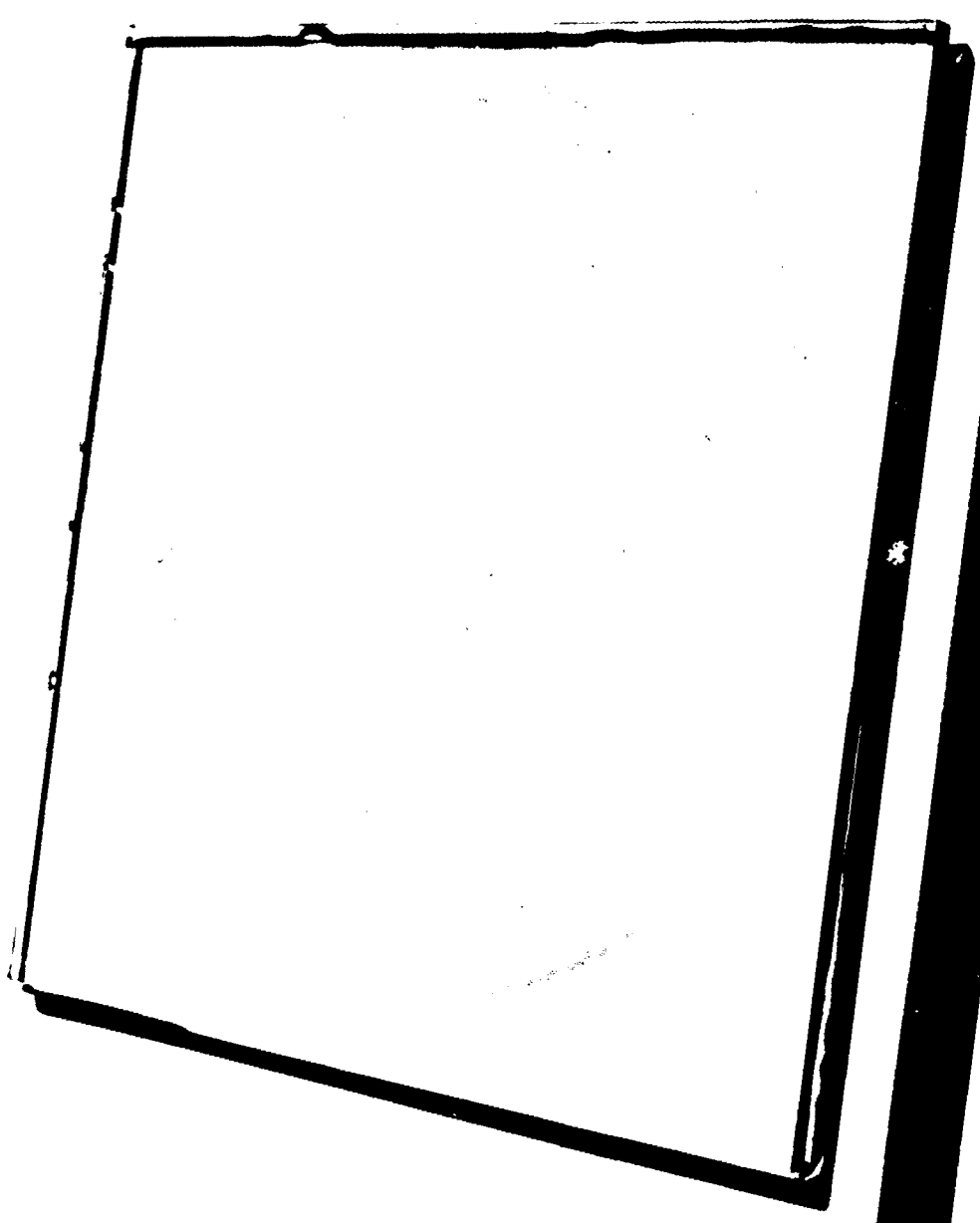
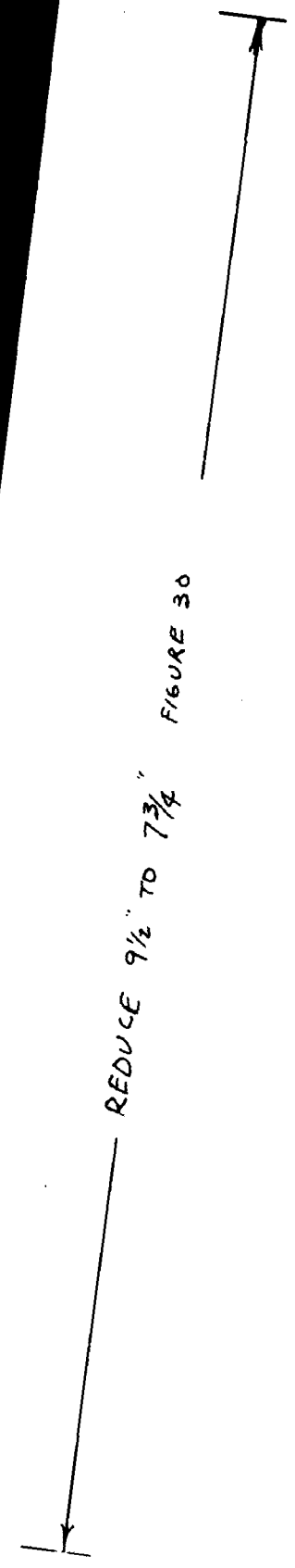


Figure 30. Photograph of a complete *Aspergillus nidulans* culture on a petri dish.



REDUCE  $9\frac{1}{2}$ " TO  $7\frac{3}{4}$ " FIGURE 30



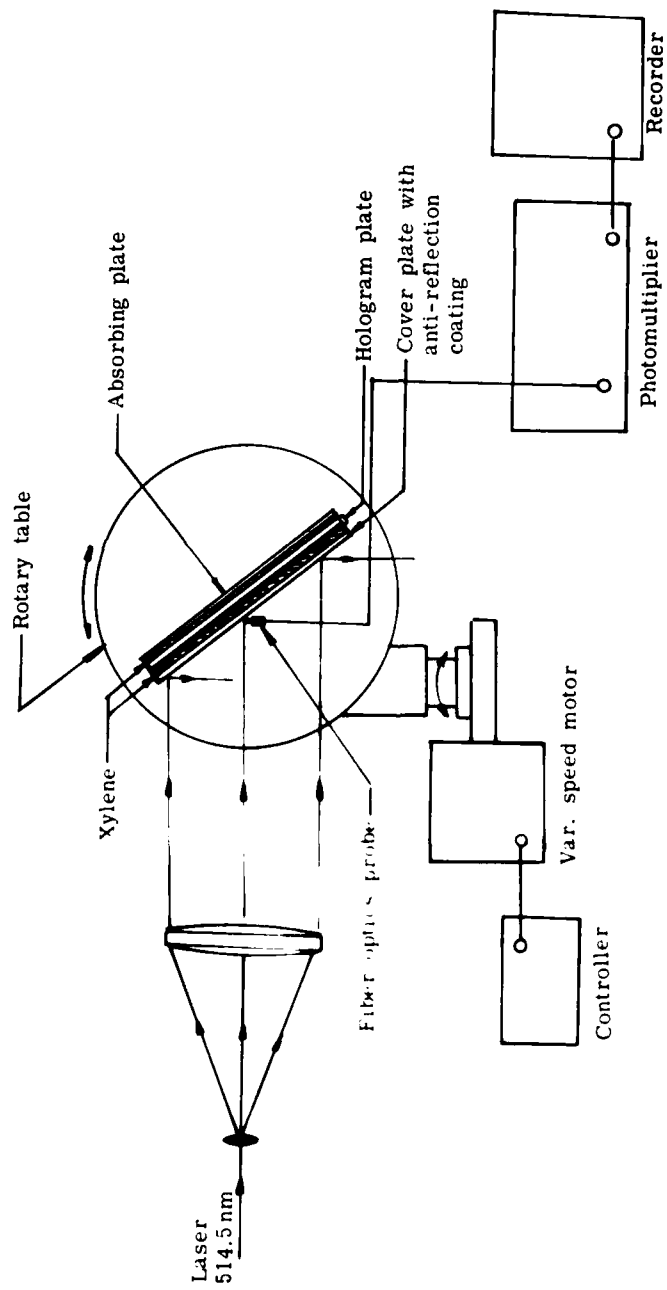
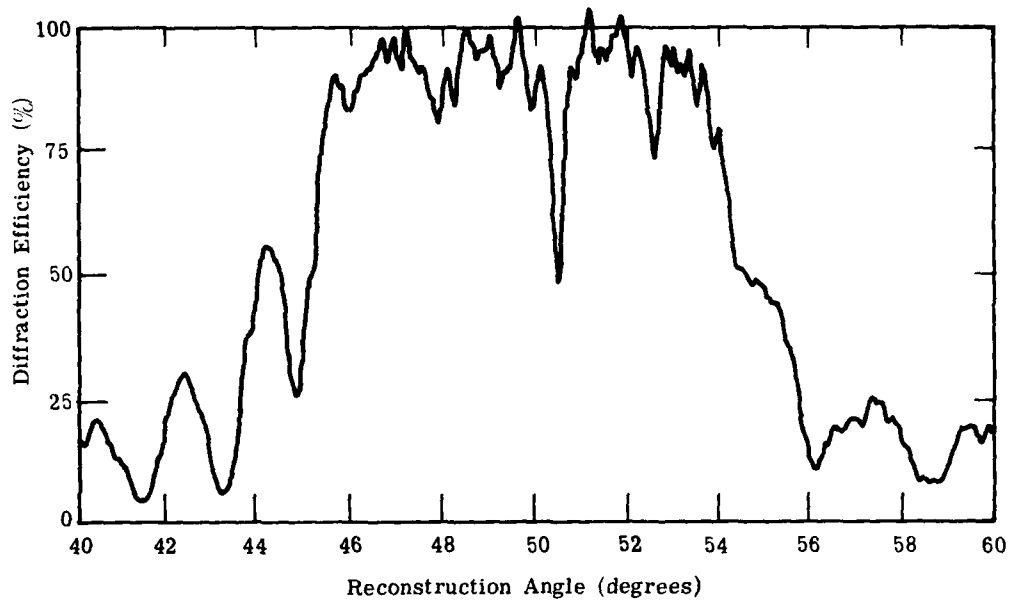
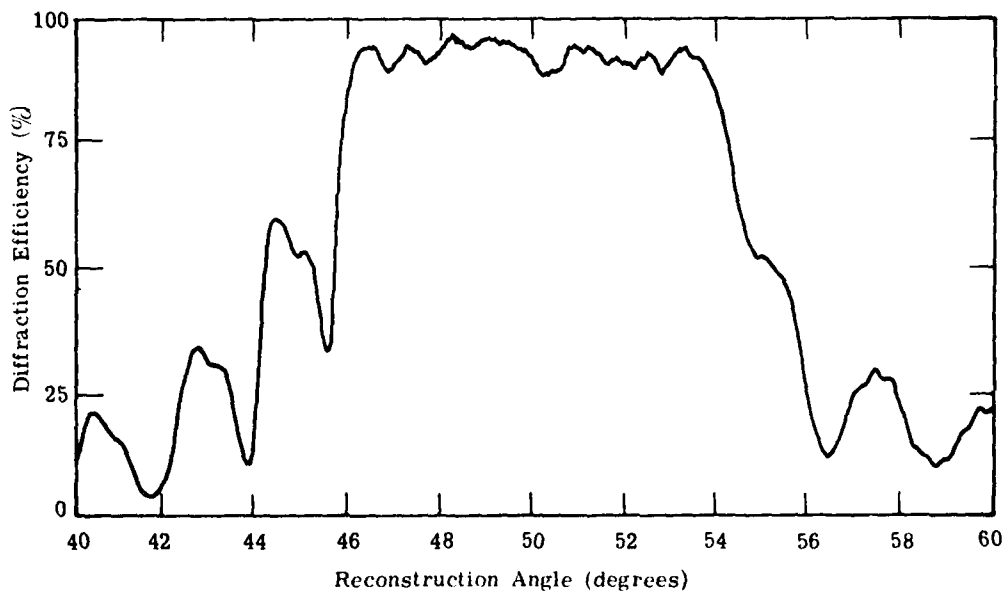


Figure 31. Measurement of angular bandwidth of the holographic combiner.



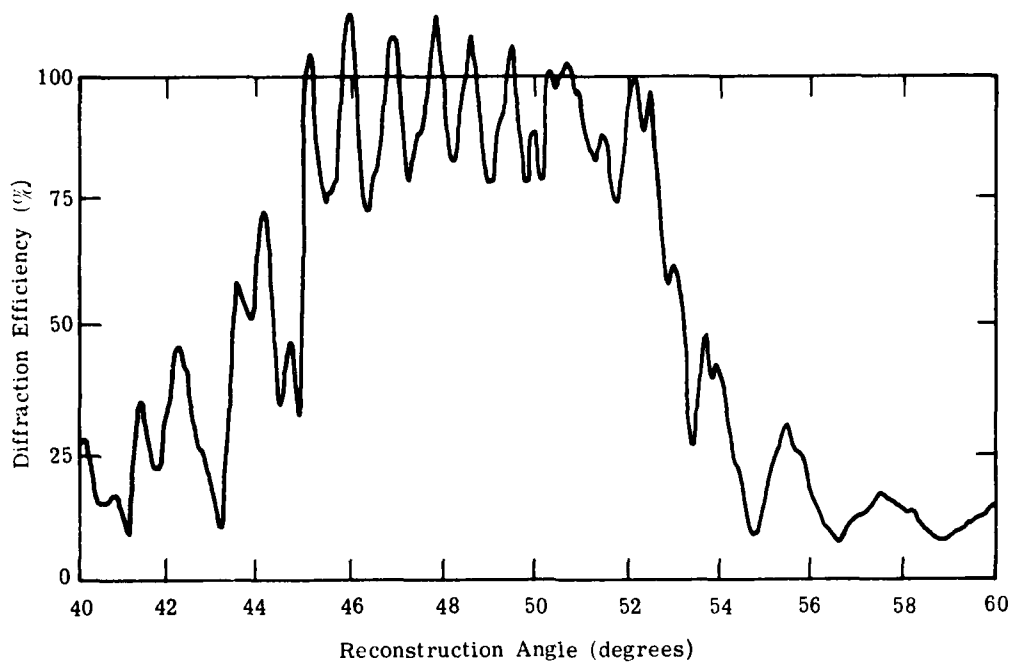
(a) Front side



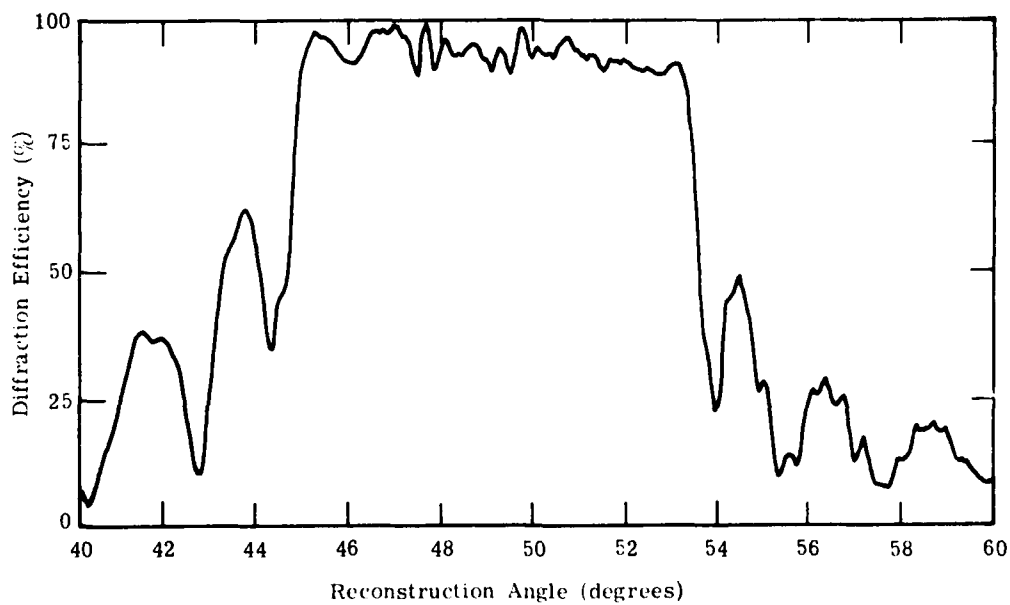
(b) Rear side

Figure 32. Angular bandwidth of holographic combiner HUD-76-1.





(a) Front side



(b) Rear side

Figure 33. Angular bandwidth of holographic combiner HUD-76-2.

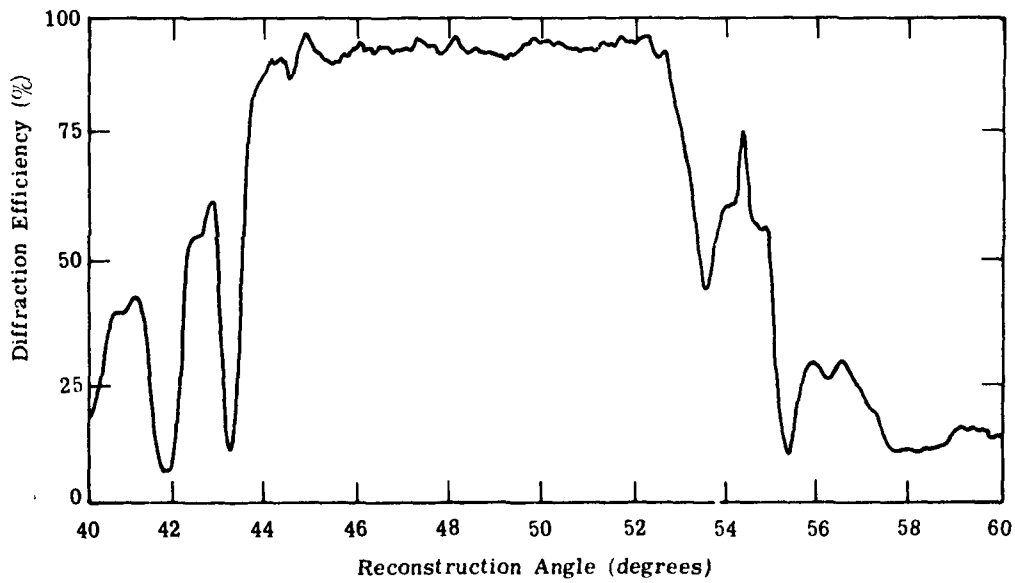
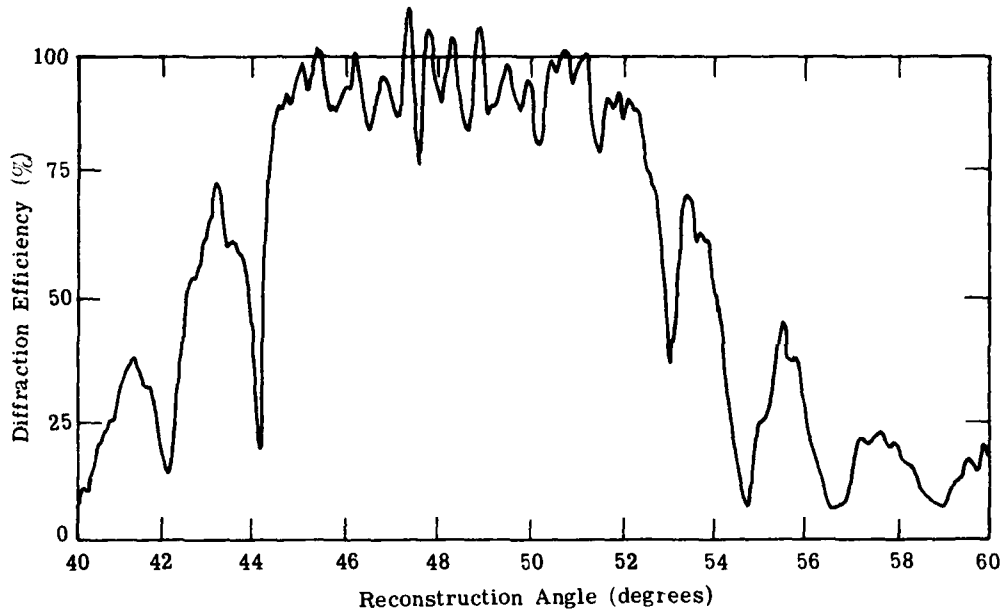
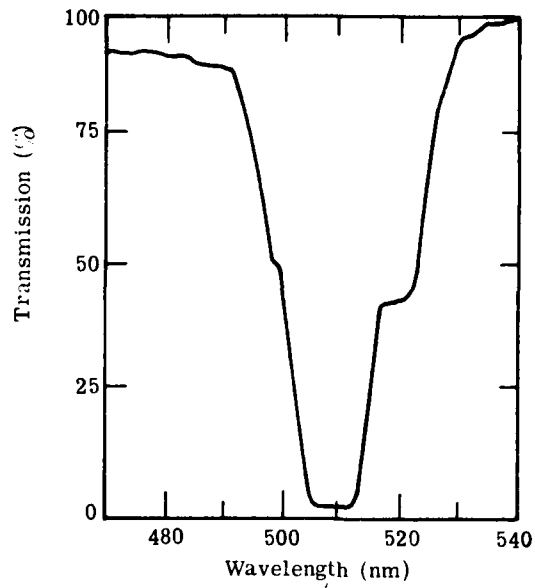


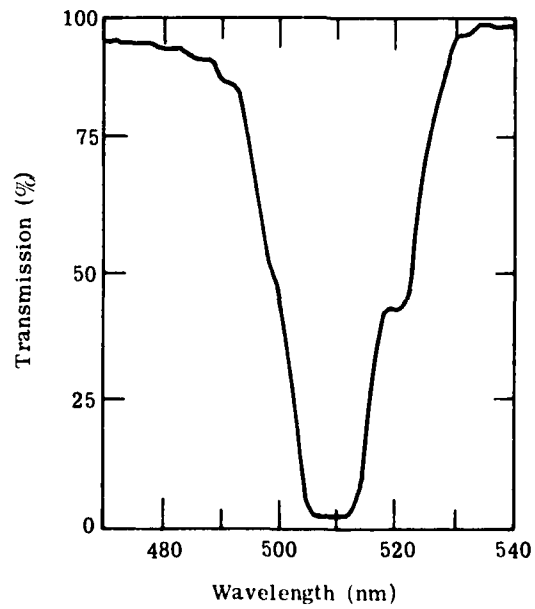
Figure 34. Angular bandwidth of holographic combiner HUD-76-3.

that generated with illumination from the rear side. There are several possible reasons for the difference. In a real hologram, the refractive index modulation varies with hologram depth because, during the exposure, absorption by the ammonium dichromate causes a depth attenuation of the incident light. The non-uniform index modulation may account for the difference in readout characteristics. Another possible reason is that very low frequency and low contrast fringes formed by multiple reflections between surfaces affect the front side of the holographic combiner more than the rear side.

The spectral bandwidth of the holographic combiners were measured with a Cary Model 14 spectrophotometer as follows. A combiner was placed in one of the sample beams and oriented such that the beam was incident at an angle of  $48^\circ$ . The transmission of the combiner was measured and plotted as a function of wavelength, as shown in Figures 35-37. Unlike the angular bandwidth curves, the spectral bandwidth curves (at least in transmission) obtained from both sides of a sample, are identical. We made two interesting observations, however. First, the transmission spectrum appears to consist of two different spectra: a wide and weak spectrum, and a narrow and strong spectrum. Secondly, these spectra have relatively wide flat bottoms of 7 nm to 10 nm. We believe that the first phenomenon originates from the non-linear index modulation due to heavy exposures. The second observation shows the large index modulation capability of dichromated gelatin as a reflection hologram recording material.



(a) Front side



(b) Rear side

Figure 35. Spectral bandwidth (shown in transmission) of holographic combiner HUD-76-1.

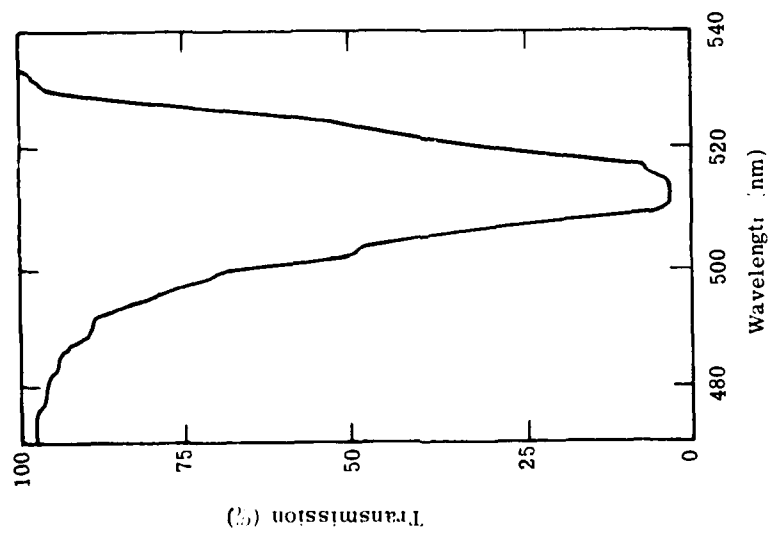
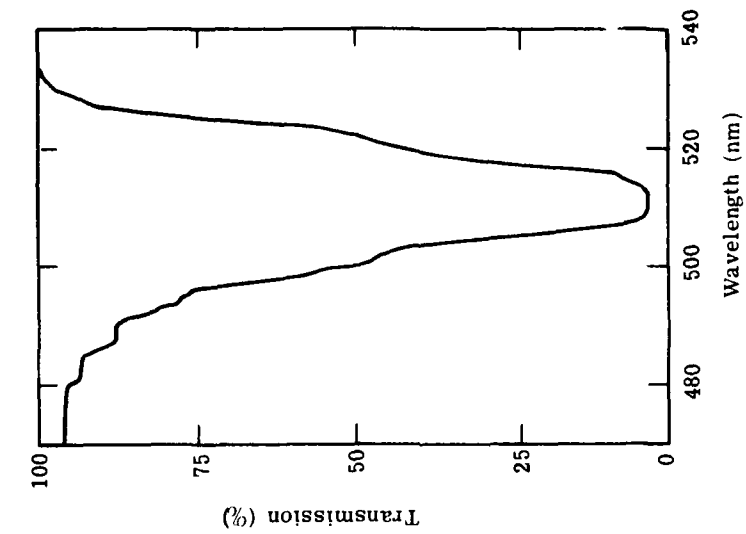
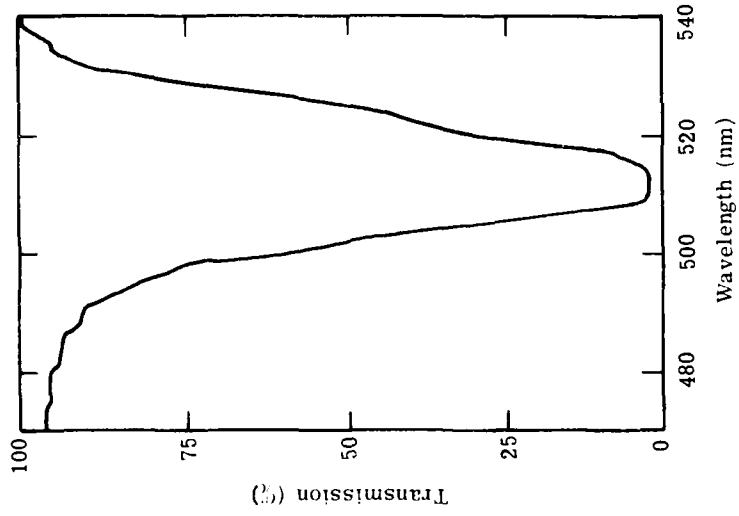
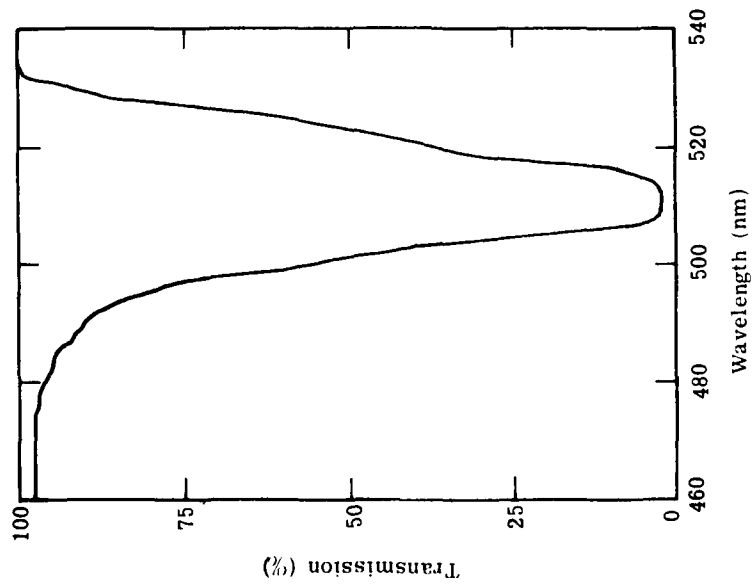


Figure 36. Spectral bandwidth (shown in transmission) of holographic combiner HUD-76-2.



(a) Front side



(b) Rear side

Figure 37. Spectral bandwidth (shown in transmission) of holographic combiner HUD-76-3.

SECTION IV  
COMPUTER ANALYSIS OF A HOLOGRAPHIC COMBINER

We carried out a computer analysis to investigate the performance improvement that can be achieved by replacing a conventional combiner in an existing system with a holographic combiner, modifying the optical train as necessary with the constraint of not exceeding the overall space requirements of the existing system. The system chosen for this investigation was the A-10 HUD system. The introduction of the holographic combiner, in this case with optical power, not only should increase the system efficiency, but also should increase the IFOV (but not necessarily the TFOV).

The A-10 HUD system is characterized by a relatively large combiner-eye separation, and by relatively large aperture optics. The TFOV is approximately  $15^{\circ}$  and the IFOV is approximately  $9.6^{\circ}$ . The primary space constraints that we used were the diameter of the last collimating element (7.0 inches) and the distance between that element and the CRT (approximately 9.8 inches). More than any of the other dimensions of the A-10 HUD Projection Unit, these two place bounds on the configuration of the optical train.

We investigated two optical configurations: one in which the holographic combiner forms the final element of the collimator optics and a second in which a relay lens forms an intermediate image between itself and the holographic combiner. In the configuration with the relay lens, the IFOV can be made to equal the TFOV, but the performance requirements on the collimator are greater.

We found in general that the imaging characteristics of the holographic combiner itself were often poor. This is due, in large part, to the off-axis nature of the hologram, dictated both by the configuration of the HUD optics

and by the requirement to separate undesired diffracted orders. Our approach, therefore, was to design a hologram with the best possible imaging characteristics, and if these were inadequate, to require correction by additional conventional optics. The penalty in weight and cost of additional optics must then be weighed against the performance improvement realized with a holographic combiner.

## 1. COLLIMATING COMBINER

In a typical refractive HUD optical system, the collimator is a Petzval, or modified Petzval, objective, a lens configuration formed by two air-spaced doublets. This design provides for color and aberration correction and low distortion over a reasonable field-of-view with an f number on the order of one [14]. Often a negative lens element is added near the CRT to provide additional field flattening. We chose to take a similar approach assuming two major lens components to collimate the light from the CRT; one of the major components, then, is the holographic combiner.

We chose the following field-of-view parameters for our design: a TFOV of  $20^{\circ}$  and an IFOV of  $15^{\circ}$ . The focal length of the collimator optics was chosen to be 9.0 inches, requiring a CRT diameter of 3.2 inches (see Figure 2). The combiner-eye separation of 33.6 inches in the A-10 requires a projected combiner diameter of 8.9 inches to satisfy the IFOV requirement, and as the collimator is actually tilted, its diameter must be approximately 15 inches, slightly less than the 16 inch diameter of the existing combiner.

It is desirable to distribute the optical power between the two major components, the holographic lens and the conventional lens element between the combiner and the CRT. The off-axis property of the hologram tends to cause field tilts and distortions, and the severity of the problem



increases as the  $f$  number of the hologram decreases. To minimize this effect, we chose to place the majority of the optical power in the conventional lens, allowing a relatively long focal length for the hologram lens. In keeping with this approach, we chose a hologram focal length of 27.1 inches, three times the system focal length. We also chose a separation between the hologram lens and the conventional lens of 11.8 inches, two thirds of the combiner-CRT distance. The hologram focal length, the lens separation, and the system focal length determine the focal length of the conventional lens, 7.6 inches. A sketch of the system is shown in Figure 38.

We are now ready to consider the hologram design. The radial distance from a hologram lens to the image it forms can be expressed as follows [15]:

$$\frac{1}{R_i} = \frac{1}{R_c} \pm \frac{\lambda_c}{\lambda_o} \left( \frac{1}{R_o} - \frac{1}{R_r} \right) \quad (4)$$

where

- $R_i$  = distance to image point
- $R_c$  = distance to reconstruction point source
- $R_o$  = distance to object beam point source
- $R_r$  = distance to reference beam point source
- $\lambda_c$  = reconstruction wavelength
- $\lambda_o$  = construction wavelength

The sign of the term in parentheses is chosen according to the diffracted order of interest. Once the hologram lens is constructed and a reconstruction wavelength is chosen, the term

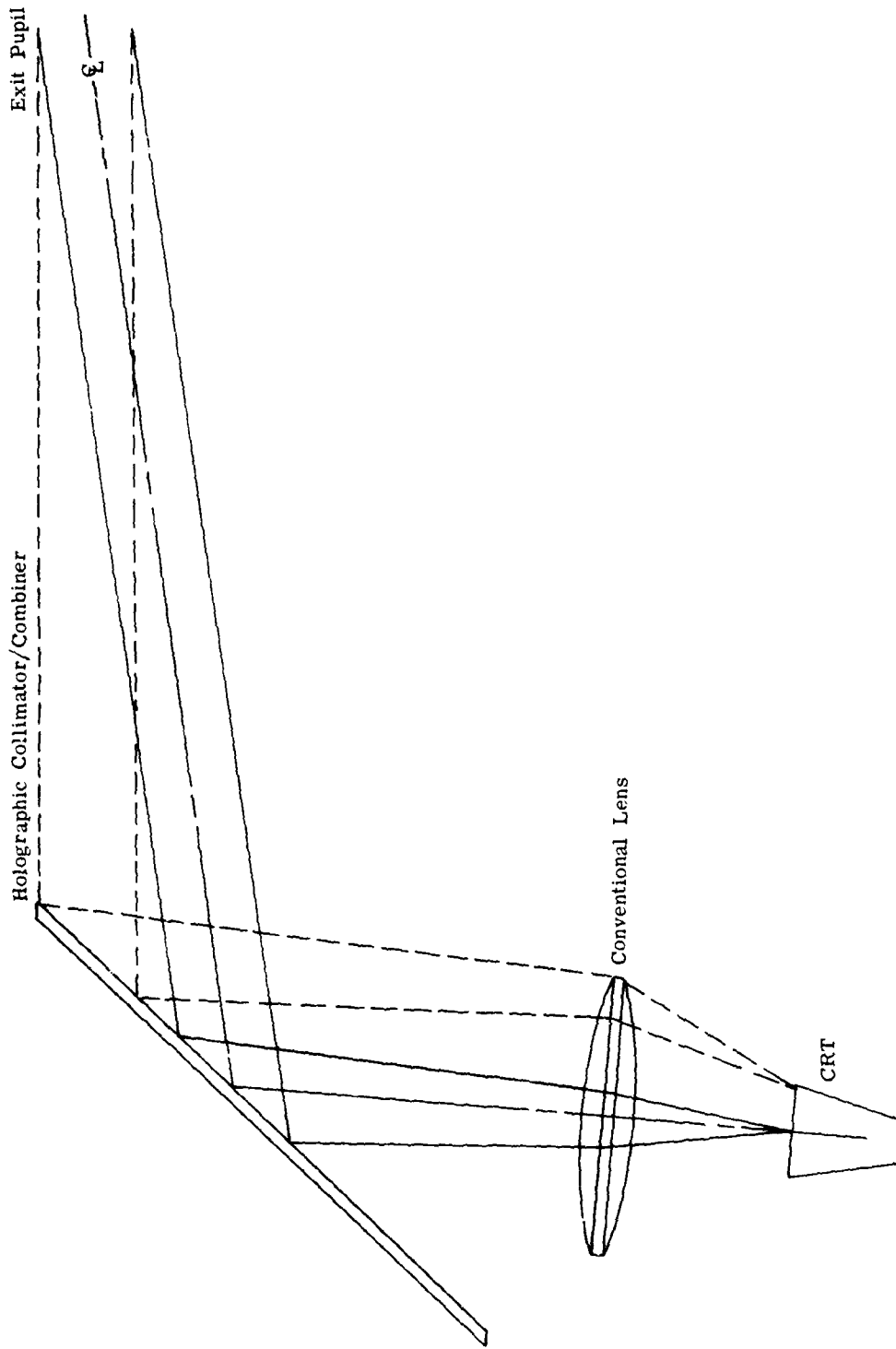


Figure 38. Configuration of the A-10 HUD with a holographic combiner/collimator.

$$\frac{\lambda_c}{\lambda_o} \left( \frac{1}{R_o} - \frac{1}{R_r} \right)$$

becomes a constant, and can be thought of as a reciprocal focal length. Equation (4) then effectively reduces to the well known thin lens equation of conventional optics. We can express the focal length of the hologram lens, therefore, as

$$f_H = \frac{\lambda_o}{\lambda_c} \left( \frac{1}{R_o} - \frac{1}{R_r} \right)^{-1} \quad (5)$$

Note that the hologram focal length varies inversely with the reconstruction wavelength; this is longitudinal dispersion, and will have to be taken into account. Note also that  $R_o$  and  $R_r$  are not determined uniquely, but that an infinite set of pairs can be chosen to produce a given focal length. This is analogous to the bending of a simple lens where a similar set of surface curvature pairs exist that determine the focal length of the lens (for a more complete discussion of the analogy, see Ref. 16).

For a hologram focal length of 27.1 inches, then, we see that there is an infinite set of reference and object beam pairs that we can choose according to the constraint

$$\left( \frac{1}{R_o} - \frac{1}{R_r} \right)^{-1} = 27.1 \quad (6)$$

and we have assumed the same reconstruction and construction wavelength.

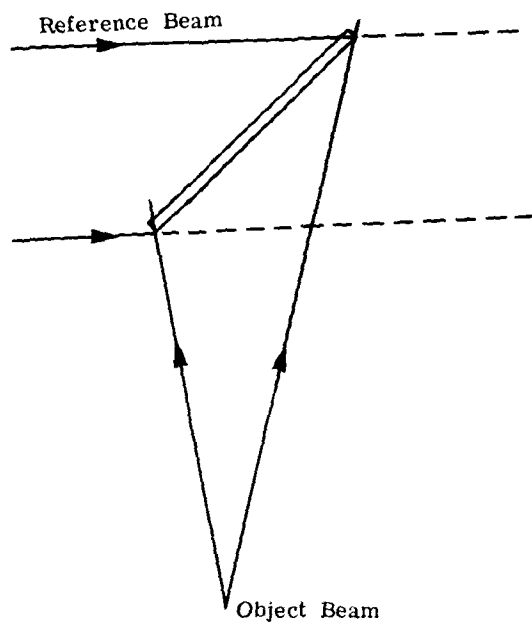
The choice of reference and object beam lengths is greatly reduced by efficiency considerations. Because rays must be near the Bragg angle to be diffracted with high efficiency, the reconstruction rays should have angles that are near those of the reference beam rays. In designing the hologram construction geometry, we reverse the process and look for a configuration in which the reference beam will approximate the reconstruction beam since the latter is determined by the HUD system geometry. Unfortunately, achieving high efficiency over a large angular field-of-view tends to be incompatible with achieving high efficiency over a large spatial field, which is required to accommodate the pilot's head motion. How well both requirements are satisfied will depend not only on the design geometry but also on the index modulation that can be achieved during fabrication (as was true for the flat combiner discussed in Section III).

The HUD system was analyzed as follows. We assumed parallel light in the vicinity of the pilot's eye traveling backward through the optical system to the CRT screen. By varying the angle of the light as it passed through the pilot's space, we could investigate the system properties over the field-of-view, and by translating the input ray bundle, we could determine the effect of allowing head motion. The first step is to trace rays from the input plane to the hologram lens, and determine the location of the image formed by the hologram as a function of field angle. As this intermediate image will form a virtual object for the conventional lens, which must then form a high quality image at the CRT surface, it is desirable for the hologram image to be as good as possible in terms of distortion, tilt, and efficiency over the field-of-view.

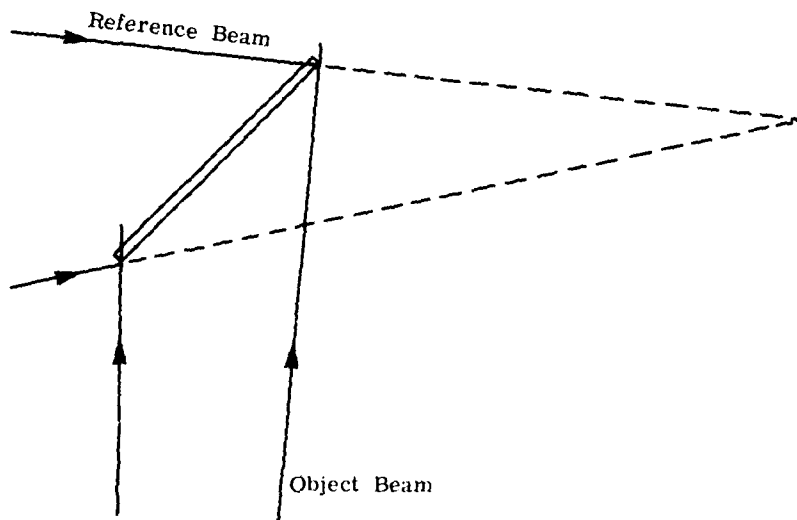
We can only optimize the hologram image quality by optimizing the hologram lens design. The variables we have to work with are rather limited, however. The requirement for approximating Bragg angles puts bounds on the lengths of the object and reference beams, although they can vary within those bounds. The tilt of the hologram can be varied somewhat within the constraints imposed by the canopy and instrument panel. The offset angle of the hologram is quite restricted by the A-10 HUD configuration. We are reasonably free, however, to introduce curvature to the hologram element.

We used the Holographic Optics Analysis and Design (HOAD) raytracing program [17] to analyze the behavior of the optical system as we varied the hologram lens design. With the program, we could determine both the image properties and the efficiency with which each ray was diffracted.

The importance of approximating Bragg angles is demonstrated by examining the hologram efficiency over the field-of-view and over the exit pupil for two sets of object and reference beam lengths. The exit pupil size is maximized if the hologram is recorded with a plane reference beam and an object beam with a point source at the focal plane of the hologram. The plane wave is aligned with the hologram-pilot axis, and the object beam with the CRT-hologram axis. At the other extreme, the field-of-view at the design eye is maximized by locating the reference beam point source at the design eye, with the object beam distance determined by Eq. (6). These recording configurations are sketched in Figure 39, and the predicted diffraction efficiency over a  $15^\circ$  field-of-view is shown for each case in Figure 40, where we have assumed an index modulation of 0.0525. Failure to keep within the angular bandwidth of the hologram can effectively reduce the field-of-view from the value expected from the geometric relationships shown in Figures 2 and 3. In



(a) Plane wave reference beam



(b) Reference beam point source at design eye

Figure 39. Two recording configurations for the holographic combiner.

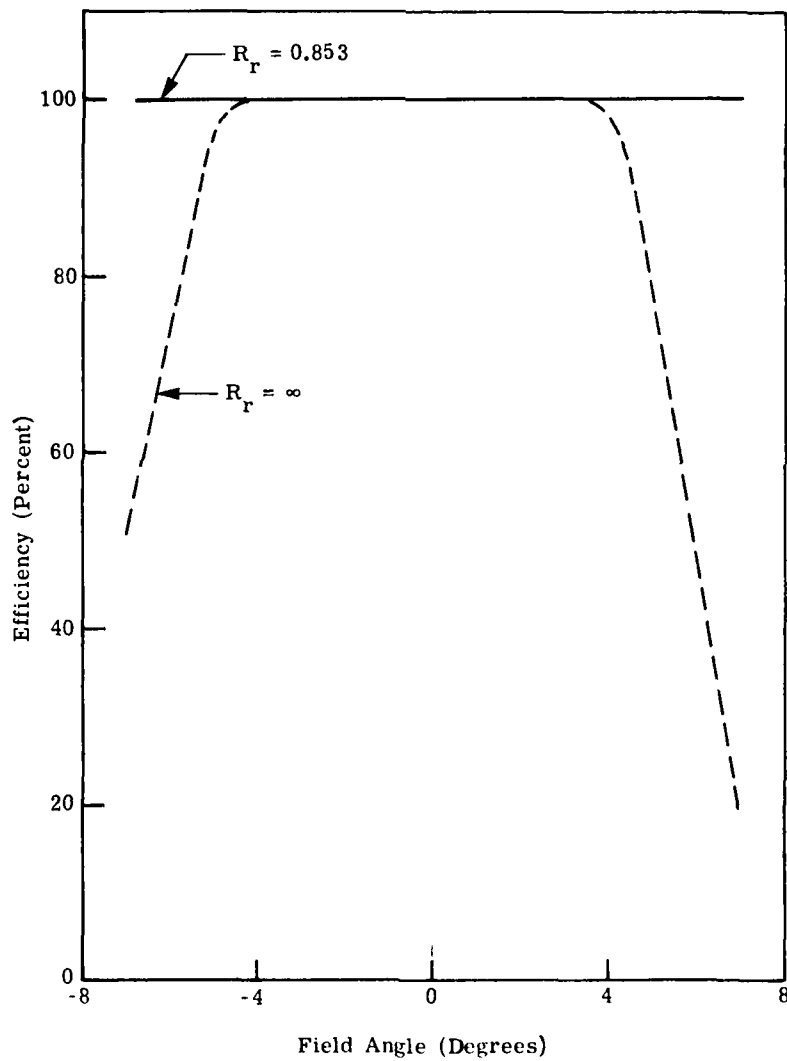


Figure 40. Diffraction efficiency as a function of field angle for the two hologram designs.

both cases, the diffraction efficiency at the central field angle exceeded 90% over an exit pupil with a five inch vertical diameter.

We observed that the hologram image surface tended to be tilted with respect to a plane perpendicular to the optic axis. This occurs in some cases because a relatively small bundle of parallel rays strikes widely different parts of the hologram at different field angles, yet focuses at roughly the same distance from the part of the hologram it illuminates. In this way, the off-axis nature of the hologram may cause the image surface to tend toward being parallel to the hologram. We found that curving the hologram affects the tilt in a manner that depends on the hologram recording beam lengths, as demonstrated by the curves in Figure 41. The curvature CV is the reciprocal of the radius of curvature, in meters, and is negative to indicate that the center of curvature is to the right of the hologram (as shown in Figure 38). The image tilt in each case was determined by tracing two orthogonal fans of rays through the system and computing the image location for several field angles. The image point at each field angle is determined as the mean of the images formed individually by the horizontal and vertical ray fans. Although in two of the cases shown in Figure 41 the field tilt is zero, the image surfaces formed by the vertical and horizontal fans are tilted but in opposite directions. This is seen more clearly in Figure 42 which shows the individual image surfaces at three hologram curvatures. Changing the hologram curvature has little effect on the horizontal image surface, but has a large effect on the rays lying in the vertical plane.

The hologram curvature affected not only the image tilt, but also aberrations. Figure 43 shows curves of the maximum wavefront deviation as a function of curvature for two reference



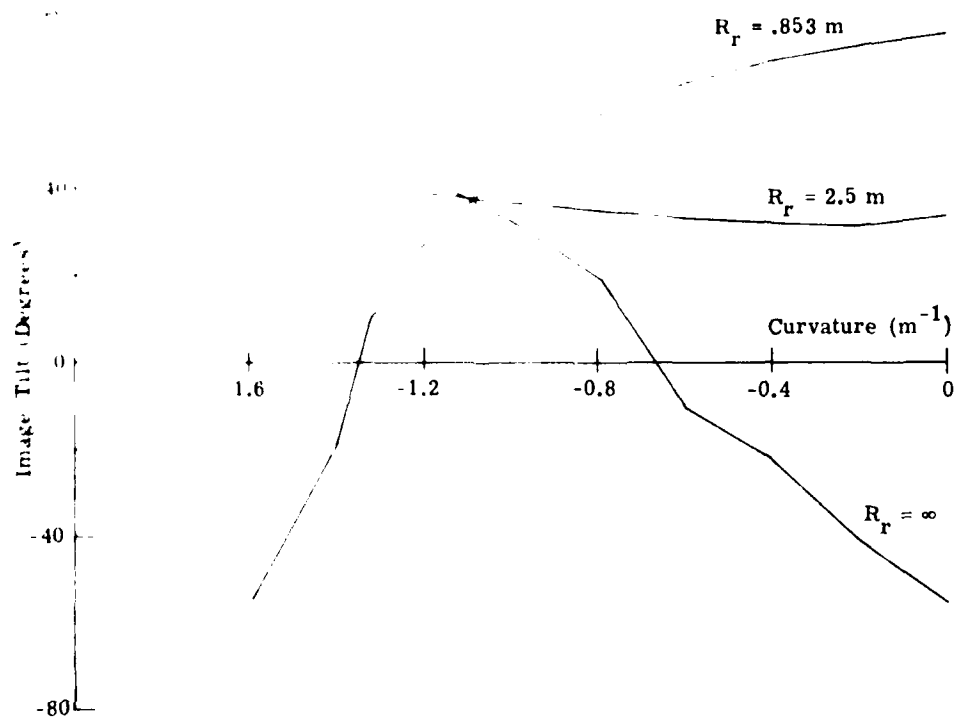


Figure 41. Effect of hologram curvature on image tilt for several hologram designs

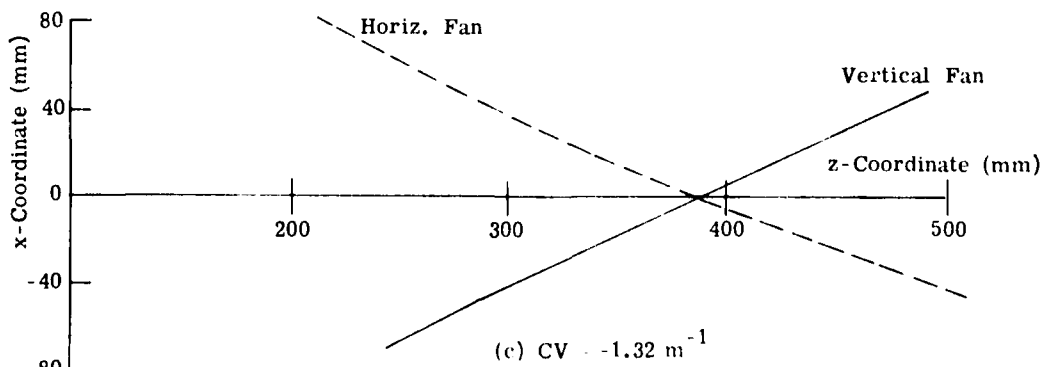
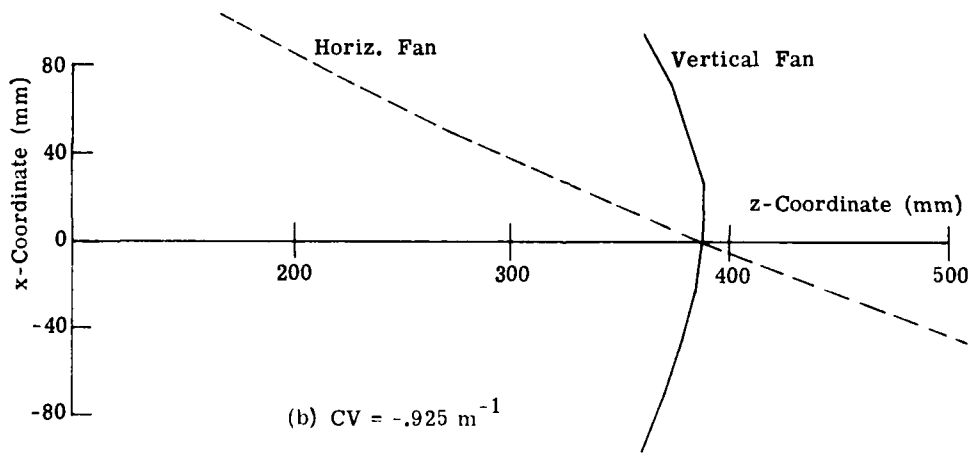
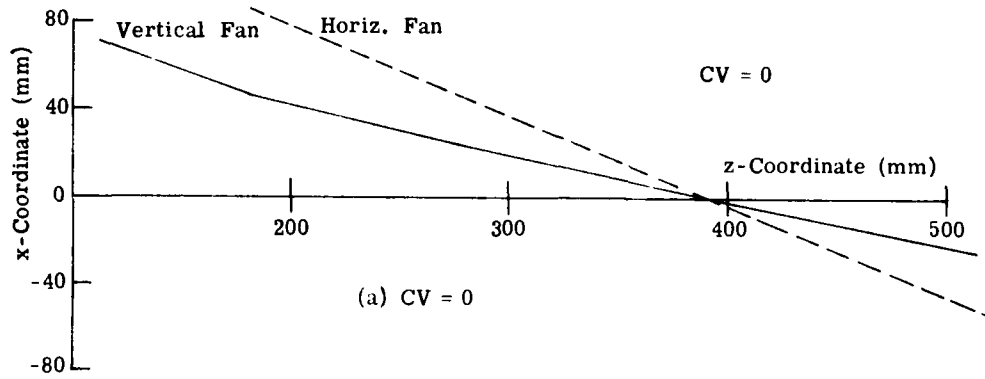


Figure 42. Image surfaces formed by varying the vertical field angle for several hologram curvatures.

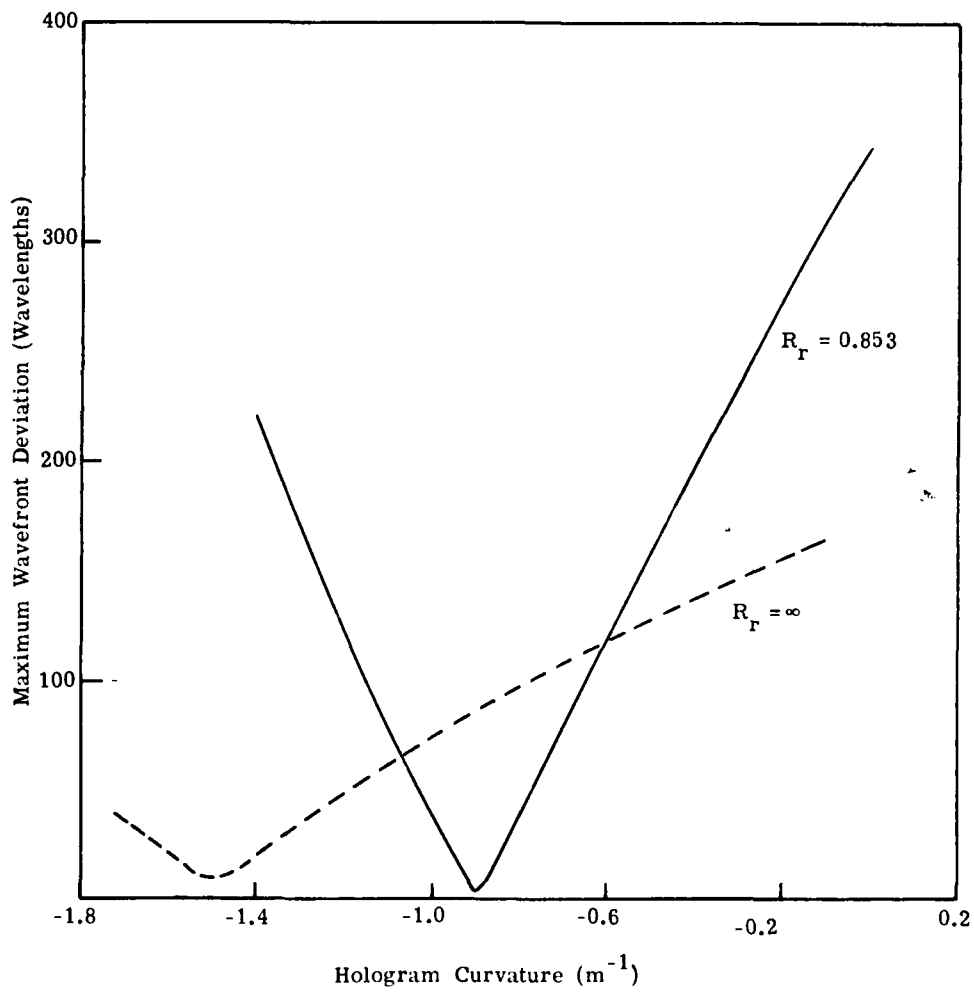
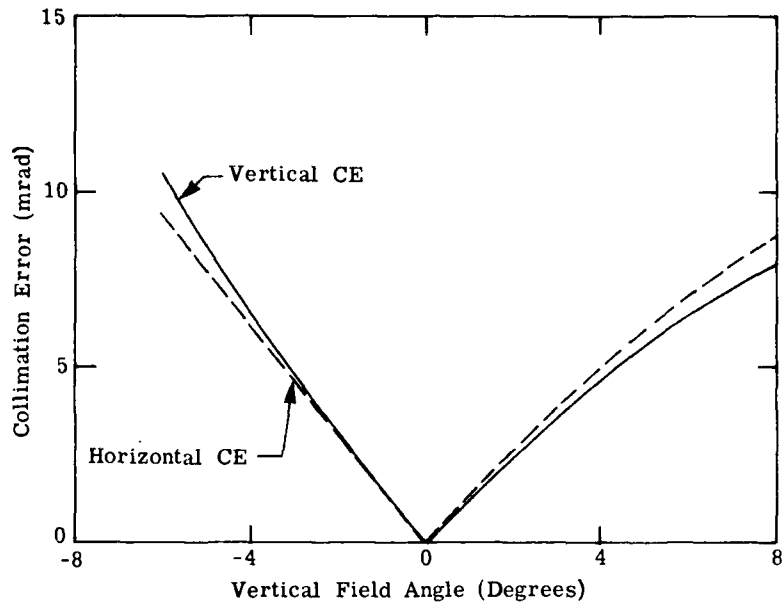


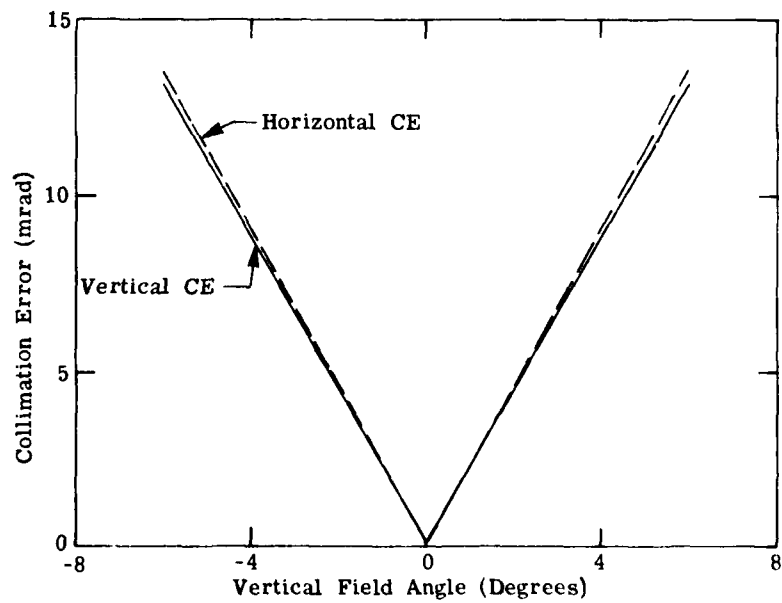
Figure 43. Effect of hologram curvature on wavefront deviations for two hologram designs.

beam lengths. We generated these curves by tracing two orthogonal ray fans, each with a height of three inches, from the exit pupil through the hologram and determining the location of the image formed by the rays. This Gaussian image location is the mean location of the images formed by the two individual fans, in each case the point of closest approach of the two rays adjacent to the central, or chief, ray. The ray tracing program defined a reference sphere about the Gaussian image point, and computed the optical path difference (OPD) along each ray between the reference sphere and a constant phase surface of the diffracted wavefront. The maximum wavefront deviation generally occurs at the edges of the wavefront. We also determined the magnitudes of the spherical, comatic, and astigmatic components of the aberrations. For the plane wave reference beam, astigmatism was predominant with a smaller amount of coma, whereas for the spherical reference beam  $R_r = .853 \text{ m}$ ), coma was dominant.

An important measure of the performance of the HUD optical system is the collimation error, with 1.0 mrad a reasonable goal, at least within the central portion of the field-of-view. The collimation error can be estimated by predicting the spot size at the image location, and dividing by the distance from the hologram to the image. Using the data shown in Figure 43 to select an optimum hologram curvature, we determined the image location and collimation error over the IFOV of the optical system. The collimation error for two hologram designs is shown in Figures 44 and 45. Again we assumed a three-inch ray bundle, so the collimation error is over a 3 x 3 inch exit pupil size. Furthermore, the image location is the mean between the horizontal and vertical image surfaces, which may be separated by a significant amount in the vertical plane (Figures 44a and 45a) as shown in Figure 42.

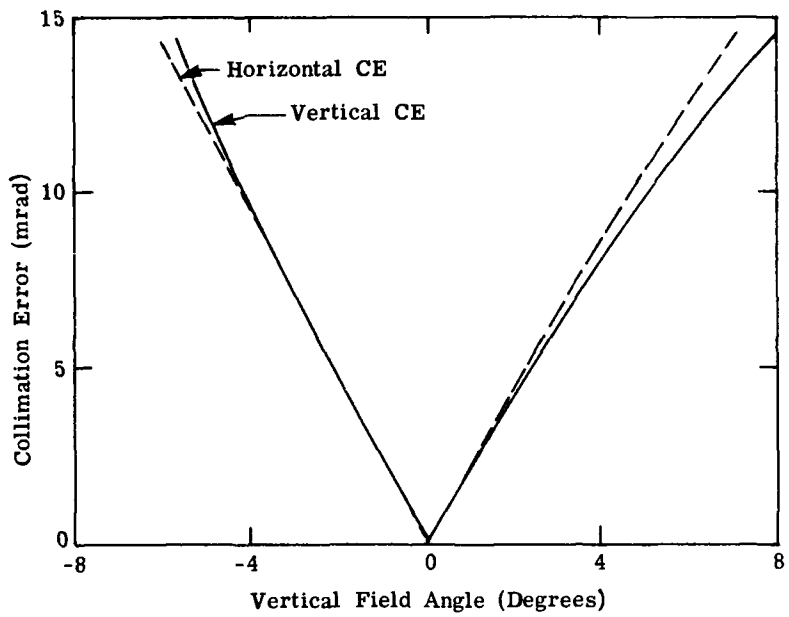


(a) Vertical field variation

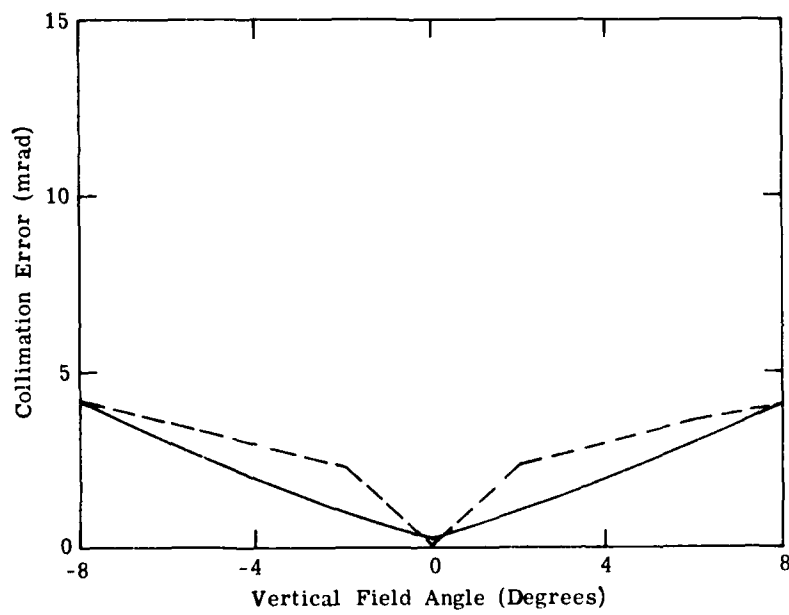


(b) Horizontal field variation

Figure 44. Collimation error as a function of field angles for a hologram made with a plane reference beam.



(a) Vertical field variation



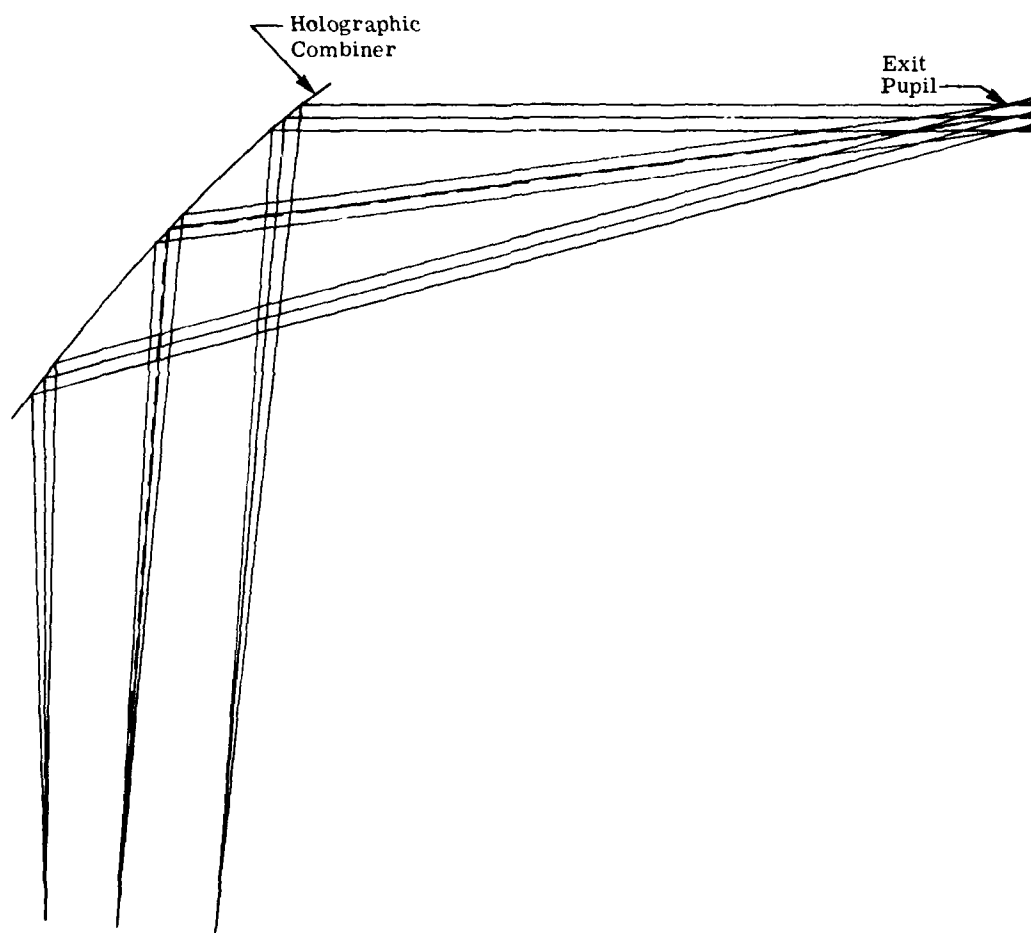
(b) Horizontal field variation

Figure 45. Collimation error as a function of field angle for a hologram made with a spherical reference beam.

Figure 46 shows the ray bundles traced through the holographic combiner at three field angles for two hologram designs. Some distortion appears evident at the intermediate image formed by the hologram in Figure 42a. The relatively low optical power of the hologram results in nearly parallel paths for the three ray bundles between the intermediate image and the hologram. This effect requires that the conventional lens, between the CRT and hologram (see Figure 38), must have a large diameter, approximately 9 inches, which is larger than the space constraint permits. (The final collimating element of the current system has a diameter of seven inches.)

As mentioned earlier, the focal length of a hologram, to a first order, is proportional to the reconstruction wavelength. For the geometry we have considered, the dispersion indicated by Eq. (4) is approximately 0.75 mm/nm, 0.75 mm change in the longitudinal, or radial, image position for every nanometer change in wavelength. Raytraces with the HOAD program indicate that the actual dispersion is 0.50 mm/nm, about two thirds that predicted by the first order theory. Without compensation for dispersion, the image position will extend over about 5 mm for a 100 nm source bandwidth. Since this amount of dispersion is excessive, either a narrowband phosphor is required for the CRT, or compensation must be introduced. Latta showed, for example, that the dispersion of a holographic element was reduced by a factor of fifty when a second compensating holographic element was added [18].

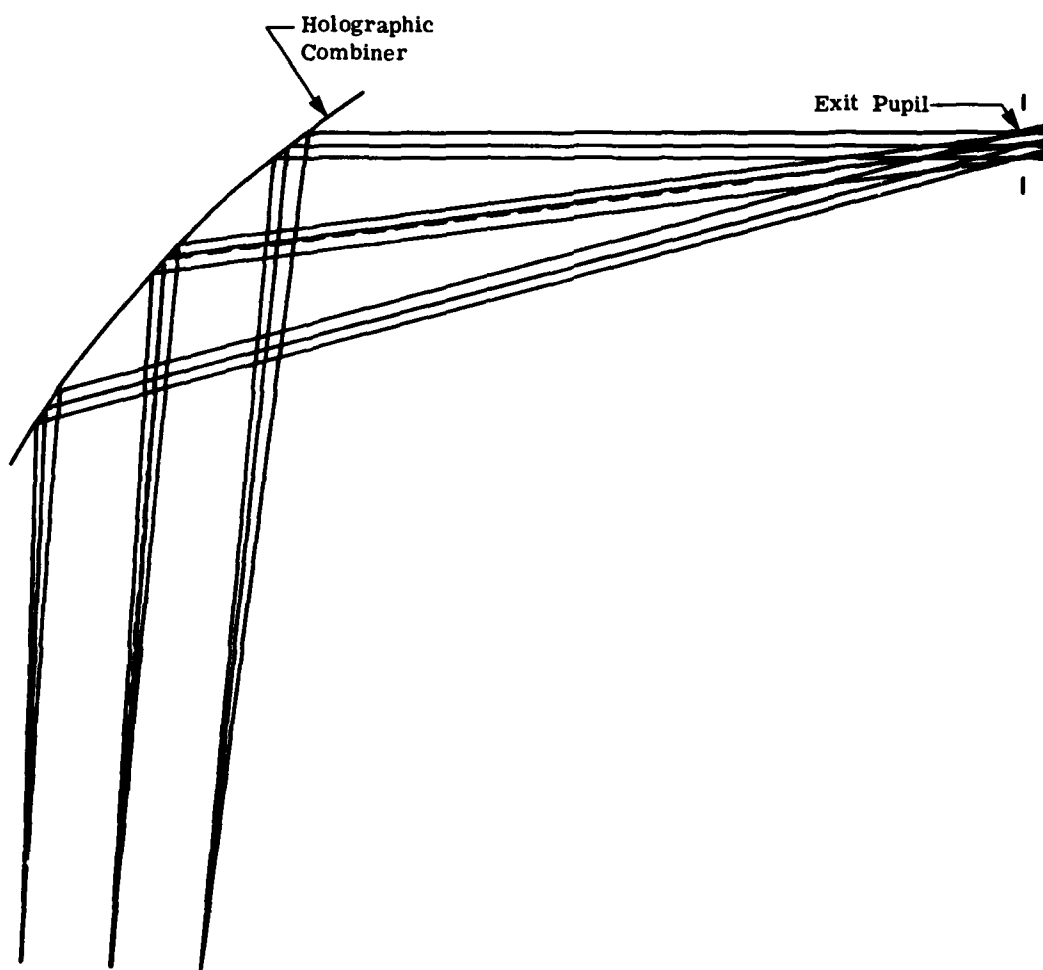
Although we chose to explore another design approach (Section IV.2) rather than optimize the hologram design here, we believe that this technique is feasible, and that with a curved holographic combiner forming the final element in a



(a) Plane reference beam:  $CV = -1.6 \text{ m}^{-1}$

Figure 46. Raytrace from exit pupil through the holographic combiner for field angles of  $0^\circ, \pm 7.5^\circ$ . (continued)





(b) Reference beam point source at design eye;  $CV = -.9m^{-1}$

Figure 46. Raytrace from exit pupil through the holographic combiner at field angles of  $0^{\circ}, \pm 7.5^{\circ}$ . (concluded)

collimating lens, the instantaneous field-of-view of the A-10 HUD can be increased to  $15^{\circ}$ . The steps required to complete the design of the optical system are optimization of the hologram lens, and design of the conventional portion of the collimating lens. In particular, the separation between the horizontal and vertical image surfaces at off-axis field angles in the vertical plane must be reduced, perhaps by the introduction of anamorphic optics into the recording beams. The hologram efficiency appears adequate given the current state-of-the-art with dichromated gelatin, but the collimation error must be reduced.

## 2. RELAY LENS SYSTEM

The advantage of this approach is that we can make the TFOV and IFOV identical, although at the expense of increased optical power required of the optical elements. A sketch of the unfolded optical system is shown in Figure 47. A conventional lens forms an intermediate image of the CRT screen at the focal plane of the hologram lens. The hologram lens then collimates the light from the intermediate image, and further, forms an image of the relay lens at the exit pupil, located at the pilot's eye. Since all of the light passing through the relay lens also passes through the exit pupil, the pilot can observe the TFOV from all points within the exit pupil. In order to form a real image between the conventional lens and the holographic lens, both lenses must be faster than in the previous case, and the task of forming a high quality image is more difficult.

For our investigations, we chose a field-of-view of  $20^{\circ}$  and an exit pupil 3.0 inches high located 33.6 inches from the hologram. The field-of-view, the hologram-CRT separation (17.7 inches by the space constraint), and the eye relief (hologram-exit pupil separation) are sufficient to determine

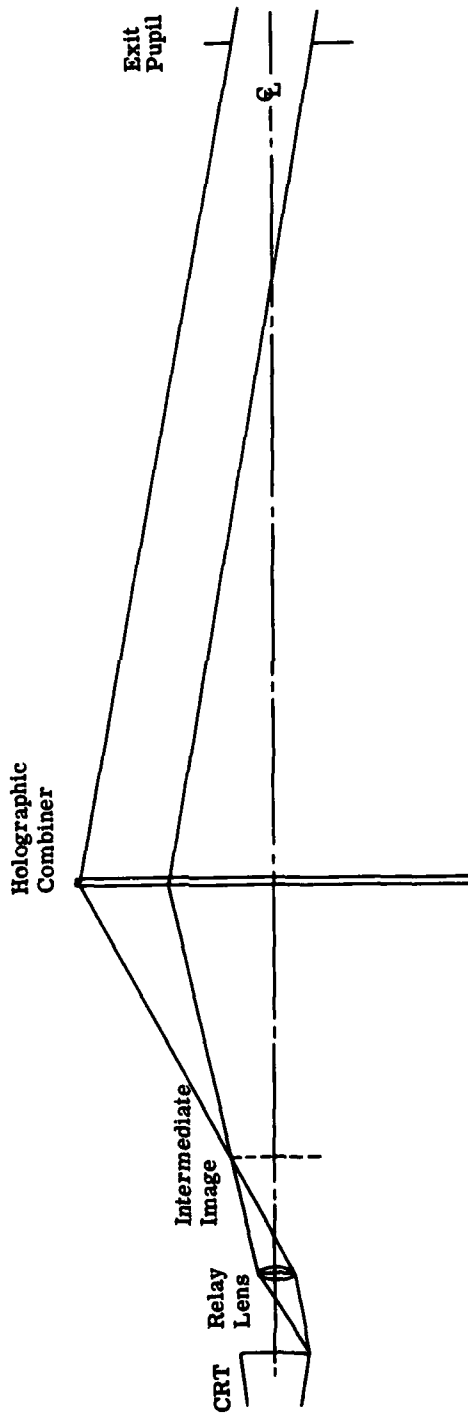


Figure 47. Unfolded optical system with a relay lens.

the location of the conventional lens and the intermediate image plane. These parameters, and the element diameters are listed in Table 5.

In analyzing this system, we used an approach similar to that described in Section IV.1; that is, we traced rays from the exit pupil to the hologram and determined the intermediate image formed by the hologram. The requirements on the relay lens are then to transfer the intermediate image to the CRT screen, correcting any defects in the intermediate image.

A reasonable design for the hologram is to locate the reference beam point source at the center of the exit pupil and the object beam point source at the center of the relay lens, since we require those to be conjugate points. With this choice for reference and object beam, all rays passing through the HUD system will be relatively near the Bragg angle (assuming no wavelength shift), and the rays passing through the center of the exit pupil will exactly satisfy the Bragg condition at all field angles.

Our analyses of the hologram generally showed that the optical performance was much less promising than in the previous configuration. Weaknesses that we observed in that configuration here were aggravated by the much greater optical power of the hologram, the focal length of which had decreased from 27 inches to 10.6 inches. The hologram curvature, for example, must be stronger to minimize the wavefront deviations, yet the minimum is not very low (see Figure 48). We observed that the image tilts and curvatures were more extreme, as shown in Figure 49 for a hologram with a curvature of  $-2.2 \text{ m}^{-1}$ . Based on these and other results, we conclude that the relay lens approach does not appear to be as promising a configuration for a holographic combiner/collimator in the A-10 HUD geometry.

TABLE 5  
DESIGN PARAMETERS OF RELAY LENS CONFIGURATIONS

Separations

CRT-Relay lens	75.7 mm
Relay lens-intermediate image	114 mm
Intermediate image-holographic lens	260 mm
Holographic lens - exit pupil	853 mm

Diameters

CRT	61.0 mm
Relay lens	33.5 mm
Holographic lens	378 mm
Exit pupil	76 mm

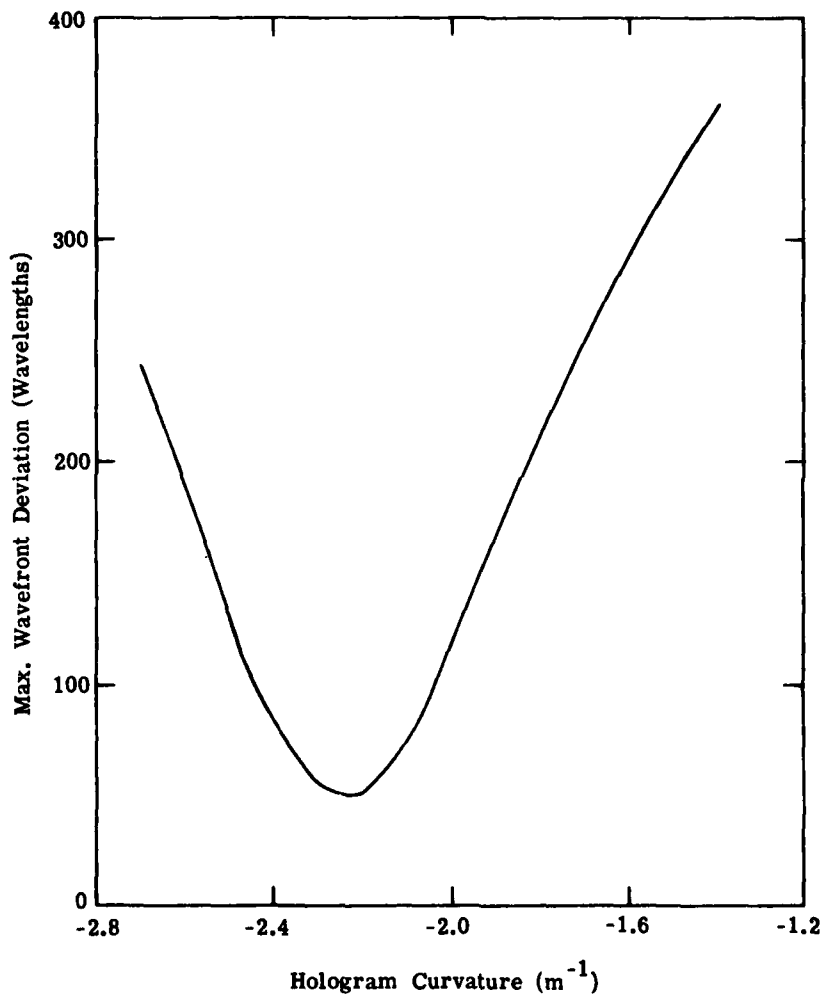


Figure 48. Effect of hologram curvature on wavefront deviations.

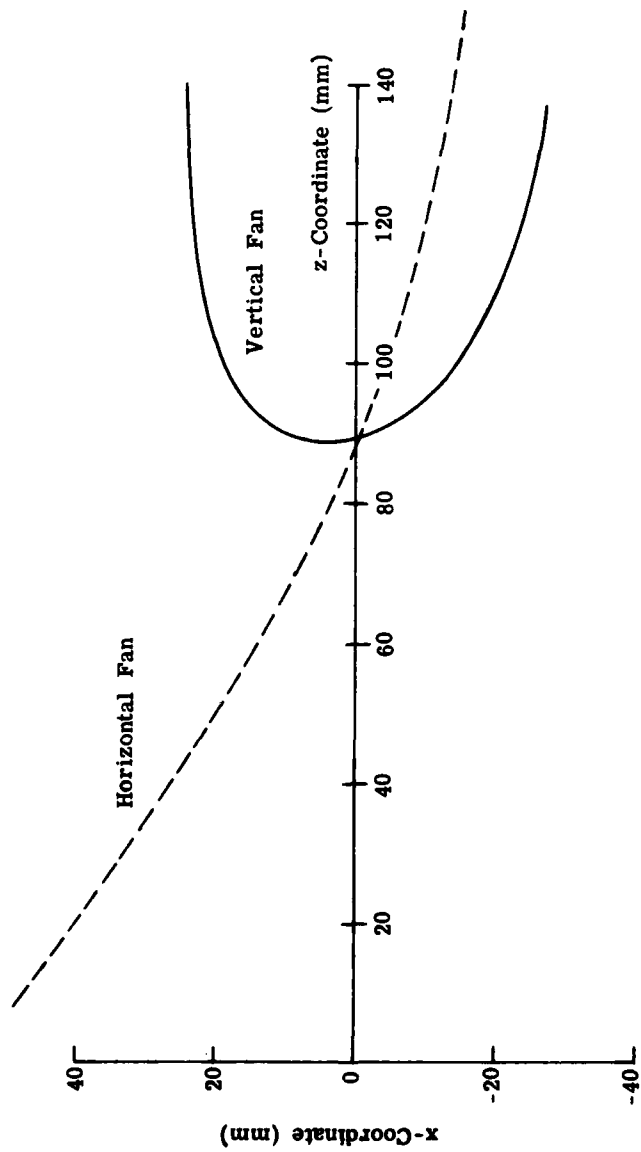


Figure 49. Image surfaces formed by varying the vertical field angle.

## SECTION V CONCLUSIONS AND RECOMMENDATIONS

In this report we have examined the effect on Head-Up Display systems of replacing the conventional combiner with a holographic combiner that may have optical power. The holographic combiner offers improved performance in two respects. The high reflectivity over a narrow spectral region of a volume phase hologram makes more efficient use of the CRT output, allowing brighter displays, lower CRT power levels, or both. Since the combiner can have optical power, it becomes part of the collimator and can increase the field-of-view of the optical system.

The design and fabrication in dichromated gelatin of a flat holographic combiner demonstrated that high quality noise free elements can be produced with high reflectivity over a limited spectral and angular extent. Since the bandwidth is approximately proportional to the refractive index modulation, it can be controlled by varying the exposure and processing steps. Using the processing procedure described in this report, we achieved refractive index modulations as high as 0.08 with a corresponding angular bandwidth of  $14^\circ$ . Three holographic combiners were fabricated as one-for-one replacements for the existing conventional combiner in the Austere F-4 HUD. These holographic combiners have wide bandwidths, diffraction efficiencies in excess of 90%, and very low scattering.

In our design investigation of a holographic combiner/collimator for the A-10 HUD, we considered two approaches. In the first, the hologram formed the second element of an airspaced two-element collimator. Although the constraint of working within the volume occupied by the existing system



limited the flexibility of the design effort, the collimator approach shows promise. At a reasonable refractive index modulation, the angular bandwidth is sufficient to allow a large angular field ( $\geq 15^\circ$ ) and a large exit pupil ( $\geq 5$  inches) simultaneously. Introducing curvature to the hologram provides an additional degree of flexibility to maximize the image quality. Dispersion caused by the diffractive nature of the hologram must be overcome, however, either by limiting the spectral bandwidth of the CRT phosphor or by providing compensation in the optical train.

The second approach, in which a relay lens forms an intermediate image, shows less promise because of the greater optical power required in each of the elements, particularly in the hologram. Although the relay lens approach is attractive in that the instantaneous field-of-view is as large as the total field-of-view, the difficulty of the design effort is considerably increased by assuming a pre-established set of constraints on the configuration of the optical system.

We recommend further design work on the holographic collimator approach to generate an optimized design of the complete optical system. This investigation would include a detailed design of the conventional portion of the optical system as well as optimization of the holographic lens. The goals of  $15^\circ$  instantaneous field-of-view and  $20^\circ$  total field-of-view appear reasonable and, in fact, might reasonably be increased to  $20^\circ$  and  $25^\circ$ , respectively. Dispersion will probably not be a significant problem if a narrow band phosphor such as the P44 phosphor is used, but other dispersion compensation techniques should be examined to allow greater flexibility in selecting the input source.

The next step is to fabricate a hologram lens according to the design developed. Since the hologram will probably

be curved, the experimental work must include preparation of gelatin layers on a curved substrate. The holograms formed under this phase of the effort should be evaluated not only in terms of efficiency and bandwidth, but also in terms of image quality, including aberrations and distortion. Finally, where the hologram fringes intersect the surface of the gelatin layer, a thin transmission hologram will be formed. Although diffraction by this transmission hologram will be weak, it may be significant if the reconstruction source is intense, as in the case of sunlight. Measurements should therefore be made to determine the amount of scattering caused in this manner.

## REFERENCES

1. R. A. Chorley, "Head-Up Display Optics," in AGARD Lecture Series No. 71, Opto-Electronics, September 1974, Paris and Bolkesjø, Norway, (AD 787 014).
2. R. J. Collier, C. B. Burckhardt and L. H. Lin, Optical Holography, Academic Press, New York, 1971.
3. H. Kogelnik, "Coupled Wave Theory for Thick Hologram Gratings," The Bell System Technical Journal, Vol. 48, 1969, p. 2909.
4. D. G. McCauley, C. E. Simpson, and W. J. Murback, "Holographic Element for Visual Display Applications," Appl. Opt. 12, 232 (1973).
5. W. S. Colburn, R. G. Zech, and L. M. Ralston, "Holographic Optical Elements," Final Technical Report AFAL-TR-72-409, January 1973.
6. A. Au, A. Graube, and L. G. Cook, "Holographic Lens for Pilot's Head-Up Display: Phase 3", Final Technical Report, N62269-75-C-0299, Hughes Research Laboratories, (1976).
7. W. S. Colburn and B. J. Chang, "Design and Evaluation of Hologram Optical Elements," Final Technical Report, AFAL-TR-76-60, ERIM No. 112100-3-F, Environmental Research Institute of Michigan, 1976 (Confidential).
8. R. K. Curran, and T. A. Shankoff, "The Mechanism of Hologram Formation in Dichromated Gelatin," Appl. Opt., 9, 1651, (1970).
9. M. Chang, "Dichromated Gelatin of Improved Optical Quality," Appl. Opt., 10, 2550 (1971).
10. B. J. Chang, "Post-Processing of Developed Dichromated Gelatin Holograms," Opt. Comm., 17, 270 (1976).
11. W. S. Colburn and B. J. Chang, "Design and Fabrication of Hologram Optical Elements," Final Technical Report, AFAL-TR-77-5, ERIM No. 119100-10-F, 1976 (Confidential).
12. B. J. Chang, and C. Leonard, "Exposure Characteristics of Dichromated Gelatin Holograms," presented at the October 1976 Annual Meeting of the Optical Society of America, in Tucson, Arizona.

13. W. S. Colburn and B. J. Chang, "Design and Fabrication of Hologram Optical Elements," Final Technical Report, AFAL-TR-74-281, ERIM No. 194500-7-F, Environmental Research Institute of Michigan, 1975 (Confidential).
14. W. J. Smith, Modern Optical Engineering, McGraw-Hill Book Co., New York, 1966.
15. E. B. Champagne, "A Qualitative and Quantitative Study of Holographic Imaging," (unpublished PhD dissertation), Ohio State University (1967), University Microfilms No. 67-10876.
16. J. N. Latta, "Computer Based Analysis of Holography," Ph.D. Thesis, University of Kansas, (1970), University Microfilms No. 71-27168.
17. J. N. Latta and R. C. Fairchild, "New Developments in the Design of Holographic Optics," Proceedings of the Seminar on Applications of Geometrical Optics (W.J. Smith, ED), Society of Photo-Optical Instrumentation Engineers, Redondo Beach, CA, 1973, pp. 107-126.
18. J. N. Latta, "Analysis of Multiple Hologram Optical Elements with Low Dispersion and Low Aberrations," Appl. Opt. 11, 1686 (1972).